The model AMBETI

A detailed description of a soil-plant-atmosphere model

von

Harald Braden

June 2012: revised version of

"The model AMBETI - A detailed description of a soil-plant-atmosphere model",

Berichte des Deutschen Wetterdienstes 195, Offenbach am Main, 1995.

Anschrift des Autors:

Dr. Harald Braden

Deutscher Wetterdienst

Zentrum für Agrarmeteorologische Forschung

Bundesallee 50

38116 Braunschweig

Corrections to pdf-version (2012) of "Braden, (1995 : 'AMBETI', Berichte des DWD 195)"

A lot of figures are damaged and could not be revised with acceptable effort.

p. 3 Fig. 1.1: lea<u>v</u>es

p. 60, 61 In Fig. 4.6 r_{lw} should be replaced by r_{pl} as in eq. (4.7a).

p. 83 Fig. 5.5 is not perfectly correct:

The resistances $r_{vl,i}$ should start at the top of the layer i.

The symbol "ρ" has been omitted five times.

Abstract

This paper gives a detailed description of the soil-plant-atmosphere model AMBETI. This model calculates transpiration and soil evaporation as well as microclimatic conditions in the canopy and in the soil. The interception of precipitation, the formation of dew and the development and melting of a snow cover on the soil surface and of soil chill are calculated. The model contains a sophisticated sub-model for the calculation of components of the net radiation fluxes of plants and of the soil surface. Another important basis for the whole model is the thorough treatment of the relevant processes in the soil: the transport of heat, of liquid water and of water vapour.

The model includes several empirical relations, namely for the calculation of the intercepted radiation fluxes, the soil thermal and hydraulic properties and the plant reactions. Most of these relations have been taken from literature or calibrated within the corresponding sub-model. The only component of the model that requires a further calibration is the bulk stomatal resistance. The corresponding coefficients have to be calibrated using the whole model.

Several results of the model are presented as case studies in order to show the possibilities for the model. The model is used in the Agrometeorological Section of the German Weather Service (DWD) for research purposes as well as for routine applications and has therefore been intensively tested.

Zusammenfassung

Mit der vorliegenden Arbeit wird ein Modell des Systems Boden-Pflanze-Atmosphäre detailliert beschrieben. Dieses Modell berechnet Transpiration und Bodenevaporation getrennt und erlaubt darüber hinaus die Bestimmung mikroklimatischer Größen in Bestand und Boden. Auch die Interzeption von Niederschlag, die Taubildung, die Entstehung und das Schmelzen einer Schneedecke an der Bodenoberfläche sowie von Frost im Boden werden bestimmt.

Das Modell enthält ein hochentwickeltes Teilmodell zur Berechnung der von den Pflanzen und der

Bodenoberfläche absorbierten Strahlungsströme. Die sorgfältige Behandlung der maßgeblichen im Boden ablaufenden Prozesse der Wärme- und Wasserhaushalte und des Dampftransports stellen eine wichtige Grundlage des gesamten Modells dar.

Das Modell enthält zahlreiche empirische Beziehungen, zum Beispiel für die Berechnung der Strahlungsinterzeption, der thermischen und hydraulischen Bodeneigenschaften und der Pflanzenreaktionen. Diese Beziehungen wurden der Literatur entnommen oder - wie bei der Strahlungsinterzeption - innerhalb des jeweiligen Teilmodells kalibriert. Die einzigen am Gesamtmodell zu kalibrierenden Größen sind die Koeffizienten zur Beschreibung der Stomatareaktionen.

Als Beispiele für die vielfältigen Möglichkeiten des Modells werden einige Ergebnisse vorgestellt. Das an der ZAMF Braunschweig entwickelte Modell wird sowohl zu Forschungszwecken eingesetzt, als auch für die Routineanwendung im Rahmen der agrarmeteorologischen Beratung und ist dadurch gründlich getestet worden.

1   Introduction

1.1   The history of the development of the model AMBETI
1.2   Model structure

This paper gives a detailed description of the model AMBETI[*], developed by the author during several years in the ZAMF. This chapter first explains the individual steps in the development of the model and the purposes of its application. The second part of the introduction gives general information about the structure of the model and its temporal and spacial discretization.

1.1   The history of the development of the model AMBETI

The first version of the model AMBETI was developed ten years ago. The initial purpose was to determine daily evapotranspiration values for the investigation of water and mass budgets in small catchments over a whole year. The energy budgets of the system had to be simulated because it was not possible to use sophisticated measuring equipment like lysimeters, eddy correlation and Bowen-ratio instruments.

When the distinction of soil evaporation and transpiration turned out to be relevant, it became necessary to determine the extinction and transmission of radiation. For this purpose a new method was developed on the basis of results of Cowan (1968, 1971) and Goudriaan (1977) with the help of a "Successive Orders of Scattering Approximations" model (Braden, 1982, p. 22). Moreover, the vertical aerodynamic transport through the canopy had to be simulated. This was done with the help of results of a numerical model of the shear stress exerted on the plants (Braden, 1982, p. 74).

The interception of precipitation by the foliage was included in the simulations (Braden, 1985) in order to allow model runs for all periods, including rainfall. Model runs during winter periods were enabled by considering soil chill in the calculation of the soil heat and water budgets, and by including the development and melting of a snow cover on the soil surface in the simulations.

In the application for agrometeorological advice, the model should provide micrometeorological conditions from inside the canopy as input quantities for phytopathological models. For this purpose, the model AMBETI was generalized to calculate air temperature and humidity at two levels inside the canopy, and to properly determine leaf wetness (Braden, 1994). This version of the model is running under MS-DOS and under UNIX-systems.

---

[*] AMBETI is the abbreviation for "Agrometeorological Model for the Calculation (in German 'Berechnung') of Evaporation, Transpiration, and Interception".

For the same purpose, the model AMBETI was supplemented with modified input/output sub-programs for direct application in the AMBER-system of the ZAMF (Löpmeier, 1990). This version of the model, called BEKLIMA[*], is running under MS-DOS and was tested intensively for different meteorological boundary conditions, crops and soil types during 1993. As of 1994, this program is routinely applied by the Agrometeorological Section of the German Weather Service (DWD). Recently, a version of the model BEKLIMA was implemented on the NOS-VE main frame of the DWD with special input/output programs for direct application with synoptic and forecasted data.

A new development in the model AMBETI/BEKLIMA, the generalized application of the so-called pedo-transfer functions for the description of the soil hydraulic properties, was advanced by cooperation inside the "Collaborative Research Program (SFB) 179"[**] of the German Research Society (Deutsche Forschungsgemeinschaft, DFG). These functions, that allow a better representation of the soil hydraulic properties, were evaluated in this project (Tietje and Tapkenhinrichs, 1993).

1.2   Model structure

In the model AMBETI the vertical transports as well as plant and soil heat and water budgets are numerically simulated in a one-dimensional manner. The plants are considered as a single layer, but the soil is divided into several horizontal layers. The temporal resolution of up to one hour is usually determined by the meteorological boundary conditions. During this global time step Δt_g, the equations of the whole system are not implicitly solved, but the time step is internally divided and accommodated to the corresponding sub-systems.

For the calculation of the soil temperatures, the time step depends on changes at the soil surface. In this context special regard is contributed to the formation and melting of snow cover and of soil chill. The time step for the calculation of the soil water content is determined by the infiltration of water at the soil surface. The time intervals also are divided for properly calculating evaporation of water intercepted by plants.

The shortest but over-simplified characterization of the model AMBETI is: "It is twice Penman-Monteith, once for the plants and once for the soil surface". Some more insight to the model will be given with the help of Fig. 1.1. Additionally the single sub-programs of the model AMBETI and their purpose are listed in appendix A1.1.

---

[*]   Abbreviation for "canopy microclimate" (in German "Bestandsklima").

[**]   'Water and Matter Dynamics in Agro-Ecosystems' (Technical University of Braunschweig)

AMBETI
overview

Input: meteorol. boundary values
R_g, R_l, T, r.h., u, P_r

Input - parameters

aerodynamic
conversion
of windspeed

separation: visible/nir radiation
direct shortwave radiation
for inclined surfaces

< site inclination

vege-
tation
?

y

absorbed radiation and aerodynamic
transport resistances for plants
and soil surface

rain
?

< plants
(height, LAI)

rainfall interception
precipitation at the soil surface

y

< soil hydraulic
properties

infiltration,
soil water
budget

evaporation of intercepted water
transpiration
energy balance, aerodyn. transp.
for plants
canopy microclimate

y

leafs
wet ?

plant water
uptake

< root-
distribution

evapotrans-
piration

snow cover, snow melt
energy balance for soil surface
soil evaporation
soil heat budget
freezing, melting of soil water

< thermal soil
properties

Fig. 1.1   Overview of the model AMBETI

The meteorological boundary conditions are recommended with temporal resolution of one hour or less. These are

-       global radiation,

-       incident long-wave radiation or cloud information,

-       temperature and humidity from a reference height (e.g. 2 m) outside the canopy,

-       wind speed from a reference height and

-       precipitation as well as irrigation, if applied.

Should values of incident long-wave radiation be missing, they can be estimated with parameterizations using cloud information. The global radiation, incident on the horizontal plane, is divided into visible and near infra-red components and transformed if the considered surface is inclined. The reference wind speed can also be converted if the corresponding input quantity does not come from the regarded surface. If vegetation is considered, the radiation components absorbed and transmitted by the plants are calculated, as well as the resistances for the vertical aerodynamic transports through the

canopy. If it is raining, the interception of precipitation by the plants is determined as well as the through-falling portion, which is considered in the soil water budget. If it does not rain, the foliage may still be wet from precipitation or dew. In this case the evaporation of the intercepted water or dew is calculated in addition to the transpiration from the energy balance of the foliage and the aerodynamic transport. Microclimatic conditions like temperature and humidity inside the canopy, as well as dew formation are also determined.

The soil evaporation and the soil heat flux are determined from the energy balance and the aerodynamic transports at the soil surface. These are used as boundary conditions for the calculation of the temperatures and water contents in the soil layers. The development and melting of a snow cover at the soil surface is considered as well as the freezing and melting of water inside the soil.

The quantities given in Fig. 1.1 and even many more can be given as output with different temporal resolution. The standard output is referred to in Chapter 6.

The details of the model are described in the following chapters:

-       **Chapter 2** deals with the calculation of the reflection, transmission and absorption of the radiation components by foliage with the aim of determining the net radiation balances of the plants and the ground surface.

-       **Chapter 3** describes the calculation of the energy budgets and the aerodynamic transports of the plants and the soil surface, as well as the development and melting of the snow cover.

-       **Chapter 4** deals with plant-water relations. The parameterization of the combined effect of the stomata is described. This is the only element requiring a calibration of the model in total. The method used for the calibration and the corresponding results are reported. Moreover, this chapter deals with the conduction of liquid water from the soil to the leaves, and with the interception of precipitation by the plants.

-       The treatment of the soil is described in **Chapter 5**. The calculation of temperatures and water contents in the soil layers considering soil chill, and the derivation of the thermal and hydraulic soil properties from the soil composition are discussed. Moreover, the treatment of water vapour transport in the top soil is explained.

-       **Chapter 6** deals with the use of the model. The recommended input quantities are summarized. The file structures for the two input-output versions of the model, called AMBETI and BEKLIMA, are discussed. Finally, some results of the model are presented as examples of the model's capabilities.

2   The net radiation of plants and of the soil surface

The exchange of radiation is treated namely in order to determine the net radiation fluxes of the plants and of the soil surface, because they are important elements of the respective energy balances. Moreover, the long-wave emission of the whole canopy is an important measure for the water supply of the crop. The remote-sensed detection of surface temperatures allows the control of evapotranspiration, respective of the water supply (Braden and Blanke, 1993).

Because of different optical properties and exchange mechanisms (Ross, 1975, p. 22; Gates, et al., 1965), three spectral ranges are distinguished:

-          the long-wave or thermal range with the wavelength $\lambda_w > 3$ μm,

-          the near infra-red radiation 0.72 μm $\leq \lambda_w \leq 3$ μm and

-          the range $\lambda_w < 0.72$ μm which includes the visible range and parts of UV and is considered to coincide with the photosynthetically active radiation (PAR).

The distinction of only two short-wave ranges is a simplification in view of spectral properties (Ross, 1975, p. 22; Gates and Tantraporn, 1952), but it seems to be acceptable for the purpose of this model. The justification for the near infra-red range is the rapid decrease of incident radiation for $\lambda_w \geq 1$ μm. For this reason, the change of optical properties beyond 1 μm is beyond consideration. The short-wave radiation which must be given as meteorological boundary condition is divided into the two short-wave components, which are distributed over nine classes of inclinations (see Section 2.1). For these distributions the scattering by the plant elements is considered, resulting in the reflection at the top of the canopy, the transmission through the plant cover and the absorption inside. In Section 2.2 basic relations for the transmission through and reflection by canopies as well as existing estimates are presented. The method used in the model AMBETI is described in Section 2.3 and the modifications required for direct solar radiation are given in Section 2.4. Some few coefficients needed for the calculation of canopy reflection and transmission have to be determined from comparisons with the results of a "Successive Orders of Scattering Approximations (SOSA)" model (Braden, 1982) (see Appendix A2.1). The direct use of that SOSA model in AMBETI would take too much computing time. So far, the treatment does not consider the reflection at the soil surface. The transmitted

components of radiation are considered to be partially reflected at the ground, with optical properties described in Section 2.5. The net short-wave radiation components of the plant cover are composed from the components considered above (see Section 2.6). The presented method is also applied to the calculation of coefficients for the exchange of long-wave radiation (Section 2.7), which are used for the absorption and emission terms in the energy balances of the plant cover as well as of the soil surface.

2.1   The components of incident radiation and their estimation

For short-wave radiation as a boundary condition, different forms of input are possible. They are

-          measured or forecasted values of global radiation, and possibly additional
-          measurements of diffuse radiation (shade ring) or
-          measurements of direct radiation or
-          observed or forecasted information about total cloudiness.

The visible and near infra-red portions R_{vi} and R_{ni}, of the global radiation R_g are determined by

$$R_{vi} = 0.52\, R_g \qquad , \tag{2.1a}$$

and

$$R_{ni} = R_g - R_{vi} \qquad . \tag{2.1b}$$

The factor 0.52 is inferred from results of Schulze (1970, p. 121) and accounts for wavelengths 0.28-0.72 μm (R_{vi}) and 0.72-3.0 μm (R_{ni}). Consequently, if no input values of the direct or diffuse radiation components are available, the separation in direct (solar) ($R_{s,vi}$, $R_{s,ni}$) and diffuse portions ($R_{d,vi}$, $R_{d,ni}$) is calculated according to results of Kasten and Czeplak (1980, p. 180),

$$R_{d,vi}/R_{vi} = R_{d,ni}/R_{ni} = d + (1 - d)\, n_{ct}^2 \qquad , \tag{2.2}$$

with the total cloudiness n_t ($0 \le n_{ct} \le 1$). The quantity d is related to the sun elevation h_{s0} by

$$d = 0.65 - 0.40 \sin h_{s0} \qquad , \qquad \text{for } h_{s0} \ge 0 \tag{2.2a}$$

otherwise $d=1$ is used.

The sun elevation h_{s0} above the horizontal earth surface is easily determined from the scalar product of the sun beam vector and the normal vector to the earth surface (Braden, 1982, p. 27; Jolly, 1986). For the horizontal surface at the geographic latitude φ ($\varphi<0$ in the southern hemisphere) the expression

$$\sin(h_{s0}) = \sin \varphi \ \sin\delta + \cos \varphi \cos \ \delta \cos(\alpha_l) \qquad (2.3)$$

results. For the sun declination δ at the day of year J the relation

$$\sin\delta = 0.3978 \sin(x - 1.3528 + 0.00335 \sin x) \qquad . \qquad (2.3a)$$

holds with the abbreviation $x=0.017202 \ J - 0.0475$ (Kasten, 1989).

The local time angle α_l is zero at noon and is related to the local time t_l as $\alpha_l = 15 \ (t_l-12)$, if the time is expressed in hours and the angle in degrees. For a slope inclined with λ to α_s , the sun height h_s is determined from

$$\sin(h_s) = \sin(h_{s0}) \cos\lambda + \cos(h_{s0}) \sin\lambda \cos(\alpha_l - \alpha_s) \qquad . \qquad (2.4)$$

For the irradiances[*)] $B(\beta)$, resulting from observations of overcast skies, a standard distribution of the radiant intensity

$$I = I_0 (1 + 2 \sin\beta)/3 \qquad (2.5)$$

is used according to Anderson (1966) and Goudriaan (1977). The integration over the solid angle results in irradiance $B(\beta_i)$ at a horizontal receiving surface as listed in (Tab. 2.1) for the nine ten-degree classes of angles of incidence β_i .

Table 2.1   The distribution of the irradiances $B(\beta_i)$ for a standard overcast sky

i	1	2	3	4	5	6	7	8	9
β (°)	0-10	10-20	20-30	30-40	40-50	50-60	60-70	70-80	80-90
$B(\beta_i)$	0.015	0.057	0.106	0.150	0.180	0.184	0.160	0.110	0.038

[*)]   The irradiance (W m^{-2}) is the incident radiant energy received per surface unit area.

2.2 Some existing solutions and estimates for the transmission and reflection of the plant cover

As already stated above, the transmission as well as the reflection of the canopy are considered without reflection at the soil surface in this section. The effect of reflection at the soil surface is considered later (Section 2.5) and superimposed on the results of this section (Section 2.6). In the radiation sub-model presented, the fractions of transmitted and reflected radiation are estimated on the basis of results for simplified situations. The generalizations work semi-empirically with coefficients resulting from comparisons with the results of a SOSA model (Braden, 1982, see Appendix A2.1).

The method used in the model AMBETI (Section 2.3) has been developed on the basis of existing analytic solutions for horizontal foliage on the one hand, and for black foliage on the other hand, as well as additional estimates for the transfer of radiation that will now be described.

Cowan (1968, 1971) examined horizontal foliage with the transmission coefficient t and the reflection coefficient r, that are randomly distributed over the horizontal plane. The leaf area index l_a is defined as the portion of the total one-sided foliage area on the area of the ground surface. Cowan (1968, 1971) considered the appropriate differential equation system for the downward and upward radiation fluxes φ^+ and φ^-, respectively

$$\partial \varphi^+ / \partial L = r \, \varphi^- - (1 - t) \, \varphi^+ \tag{2.6a}$$

and

$$\partial \varphi^- / \partial L = - r \, \varphi^+ + (1 - t) \, \varphi^- \qquad . \tag{2.6b}$$

In contrast to Cowan, here the cumulative leaf area index L is defined with zero at the top of the canopy and l_a above the soil surface. From the corresponding solution with the boundary conditions $\varphi^+(L=0)=\varphi_0^+$ at the upper boundary and $\varphi^-(L=l_a)=r_g \, \varphi^+(l_a)$ (r_g=ground reflection) the transmitted portion results as

$$T = \exp\{-K_h \, l_a\} / [1 - d \, (1 - T_h^2)] \tag{2.7}$$

with the abbreviations

$$d = ½ - ½ (1 - t)/K_\mathrm{h} \tag{2.8}$$

and

$$T_\mathrm{h}^2 = \exp\{ - 2 K_\mathrm{h} l_\mathrm{a}\} \qquad . \tag{2.9}$$

In this case the extinction coefficient is

$$K_\mathrm{h} = [(1 - t)^2 - r^2]^{1/2} \qquad , \tag{2.10}$$

which for $r=t$ simplifies to

$$K_\mathrm{h} = (1 - 2r)^{1/2} \qquad . \tag{2.10a}$$

From the same differential equation system the canopy reflection ρ_h results as

$$\rho_\mathrm{h} = r (1 - T_\mathrm{h}^2) / [K_\mathrm{h} + 1 - t + (K_\mathrm{h} + 1 - t) T_\mathrm{h}^2] \qquad . \tag{2.11}$$

The index h of T_h, K_h and ρ_h stands for the horizontal foliage. For $(K_\mathrm{h} l_\mathrm{a}) \geq 1.5$ the canopy reflection (2.11) simplifies to

$$\rho_\mathrm{hl} = (1 - t - K_\mathrm{h})/r = r/(1 - t + K_\mathrm{h}) \qquad . \tag{2.11a}$$

On the other hand, a solution can be given for black leaves ($t=r=0$) with inclinations λ that are again randomly distributed over the horizontal plane and, moreover, randomly distributed over the azimuths. For this case of black leaves Anderson (1966) gave the extinction coefficient

$$K_\mathrm{b}(\beta) = P'(\beta)/\sin\beta \qquad , \tag{2.12}$$

where β is the angle between the penetrating beam of radiation and the horizontal plane, and $P'(\beta)$ is the average leaf projection into a plane vertical to the angle of incidence. For a continuous leaf inclination distribution $F(\lambda)$ with

$\int F(\lambda)\, d\lambda = 1$

the average projection $P'(\beta)$ is

$$P'(\beta) = \int F(\lambda)\, P(\beta,\lambda)\, d\lambda \qquad . \tag{2.13}$$

Here, the quantity

$$P(\beta,\lambda) = \int |\sin \Theta|\, d\alpha\, /(2\pi) \tag{2.14}$$

is the projection for the leaf inclination λ averaged over the azimuths α, where Θ is the angle of incidence between the beam of radiation (β) and the leaf element (λ,α). The integration results in the expression

$$P(\beta,\lambda) = \begin{cases} |\sin\beta|\, \cos\lambda & \text{for } 0 \le \lambda \le |\beta| \\[2mm] 2/\pi \left\{ Y \sin\beta\, \cos\lambda + (\sin^2\lambda - \sin^2\beta)^{1/2} \right\} & \text{for } 0 \le |\beta| \le \lambda \end{cases} \tag{2.13a}$$

with the abbreviation

$$Y = \arcsin(\, \tan\beta\, /\, \tan\lambda\,) \qquad . \tag{2.13b}$$

For reasons of practicability, discrete inclination distributions $F(\lambda_i)$ with nine classes of inclination and $\Sigma_i\,F(\lambda_i)=1$ are used in the following, and the integral in (2.13) is replaced by summation. Three inclination distributions are given as examples in Tab. 2.2 and Fig. 2.1. The spherical distribution is equivalent to the surface distribution of a sphere, and thus has the same projection for all angles of incidence. For this reason spherical distribution is frequently used in models of radiation transfer (e.g. Goudriaan,
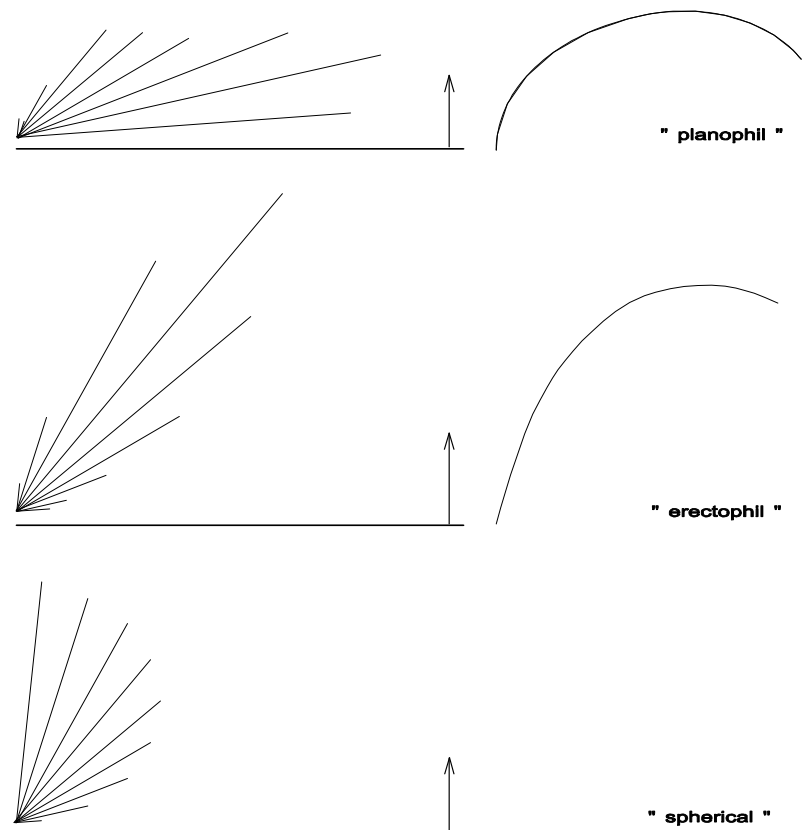
Fig. 2.1   The inclination distributions (in polar coordinates) and the corresponding leaf shapes

1977). However, it can be seen in Fig. 2.1, that this distribution represents only extremely upright plant elements. In contrast, typical distributions $F(\lambda)$ have been empirically evaluated from two typical leaves of maize. They are denoted as "planophil" and "erectophil", and illustrated in Fig. 2.1 in a projection to a vertical plane.

Table 2.2   The inclinations distributions and corresponding leaf shapes

angle of inclination λ (°)		0-10	10-20	20-30	30-40	40-50	50-60	60-70	70-80	80-90
class i		1	2	3	4	5	6	7	8	9
"planophil"	$F(\lambda_i)$	0.202	0.228	0.179	0.125	0.105	0.093	0.041	0.013	0.014
"erectophil"	$F(\lambda_i)$	0.020	0.030	0.060	0.120	0.200	0.280	0.200	0.070	0.020
spherical $F(\lambda_i)$		0.015	0.045	0.074	0.099	0.124	0.143	0.158	0.168	0.174

For horizontal black leaf elements the solution (2.7) reduces to

$$T_b = \exp\{-K_{hb}\,l_a\} \tag{2.15}$$

with $K_{hb}=1$.

The extinction coefficient $K_h(r,t)$ (2.10) for horizontal leaves with optical properties (t,r) together with $K_b(\beta)$ (2.12) for black leaves with inclination distribution $F(\lambda_i)$ represent the most important canopy properties which influence the transmission. For this reason the simple exponential expression (2.15) was used by Goudriaan (1977) with a generalized extinction coefficient

$$K_m = a\, K_h\, K_b + c \qquad , \qquad\qquad\qquad\qquad\qquad (2.16)$$

where the constants a and c have been determined by a regression of (2.15) to the results of Goudriaan's SOSA model.

With the irradiances $B(\beta_i)$ for the standard overcast sky (Tab. 2.1) the foliage transmission for diffuse radiation is determined from

$$T_d = \Sigma_i\, B(\beta_i)\, \exp\{ -K_h\, K_b\, l_a \} \qquad . \qquad\qquad\qquad\qquad (2.17)$$

However, that method has some essential shortfalls and fails in some common situations:

-        The transmission and reflection coefficients of the leaves are assumed to be identical.

-        Stems are ignored.

Moreover, the SOSA model of Goudriaan (1977) works with some simplifying assumptions, e.g., the radiant emittances scattered by the leaves are assumed to be distributed like the radiance of a horizontal Lambertian emitter.

For the reflected portion of the incident radiation Goudriaan (1977, p. 30) gave the expression

$$\rho'_d = \Sigma_i\, B(\beta_i)\, (1 - \exp\{ - 2\, \rho_h\, K_b(\beta_i)/[\, 1 + K_b(\beta_i)\,] \}) . \qquad\qquad (2.18)$$

This expression does not hold for low l_a, moreover, it ignores stems.

For these reasons the attempt was made to generalize the solution (2.7, 2.11) given by Cowan (1968, 1971) for horizontal elements, allowing all optical properties and leaf inclinations. However, the generalization of the differential equation system (2.6) would result in integro-differential equations which cannot be resolved analytically. Moreover, the attempt failed to find acceptable estimates of the transmitted and reflected portions including the special cases of the horizontal and the black foliage.

2.3   The determination of the reflected and transmitted portions in the model AMBETI

Instead of a real generalization, another estimate has been developed, improving on the one discussed in Section 2.2 in several regards:

-        The transmission coefficient of the leaves may differ from the reflection coefficient.

-        Stems can be considered with independent optical properties (transmission coefficient$\equiv 0$, reflection coefficient r_s).

-        The canopy reflection also is valid for small crop densities.

The resulting formulae have been determined with the help of the relations presented in Section 2.2 and additional empiric relations which have been drawn from comparisons with results of the SOSA model (see Appendix A2.1). The transmission of diffuse radiation is determined as the sum over the nine classes (i) of incident radiation considered (see Tab. 2.1)

$$T_d = \Sigma_i \, B(\beta_i) \, \exp\{ \, - K_{ml,i} \, l_a/F_{li} - K_{ms,i} \, s_a/F_{si} \, \} \qquad\qquad , \qquad\qquad\qquad (2.19)$$

where the two terms in the exponential function correspond to leaves and stems. The expression is evaluated separately with the individual optical properties (t, r and r_s) for the three spectral ranges distinguished. The coefficient $K_{ml,i}$ is determined similar to (2.16) as

$$K_{ml,i} = b_0 + b_1 \, K_{bl}(\beta_i) \, K_h(t,r) \qquad\qquad , \qquad\qquad\qquad (2.20a)$$

with the coefficient (2.10) for horizontal **leaves** and the transmission and reflection coefficients for the corresponding spectral range t and r. The coefficient $K_{bl}(\beta_i)$ is the extinction coefficient for <u>b</u>lack <u>l</u>eaves (2.12). The coefficients b_0 and b_1 (see Tab. 2.3) have been determined from comparisons with the results of the SOSA model (Braden, 1982), explained in Appendix A2.1.

Table 2.3   The coefficients used in the equations of section 2.3

b_0	b_1	b_{s0}	b_{s1}	f_c
0.0917	0.8961	0.01264	0.84329	1.21

From these comparisons the correction term

$$F_{li} = 1 - f_c \, T'_{li} \, \rho^{*}_{li}{}^{2} \qquad\qquad\qquad\qquad\qquad\qquad (2.21a)$$

with the abbreviation

$$T'_{li} = \exp\{-K_{ml,i}\, l_a\} \qquad . \tag{2.22a}$$

also has been found to be suitable. The quantity

$$\rho^{*}_{li} = 1 - \exp\{ - \rho_{hl}\, c\, K_{bl}(\beta_i)\, /[\pi^{-1} + K_{bl}(\beta_i)] \} \tag{2.23a}$$

with the abbreviation

$$c = [\, 2 + t - K_h(t,r)\,]^{1/2} / [t + K_h(t,r)]$$

is a modification of the "limiting reflection" (2.18) proposed by Goudriaan (1977, p. 30) with ρ_{hl} according to (2.11a).

In general the reflection of the leaves is determined from the sum of the nine classes of incident radiation

$$\rho_l = \Sigma_i\, B(\beta_i)\, \rho_{li} \tag{2.24a}$$

with

$$\rho_{li} = \rho^{*}_{li}\, [\, 1 - \exp(- 2\, K_{ml,i}\, l_a)\,] \qquad . \tag{2.25a}$$

The transmission (2.19) and reflection of **stems** are calculated similarly to equations (2.20a) to (2.25a) with the following modifications. The stem area index for cylindric stems is defined as

$$s_a = (\pi/2)\, n_s\, d_s\, z_s \tag{2.26}$$

with the number of stems per square meter n_s, the stem diameter d_s and the height of the stems z_s, and the extinction coefficient (2.12, 2.14) for black stems $K_{bs}(\beta)$ is

$$K_{bs}(\beta_i) = (2/\pi)\, \cot\beta_i \qquad . \tag{2.27}$$

Since the transmission of stems is zero, the effect of the stem reflectivity r_s is considered with

$$K_{os} = (1 - r_s^2)^{1/2} \tag{2.28}$$

according to (2.10), where the index stands for 'optical properties of stems'. Similar to (2.20a) the coefficient $K_{ms,i}$ is determined from

$$K_{ms,i} = b_{s0} + b_{s1} \, K_{bs}(\beta_i) \, K_{os} \qquad , \tag{2.20b}$$

where the coefficients b_{s0} and b_{s1} (see Tab. 2.3), once again, result from the comparison with the SOSA model of Braden (1982), see Appendix A2.1. The correction term F_{si} in (2.19) is determined similar to (2.21a)

$$F_{si} = 1 - f_c \, T'_{si} \, \rho^{*}_{si}{}^2 \tag{2.21b}$$

with the abbreviation

$$T'_{si} = \exp\{-K_{ms,i} \, s_a\} \qquad . \tag{2.22b}$$

The "limiting reflection" for stem canopies

$$\rho^{*}_{si} = 1 - \exp\{ -\rho_{os} \, K_{bs}(\beta_i)/[\pi/4 + K_{bs}(\beta_i)] \} \qquad . \tag{2.23b}$$

Here the quantity

$$\rho_{os} = r_s (2 - K_{os})^{1/2} / [(1 + K_{os}) \, K_{os}] \tag{2.11b}$$

is an empirical modification of (2.11a) representing the reflection of the stems.
Like in (2.24a), the reflection of a stem canopy is calculated from

$$\rho_s = \Sigma_i \, B(\beta_i) \, \rho_{si} \tag{2.24b}$$

with the abbreviation

$$\rho_{si} = \rho^{*}_{si} / [\ 1 + \exp\{-(2/\pi)\ K_{ms,i}\}/s_a\ ] \qquad . \qquad (2.25b)$$

In contrast to the simple expression (2.19) for the transmission of stems and leaves, the combined reflectance ρ_c has been elaborated - generalizing the individual reflectances of the leaf and stem canopies (2.25a,b) and comparing with the results of the SOSA model - to the following formula:

$$\rho_c = \Sigma_i\ B(\beta_i)\ \{\ \rho_{li}/[\ 1 + \exp(-T'_{si})\ (2 - K_{os} - T'_{li})\ K_{os}\ (1 + K_{ol})]$$
$$+\ \rho_{si}/[\ 1 + \exp(-T'_{li})\ (2 - K_{ol} - T'_{si})\ K_{ol}\ (1 + K_{os})]\ \}. \qquad (2.29)$$

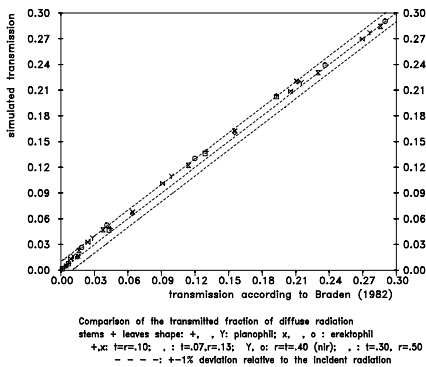Here T'_{li} and T'_{si} are the abbreviations of (2.22a,b).

Fig. 2.2 Transmitted portions of diffuse radiation for different optical properties, densities p_a and leaf shapes (see text)

Some typical comparisons of simulated results using (2.19) and (2.29), with results obtained by the SOSA model (Braden, 1982) (see Appendix A2.1) are presented in Figures 2.2 and 2.3. The dashed

curves indicate a deviation of the simulated radiation fluxes of ±1% relative to the incident radiation. The corresponding transmitted and reflected portions are given for a variety of different optical properties, i.e. two leaf shapes (see Tab. 2.4) and five plant densities ($p_a=l_a+s_a$=1.2, 2.4, 5.0, 8.7, 10.7). These canopies consists of leaves (with l_a= 0.5, 1.0, 2.0, 4.0, 6.0) and 600 stems/m^2 with diameters and heights as listed in Tab. 2.6. The results for the different plant densities are designed with identical symbols if the other properties are the same (see Tab. 2.4). In all cases a good agreement is achieved with deviations less than about 1% of the incident radiation for the transmitted radiation and up to 3% for the reflected near infra-red radiation.

For stems without leaves as well as for leaves without stems the agreement is remarkably better, with deviations usually less than 1% of the incident radiation.

Table 2.4   The optical properties and leaf inclination distributions used in Figs. 2.2 and 2.3

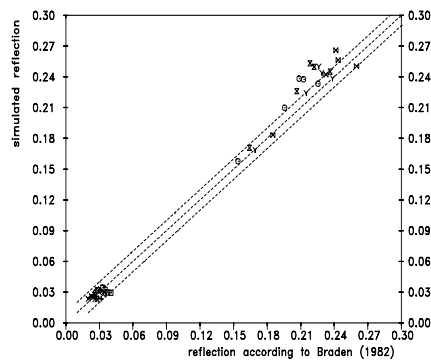| "leaf shape": optical properties	"erectophil"	"planophil"
t=0.10, r=0.10; r_s=0.10	x	+
t=0.07, r=0.13; r_s=0.13	◊	□
t=0.40, r=0.40; r_s=0.60	⊙	Y
t=0.30; r=0.50; r_s=0.60	_	⧗

Fig. 2.3   Reflected portions of diffuse radiation for different optical properties, densities p_a and leaf shapes (see text)

2.4   The treatment of direct radiation

 To calculate the transmitted and reflected portions of the incident direct (solar) radiation, the equations of Section 2.3 are evaluated in a similar manner without summations in (2.19) and (2.24a) and (2.24b). For leaves combined with stems the reflected portion $\rho_\text{ß}$ of the direct component from β is calculated similarly to (2.29) but without summation. For $K_\text{bl}(\beta)$ and $K_\text{bs}(\beta)$ instead of β_i , the angle of incidence β is used in the Equations (2.20) and (2.17). From the resulting transmitted portion $T_\text{ß}$ the corresponding extinction coefficient $K_\text{ß}$ is determined by

$$K_\text{ß} = -\ln(T_\text{ß}) / (l_\text{a} + s_\text{a}) \qquad . \tag{2.30}$$

However, this is only the first step for the transmission, since the resulting extinction coefficient will generally not remain constant during the transmission through the canopy. For example, a direct beam of radiation from a small angle of incidence will be scattered strongly into different directions at the top of the canopy. Below the top of the canopy the resulting downward distribution of the radiances changes towards a diffuse distribution. Therefore, the further extinction will be similar to that of diffuse radiation as determined with (2.19). The corresponding extinction coefficient K_d for the diffuse radiation is obtained from

$$K_\text{d} = -\ln(T_\text{d}) / (l_\text{a} + s_\text{a}) \qquad . \tag{2.31}$$

In the model this effect is considered in the following manner:
The effective extinction exponent E is calculated from the integral over the profile of the extinction coefficient $K(L)$

$$E = \int K(L) \, dL \qquad . \tag{2.32}$$

The integration is carried out with the cumulative plant area index L from zero at the top of the canopy to $L=l_a+s_a$ just above the soil surface. The extinction coefficient is allowed to vary from K_β to K_d (see Fig. 2.4).

Fig. 2.4   The extinction coefficient for direct radiation (small angle of inclination)

The transition point L_a of the $K(L)$ profile is determined with the prerequisite that the remaining direct portion $d(L_a)$ of the irradiance is reduced to a certain ratio a of the scattered portion $s(L_a)$ of the irradiance, i.e.

$$d(L_a) = a\, s(L_a) \qquad .(2.33a)$$

Similar at L_b the remaining direct irradiance $d(L_b)$ is further reduced to the portion $b<a$ of the scattered irradiance $s(L_b)$, i.e.

$$d(L_b) = b\, s(L_b) \qquad .(2.33b)$$

For the determination of L_a and L_b the direct portion of the irradiance is estimated as

$$d(L) = \exp(-K_b'\, L) \qquad\qquad (2.34)$$

with the weighted mean extinction coefficient of (2.12) and (2.27) for black plant elements

$$K_b' = [\, K_{bl}(\beta)\, l_a + K_{bs}(\beta)\, s_a\,]/(l_a + s_a) \qquad\qquad . \qquad (2.35)$$

The scattered portion s of the irradiance for $L \leq L_a$ is estimated as the difference of the remaining total and direct portions
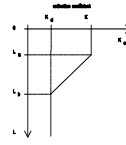
$$s(L) = \exp(-K_\text{ß}\, L) - d(L) \qquad .$$ (2.36)

From the demand (2.33a) the first transition point L_a results as

$$L_\text{a} = \ln(1 + 1/a)/(K_\text{b}' - K_\text{ß}) \qquad .$$ (2.37)

At the second transition point L_b the scattered portion $s(L_\text{b})$ of the irradiance is estimated as

$$s(L_\text{b}) = \exp\{ -\!\!\int K(L)\, dL \} - d(L_\text{b}) \qquad ,$$ (2.38)

where the integration has to be carried out from $L=0$ to $L=L_\text{b}$. From (2.33b) the second transition point results as

$$L_\text{b} = [\ \ln(1 + 1/b) + L_\text{a}\,(K_\text{ß} - K_\text{d})/2\ ]/[\ K_\text{b}' - (K_\text{ß} - K_\text{d})\ ] \qquad .$$ (2.39)

With this profile of $K(L)$ the portion of the total irradiance $\tau_\text{ß}(L_0)$ at the bottom of the canopy is determined from

$$\tau_\text{ß} = \exp\{ -\!\!\int K(L)\, dL \}$$ (2.40)

with the integration in the boundaries $L=0$ to $L=l_\text{a}+s_\text{a}$. Since $K(L)$ has a simple shape (Fig. 2.4), the integration is carried out analytically.

From the comparison with the results of the SOSA model (see Appendix A2.1) the ratios a and b have been calibrated as listed in Tab. 2.5. In Figs. 2.5 to 2.13 the resulting transmitted and reflected portions of the direct radiation are presented for the angles of incidence $5° \leq \beta \leq 85°$ [*)]. The results of the SOSA model, which works only for discrete mean values of the ten degree-

Table 2.5   The coefficients a and b used for the calculation of the transmitted direct radiation

	a	b
leaves $t+r<0.5$	3.90	0.08
leaves $t+r\geq0.5$	3.70	0.05
stems $r_s<0.3$	3.10	0.05
stems $r_s\geq0.3$	3.30	0.07
plants:		
$[(t+r)\,l_a + r_s\,s_a]/p_a < 0.3$ 3.50	0.05	
$[(t+r)\,l_a + r_s\,s_a]/p_a < 0.3$ 4.60	0.04	

classes, are represented by the symbols. In each figure, the results of both methods are compared for canopies with different densities as described in the captions. The deviations between the results of both models are expressed in the comments as percent of the incident radiation flux (irradiance).

The results for leaf canopies with different densities of the leaf area index l_a are shown in Figs. 2.5, 2.6 and 2.7. The agreement for the transmitted visible radiation (Fig. 2.5) is good with deviations of less than 1.5% of the incident radiation in all cases. For the transmission of near infra-red radiation (Fig. 2.6) the deviations are somewhat larger. But the deviations amount up to 5% only for radiation incident from small angles ($\beta \leq 5°$) on small leaf densities. In the other cases the deviations of the transmitted near infra-red radiation do not exceed 2% of the incident radiation.

Also, for the reflection, the agreement is generally good with deviations of less than 1.5% of the incident radiation, except for radiation from angles $\beta=5°$, where deviations of about 3% occur. However, these small angles of incidence are less important, since they usually occur with only small amounts of the incident radiation during sunrise and sunset. The results for the "erectophil" distribution of the leaf inclinations are similar.

[*)]   The simulations with the method presented in this section have been carried out for $\beta=5°$, $10°$, $15°$, $20°$, $25°$, $35°$, $45°$, $55°$, $65°$, $75°$, $85°$. The intermediate values in the plots have been interpolated with third order polynoms.
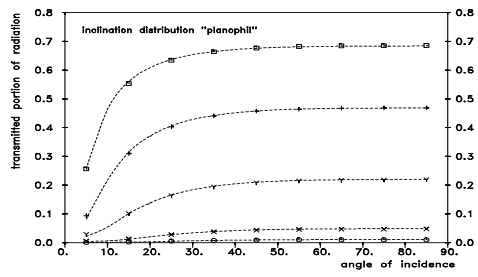
Fig. 2.5   Transmitted portions of direct visible radiation for leaves (t=0.10, r=0.15) with l_a=0.50 (□), 1.00 (+), 2.00 (Y), 4.00 (x), 6.00 (⊙)
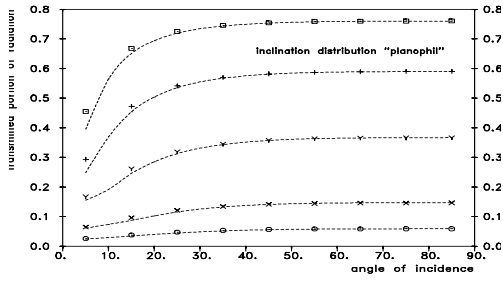
Fig. 2.6   Transmitted portions of direct near infra-red radiation for leaves (t=0.30, r=0.50) with l_a=0.50 ($\Box$), 1.00 (+), 2.00 (Y), 4.00 (x), 6.00 ($\odot$)
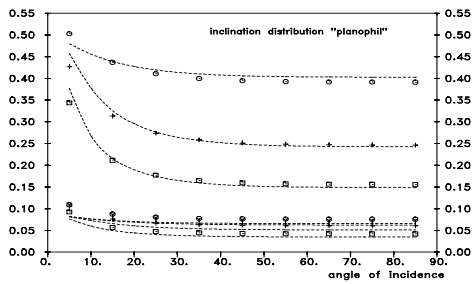
Fig. 2.7   Reflected portions of direct visible and near infra-red radiation for leaves (t=0.10, r=0.15; t=0.30, r=0.50) with l_a=0.50 ($\Box$), 1.00 (+), 2.00 (Y), 6.00 ($\odot$)

Fig. 2.8   Transmitted portions of direct visible radiation for stems (r_s=0.15) with s_a=0.39 ($\square$), 0.79 (+), 1.57 (Y), 3.14 (x), 4.71 ($\odot$)

Fig. 2.9   Transmitted portions of direct near infra-red radiation for stems (r_s=0.50) with s_a=0.39 ($\square$), 0.79 (+), 1.57 (Y), 3.14 (x), 4.71 ($\odot$)
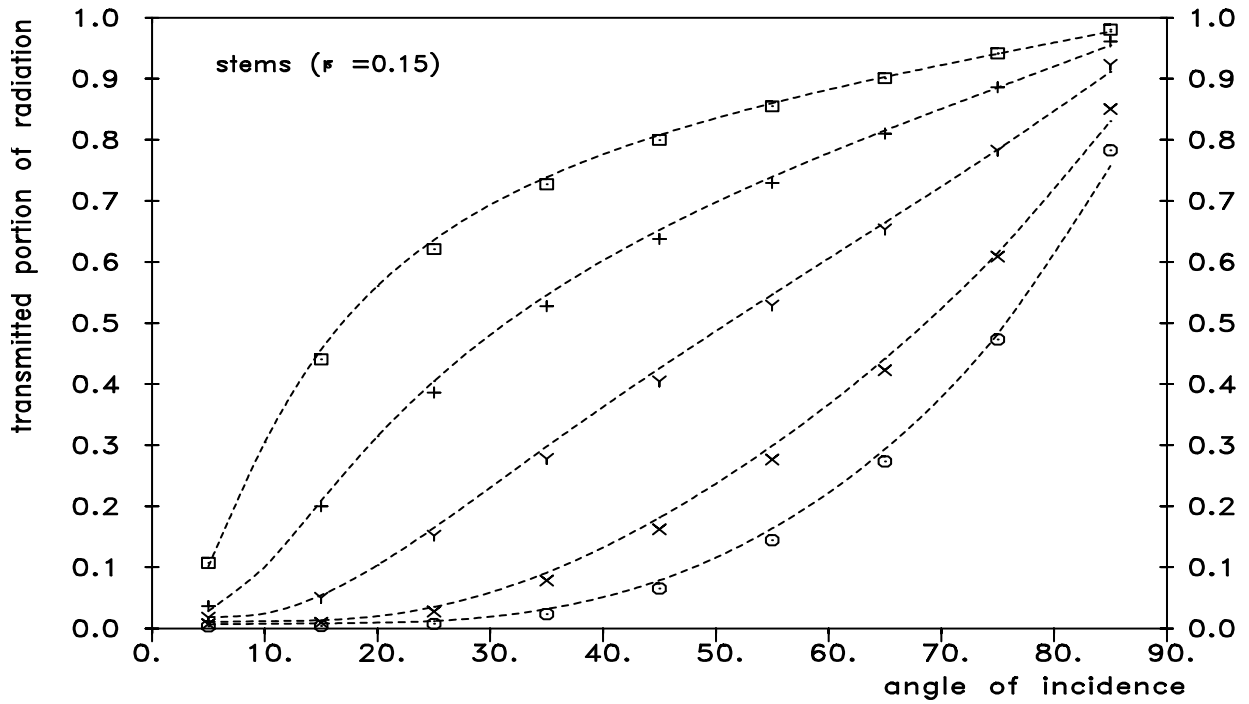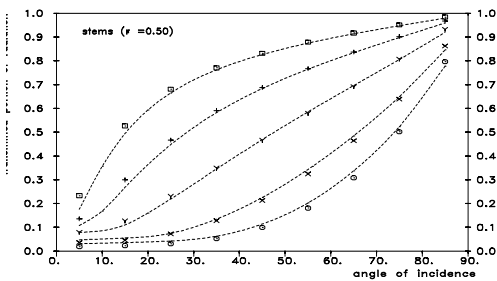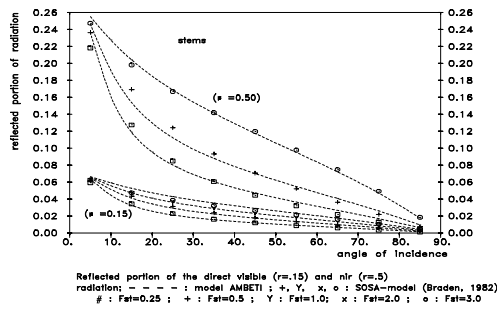
Fig. 2.10   Reflected portions of direct visible and near infra-red radiation for stems (r_s=0.15, 0.50) with s_a=0.39 (□), 0.79 (+), 1.57 (Y), 4.71 (⊙)

The results for stem canopies with five different densities s_a are presented in Figs. 2.8, 2.9 and 2.10. For the transmission of visible radiation (Fig. 2.8) good agreement is obtained for each stem density and angle of incidence. The deviations do not exceed 1% of the incident radiation. For the transmission of the near infra-red radiation (Fig. 2.9) the agreement is somewhat poorer, with deviations mostly of less than 1.5% of the incident radiation. Only for radiation from angles $\beta \leq 15°$ on small stem densities deviations of up to 5% are reached.

The reflectances of stem canopies are presented in Fig. 2.10 for two different reflection coefficients r_s=0.15 (lower part) and r_s=0.50 (upper part). Obviously good agreements were achieved for each case.

The results for plants consisting of leaves and stems are presented in Figs. 2.11, 2.12 and 2.13. The plants have been combined from n_s=600 stems/m^2 and leaves with "planophil" inclination distribution. The combination of

Table 2.6   The combinations of leaf densities and stem geometries used for Figs. 2.11, 2.12 and 2.13

symbol	□	+	Y	x	⊙
l_a	0.50	1.00	2.00	4.00	6.00
d_s (m)	0.003	0.003	0.004	0.005	0.005
z_s (m)	0.25	0.50	0.80	1.00	1.00
s_a	0.71	1.41	3.02	4.71	4.71
p_a	1.2	2.4	5.0	8.7	10.7

leaves (leaf area index l_a) and stems used for the different curves are listed in Tab. 2.6. The plant area

density p_a is the sum of l_a and the stem area index s_a, which results from the stem density n_s, the stem diameter d_s and the length of the stems z_s according to (2.26).

In general the results for plants combined of stems and leaves are not as good as those for only leaves or only stems, except for the transmission of visible radiation, where good agreements are attained (see Fig. 2.11). For near infra-red radiation (Fig. 2.12), deviations of up to 5% appear for small angles of incidence, as well as for high plant densities. The reflected portions of visible and near infra-red radiation are presented in the lower and upper parts of Fig. 2.13. The deviations account for up to about 2% of the incident radiation for near infra-red radiation and ≤1.5% in the visible range.
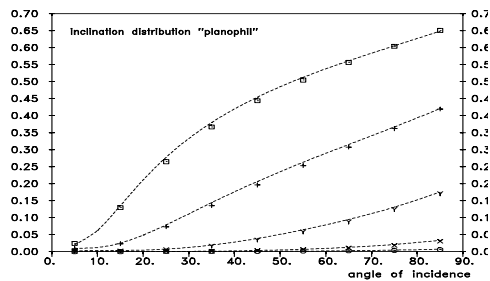
Fig. 2.11   Transmitted portions of direct visible radiation for plants (t=0.10, r=r_s=0.15) with
                      p_a=1.21 (□), 2.41 (+), 5.02 (Y), 8.71 (x), 10.71 (⊙)

The remaining deviations between the radiation fluxes calculated with the presented method and the SOSA model taken as reference (see Appendix A2.1) could probably be diminished with a more thorough fit of the model. However, it should be kept in mind that the larger deviations appear only for the direct near infra-red components of the radiation that account

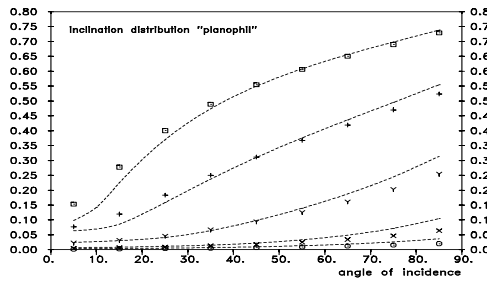**Fig. 2.12**   Transmitted portions of direct near infra-red radiation for plants (t=0.30, r=0.50, r_s=0.60) with p_a=1.21 (□), 2.41 (+), 5.02 (Y), 8.71 (x), 10.71 (☉)
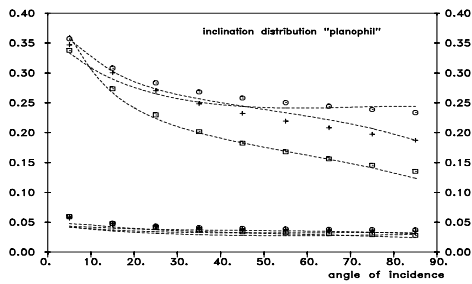

Fig. 2.13   Reflected portions of direct visible (t=0.07, r=r_s=0.13) and near infra-red (t=0.30, r=0.50, r_s=0.60) radiation for different plant densities (see text)

for less than 50% of the total global radiation. Moreover, most of the stronger deviations occur for small angles of incidence, which usually appear only during sunrise and sunset with small fluxes of direct radiation.

Consequently, the presented method acceptably estimates the radiation transmitted through and reflected by plant stands for arbitrary values of

-        the transmission and reflection coefficients of the leaves and the stems,

-        angles of incidence β,

-        canopy densities and structures as well as

-        different distributions of leaf inclinations.

These capabilities of the presented radiation model, together with its low amount of computing time required are good precautions for its use in models like AMBETI.

2.5   The optical properties of the ground surface (soil or snow surface)

In the foregoing treatment the reflectance at the ground surface was not taken into account. Before the calculation of the net radiation fluxes is described in Section 2.6, the determination of the optical properties of the ground surface will be explained. These optical properties are distinguished in the visible ($\lambda_w < 0.72$ µm), the near infra-red ($0.72 \leq \lambda_w \leq 3.0$ µm) and the infra-red (thermal) ($\lambda_w > 3$ µm) spectral ranges. For the direct radiation in the case of bare soil only hemispherical reflection coefficients are considered. In each spectral range, the type of the ground surface, soil or snow, is considered.

The reflectance r_{sd} of dry **soils** have to be given as input parameters for the visible and near infra-red ranges (see Section 6.1). From these, the corresponding wet soil reflectances r_{sw} are determined with a semi-empirical relation of Ångström (1925)

$$r_{sw} = r_{sd}/[\, n^2\,(1 - r_{sd}) + r_{sd}\,] \qquad\qquad , \qquad\qquad\qquad\qquad\qquad (2.41)$$

where the refraction index n of water takes the values 1.33 in the visible and 1.32 in the near infra-red range. Between the two extremes the reflectances are varied with the water content w_1 of the uppermost layer by an empirical relation according to Graser and van Bavel (1982)

$$r_{soil} = (r_{sd} + r_{sw})/2 + 0.75\,(w_1 - 0.13) \qquad\qquad . \qquad\qquad\qquad\qquad (2.42)$$

Relation (2.41) has been validated with reflectances measured for different plots of soil. Fig. 2.14 shows the measured reflectances for sand (+), loam (x), loamy sand (☉) and sandy loam (Y) together with the simulated relations (----) according to (2.41) and (2.42). The agreement for the considered soil types seems to be acceptable.
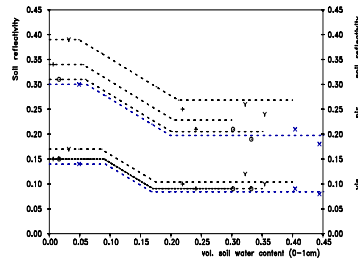
Fig. 2.14   Measured and simulated soil reflectances for visible and near infra-red radiation of different types of soil (see text)

According to van Bavel and Hillel (1976) the emissivity of the soil surface ε_{soil} is varied between the values 0.98 and 0.90 for wet and dry soil surfaces, by

$$\varepsilon_{soil} = 0.90 + 0.18\ w_1 \qquad \text{for } 0 \leq w_1 \leq 0.44 \qquad . \qquad (2.43)$$

The reflectances for fresh **snow** covers are taken as $\rho_{sn0}=0.95$ in the visible and $\rho_{sn0}=0.65$ in the near infra-red range. For older snow covers, the snow is allowed to compact and the snow density, w_{sn}/d_{sn}, to increase (see Section 3.6). With the increase of w_{sn}/d_{sn} from 100 kg m^{-3} for fresh snow to 500 kg m^{-3} for old snow the reflectances are linearly decreased to $\rho_{sn0}=0.75$ for the visible and $\rho_{sn0}=0.33$ for the near infra-red range. For direct radiation from small angles of incidence h_s the reflection is augmented as used by Dickinson et al. (1986)

$$\rho_{snow}(h_s) = \rho_{sn0} + 0.4\ (\ 1 - \rho_{sn0}\ )\ f(h_s) \qquad . \qquad (2.44)$$

The function $f(h_s)$ is zero for $h_s \geq 30°$ and else increases up to unity for $h_s=0°$ according to

$$f(h_s) = [\ (a+1)/(1 + 2\ a\ \sin(h_s)) - 1\ ]/a \qquad (2.44a)$$

with a=2. Relation (2.44) is also used for the relectivities ε_{soil} of bare soil for small angles of incidence.

The emissivities are linearly decreased from the value $\varepsilon_{snow}=0.99$ for fresh snow to $\varepsilon_{snow}=0.82$ for old snow, according to Oke (1978, p. 15).

For thin snow covers, $d_{sn}<1mm$ of H_2O, the optical properties of the surface are linearly varied between the values for the snow cover and the values for the snow-free soil surface.

2.6   The calculation of the net short-wave radiation fluxes for the plants and the ground surface

In this section the calculation of the net short-wave radiant fluxes of the plants and the ground surface is described. In addition to the portions of the reflected and transmitted fluxes considered in Sections 2.3 and 2.4, the reflectances of the ground surface also are taken into account. The procedure as illustrated by Fig. 2.15 is carried out separately for the visible and near infra-red ranges:

From the incident radiant flux ("1") with its diffuse and possibly direct components (see Section 2.1), the portions reflected at the top of the canopy ("ρ_0" in Fig. 2.15) are first calculated according to (2.29). The portions transmitting the plant cover ("τ") are determined with (2.19) and (2.40) for the incident diffuse and direct components.
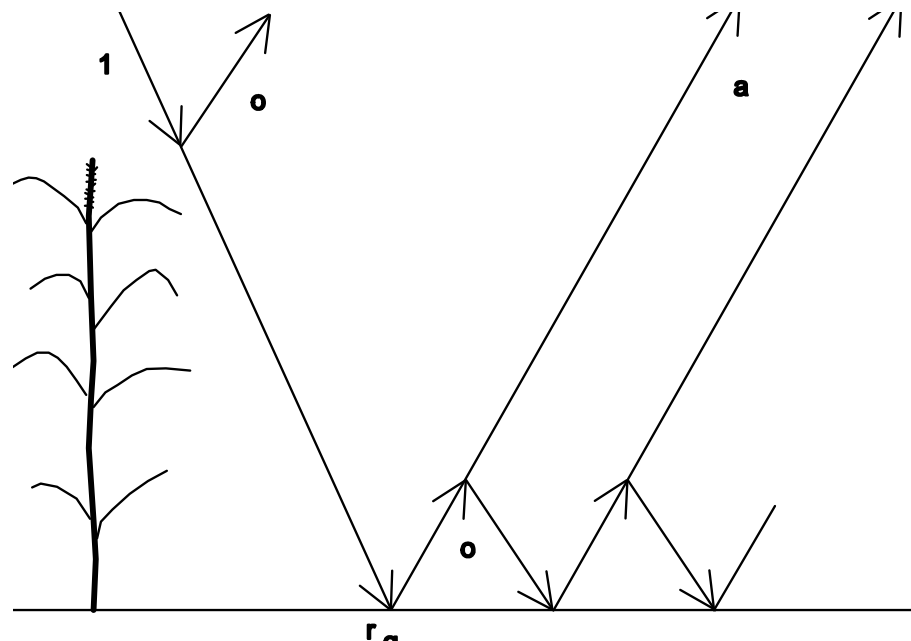
Fig. 2.15   The components of the net radiation fluxes

From then on, the remaining fluxes are assumed to be diffuse (see Section 2.4). At the ground surface partly diffuse reflection is considered with the reflection coefficient r_g, equal to the reflectance of the soil or snow according to Section 2.5. The remaining upward reflected portion is allowed to be partly reflected at the bottom side of the plant cover and partly transmitted through the canopy. In

consequence of the reflections at the bottom of the plant cover and at the ground surface, the remaining portions are repeatedly reflected. The resulting effects can be expressed by geometrical series in the relations for the additionally reflected radiant fluxes ("ρ_a"), as well as in the relations for the fluxes absorbed by the plants and absorbed by the ground surface.

For reflection at the bottom of the plant cover, as well as for the transmission directed upward, the relations for the diffuse reflection ρ_d and transmission T_d, (2.29) and (2.19), are used. Therefore the geometrical series all include the term $1/(1-r_g \rho_d)$, which remarkably deviates from unity only for near infra-red radiation. For the direct component of the incident radiation the total portion reflected by the canopy is

$$\rho_{t\text{ß}} = \rho_\text{ß} + \tau_\text{ß} \, r_g \, (1 - \rho_d) \, T_d \, /(1 - r_g \, \rho_d) \tag{2.45}$$

with the direct and diffuse portions reflected at the top of the canopy, $\rho_\text{ß}$ and ρ_d, according to (2.29). The transmissivities for direct ($\tau_\text{ß}$) and diffuse (T_d) radiation are determined with (2.40) and (2.19). For the diffuse components of the incident radiation the total reflected portion ρ_{td} is calculated similar to (2.45) with $\rho_\text{ß}$ and $\tau_\text{ß}$ replaced by ρ_d and T_d, respectively:

$$\rho_{td} = \rho_d + T_d^2 \, r_g \, (1 - \rho_d)/(1 - r_g \, \rho_d) \qquad . \tag{2.46}$$

The portion of the incident direct radiation flux absorbed by the soil surface is

$$A_{s\text{ß}} = \tau_\text{ß} \, (1 - r_g)/(1 - r_g \, \rho_d) \qquad . \tag{2.47}$$

The portion of the direct radiation flux absorbed by the plants is given by

$$A_{p\text{ß}} = 1 - \rho_\text{ß} - \tau_\text{ß} + \tau_\text{ß} \, r_g \, (1 - \rho_d)(1 - T_d)/(1 - r_g \, \rho_d) \qquad . \tag{2.48}$$

Similar to the diffuse reflection, the absorbed portions A_{sd} and A_{pd} of the diffuse incident radiation are determined according to (2.47) and (2.48). With the direct (solar) and diffuse components of the visible radiances, $R_{s,vi}$ and $R_{d,vi}$, (see Section 2.1) the visible net radiation flux of the plants is determined as

$$R_{n\,vi,pl} = R_{s,vi} \, A_{p\text{ß}} + R_{d,vi} \, A_{pd} \qquad . \tag{2.49}$$

This visible net radiation flux controls the stomatal resistance according to Section 4.1. The visible net radiation flux of the ground surface is

$$R_{n\ vi,g} = R_{s,vi}\,A_{sß} + R_{d,vi}\,A_{sd} \qquad . \tag{2.50}$$

For the near infra-red range, the net radiation fluxes $R_{n\ ni,pl}$ and $R_{n\ ni,g}$ are determined in the same way with the corresponding optical properties used for ρ_d, $\rho_ß$, r_g, T_d and $\tau_ß$. The net short-wave radiation fluxes of the plants $R_{n\ s,pl}$ and the ground surface $R_{n\ s,g}$ are the sum of the corresponding net fluxes in the two short-wave ranges

$$R_{n\ s,pl} = R_{n\ vi,pl} + R_{n\ ni,pl} \tag{2.50a}$$

$$R_{n\ s,g} = R_{n\ vi,g} + R_{n\ ni,g} \qquad . \tag{2.50b}$$

2.7   The exchange of thermal radiation

With the emissivity of the ground cover ε_g equal to the emissivity of soil surface or of snow cover (see Section 2.5), and the emissivity $\varepsilon_{pl}=0.96$ of the plant elements, the absorbed portions of the incident long-wave radiation are determined the same way as described for the diffuse short-wave radiation. For the incident long-wave radiation, the inclination distribution of the standard overcast sky (see Tab. 2.1) is used. The reflection coefficients of the plant elements and the ground surface in the above equations have to be replaced by $1-\varepsilon_{pl}$ and $1-\varepsilon_g$, and the transmission coefficient is zero.

The transmitted and reflected portions T_{IR} and ρ_{IR} of the incident flux of long-wave radiation are calculated with (2.19) and (2.29). The portions absorbed by the plants and the ground surface are determined similar to (2.48) and (2.47), resulting in coefficients for the equations (3.5) and (3.2). The geometrical series can be omitted, since the corresponding term $1/[1-(1-\varepsilon_g)\,\rho_{IR}]$ is very close to unity. Thus, the coefficient in (3.2) for the absorption of the incident long-wave radiation by the plants results as

$$a_{plu} = [\ 1 - \rho_{IR} - T_{IR} + T_{IR}\ (1 - \varepsilon_g)(1 - \rho_{IR})(1 - T_{IR})\ ]/\varepsilon_{pl}. \tag{2.51}$$

The coefficient in (3.5) for the absorption of the ground surface is $a_{sas}=T_{IR}$.

The exchange of long-wave radiation, due to the "active" emission of the plant elements and the ground cover, is considered in the energy budget equation of the plants (3.2) with the coefficients ε_{pl} a_{plo} ε_g and ε_{pl} a_{ple} and in the budget equation for the ground surface (3.5) with ε_g a_{sap} ε_{pl} and ε_g a_{sae} . These coefficients are estimated from T_{IR} and ρ_{IR} : For the absorption of thermal radiation from the ground surface by the plants

$$a_{plo} = (1 - T_{IR})/\varepsilon_{pl} \qquad (2.52)$$

is used. The coefficient describing the upward and downward long-wave emission of the plants is

$$a_{ple} = (1 - T_{IR}) [2 - (1 - \varepsilon_g) \rho_{IR} (1 - T_{IR})] / \varepsilon_{pl} \qquad . \qquad (2.53)$$

In the net radiation balance of the ground surface the coefficients $a_{sap}=1-T_{IR}$ for the radiation emitted by the plants and

$$a_{sae} = 1 - \rho_{IR} (1 - \varepsilon_g) \qquad (2.54)$$

for the emission by the ground surface are used.

For the interpretation of <u>remotely sensed long-wave radiation</u> from crops in general the origin of the single components has to be considered. These are

-       parts of the incident long-wave radiation flux that are reflected by the plants and the ground surface according to (2.45) and (2.46),
-       radiation emitted by the plants and
-       radiation emitted by the ground surface.

For narrow spectral ranges, the Planck law results in strong deviations from the $\sigma\, T^{\,4}$-emission according to the Boltzmann law (see Widger and Wodall, 1976), which are not considered here. The hemispherical emission in broad spectral ranges can be derived with the above relations. For the detection of radiation emitted to an angle β, the single components can be derived according to the above equations for direct radiation with the corresponding transmissivities and reflectances. To a high degree of accuracy the long-wave radiant intensity detected with the inclination β from a canopy is proportional to

$$R_{e\beta} = \sigma\,T_a^{\,4} = [\ \rho_\beta + T_{IR}\,(1 - \varepsilon_g)(1 - \rho_\beta)\,\tau_\beta\ ]\,R_l$$

$$+\ [\ (1 - \tau_\beta) + (1 - T_{IR})(1 - \varepsilon_g)(1 - \rho_\beta)\,\tau_\beta\ ]\ \sigma\,T_{pl}^{\,4} \qquad\qquad (2.55)$$

$$+\ \varepsilon_g\,(1 - \rho_\beta)\,\tau_\beta\ \sigma\,T_{sa}^{\,4} \qquad\qquad .$$

Here T_a is the "apparent surface temperature" or equivalent black body temperature and ρ_β, ρ_{IR}, τ_β, and T_{IR} are the canopy reflections and transmissions for direct and diffuse radiation according to (2.29), (2.40) and (2.19) with the corresponding optical properties $t=0$, $r=r_s=1-\varepsilon_{pl}$. The above equation considers that for small plant densities the "visible" amount of the ground surface increases with the angle β. For example in a typical situation with the temperatures $T_{pl}=30$ °C, $T_{sa}=22$ °C and $R_l=250$ W m^{-2} the apparent surface temperature T_a varies between 28.3 °C for $\beta=15°$ and 24.6 °C for $\beta=65°$, which amounts to a difference of 3.7 K depending only on the angle of incidence.

For dense crops, the transmission can be neglected and the above equation simplifies to

$$R_e = \sigma\,T_a^{\,4} = \rho_{IR}\,R_l + (1 - T_{IR})\,\sigma\,T_{pl}^{\,4} \approx (1 - \varepsilon_{pl})\,R_l + \varepsilon_{pl}\,\sigma\,T_{pl}^{\,4}, \qquad\qquad (2.55a)$$

which is valid for hemispherical emission and can also be used for the radiant intensities detected from discrete angles of view.

The correction by (2.55a) still accounts for an apparent temperature T_a of about 1.5 K below the actual surface temperature for the above conditions with $\varepsilon_{pl}=0.96$. For crops with smaller ε_{pl} (Gates and Tantraporn, 1952) the deviations may be several degrees.

With the help of the remotely sensed control of the (apparent) surface temperatures, the results of models like AMBETI are allowed to be validated and adjusted in large scale applications as pointed out by Braden and Blanke (1993). Examples of apparent surface temperatures simulated with (2.55a) and measured are given in Section 6.3.

3   Energy budget and transport inside and above the canopy

This chapter deals with the heat budget equation for plants and for the soil surface; the arrangement of the resistances for the aerodynamic transport of sensible and latent heat inside the canopy, and the solution of the resulting equations in the model AMBETI. Since the model is one-dimensional, only the vertical turbulent components of the aerodynamic transports are considered. The heat budget and transport equations are solved for discrete time steps, Δt, which usually are chosen equal to the time step of the meteorological boundary conditions.

In order to allow for a simple notation, the aerodynamic transports are expressed in the form

flux density = - concentration difference /(aerodynamic resistance)

(see Thom, 1975, p. 65). This notation has been adapted from the Ohm's law in electricity and is commonly used in agrometeorological models (see e.g. Waggoner et al., 1969; Goudriaan, 1977). The aerodynamic resistance replaces the diffusivity K, (e.g. eddy diffusivity or molecular diffusivity), by the integral of the reciprocal diffusivity

$$r_a = \int K^{-1}\, dz \qquad .$$

The notation with the resistances offers the advantage that Kirchhoff's laws for the calculation of fluxes in networks can be used.

Two varieties of the model exist, differing in the arrangement of the transport resistances: in the older version, the aerodynamic transports of the plants and the soil surface are treated without an aerodynamic coupling inside the canopy (see Section 3.2). In the more sophisticated version, used for the calculation of microclimate, the aerodynamic transports are linked to each other inside the canopy (see Section 3.3). A few comments for the modifications recommended for wet leaves (from dew or intercepted precipitation) are offered in Section 3.4. The determination of the transport resistances is described in Section 3.5. Section 3.6 deals with the development and melting of the snow cover at the soil surface and its insulating effect.

3.1   The energy budget of the plants and the energy balance of the soil surface

In this section, only the basic form of the energy budget equations is presented. The determination of the additional flux densities and the solution of the equations are described afterwards. In the energy budget of the plants the fluxes of sensible heat H_{pl} and latent heat V_{pl} are regarded as well as the net radiation flux densities $R_{n\,pl}$ and the heat storage term

$$S = c_{pl}\,(\,T_{plo} - T_{pl}\,)/\Delta t \qquad . \tag{3.1}$$

For the specific heat capacity c_{pl} of the plant a value of $(4.18\,p_a)$ J K^{-1} m^{-2} is used with the plant area index p_a (see Chapter 2). This corresponds with the specific heat of water and the estimate of 100 g m^{-2} of plant area, which is reasonable for many crops. The plant temperatures T_{pl} and T_{plo} correspond to the actual and the previous time step, respectively. As described in Sections 2.6 and 2.7 the net radiation is expressed as

$$R_{n\,pl} = R_{n\,s,pl} + \varepsilon_{pl}\,(a_{plu}\,R_l + a_{plo}\,\varepsilon_g\,\sigma\,T_{sa}{}^4 - a_{ple}\,\sigma\,T_{pl}{}^4\,). \tag{3.2}$$

Here $R_{n\,s,pl}$ is the net short-wave balance of the plant elements, R_l is the incident long-wave radiation and T_{sa} the temperature of the soil surface or the temperature of the snow cover (see Section 3.6). The emissivities ε_{pl} and ε_g of the plants and the ground surface are described in Section 2.5. The determination of the coefficients a_{plu} for the absorption of the incident long-wave radiation, a_{plo} for the interception of thermal emission of the ground surface and a_{ple} for the thermal emission of the plants is explained in Section 2.7.

For the simplification of the solution $T_{pl}{}^4$ is linearized by

$$T_{pl}{}^4 = T_x{}^4 + 4\,T_x{}^3\,(T_{pl} - T_x) \qquad , \tag{3.2a}$$

where T_x is a suitable estimate like T_{plo} or the air temperature T_r at reference level.

When all signs of fluxes towards the plants are positive, the energy budget reads

$$R_{n\,pl} + H_{pl} + V_{pl} + S = 0 \qquad . \tag{3.3}$$

For soil, only the surface energy balance is regarded in this chapter. The heat and water budgets in the

soil layers are calculated from the surface conditions as described in Chapter 5.

With the vertical turbulent flux densities of sensible heat H_{sa} and latent heat V_{sa} at the soil surface, the net radiation flux density $R_{n\,sa}$ and the ground heat flux density G the energy balance is

$$R_{n\,sa} + H_{sa} + V_{sa} + G = 0 \qquad . \tag{3.4}$$

Again, all fluxes towards the soil surface are positive.

The latent heat flux density at the soil surface V_{sa} is regarded in this balance equation only in the cases of dew formation and when the soil water potentials of the uppermost soil layer $|\psi_1|$ are less than 10 J/kg (see Section 5.5), which is equivalent to a wet surface. Otherwise, the corresponding latent heat flux densities are regarded as sink terms in the calculation of the soil heat budgets (see Section 5.1), since the vapour is extracted from below the surface (see Section 5.6).

The net radiation at the ground surface is calculated with

$$R_{n\,sa} = R_{n\,s,g} + \varepsilon_g \, (a_{sas} \, R_l + a_{sap} \, \varepsilon_{pl} \, \sigma \, T_{pl}^{\,4} - a_{sae} \, \sigma \, T_{sa}^{\,4}). \tag{3.5}$$

The calculation of the short-wave component of the ground surface net radiation $R_{n\,s,g}$ and the coefficients a_{sas}, a_{sap} and a_{sac} for the exchange of long-wave radiation are described in Sections 2.6 and 2.7.

The expressions for the fluxes of sensible and latent heat and the solution of the equations are different for the two model versions.

3.2   The aerodynamic transports in the "no-microclimate" option

In the "no-microclimate" option, the vertical turbulent fluxes of sensible and latent heat from the soil surface on the one hand, and from the plants on the other hand, are calculated separately corresponding to Fig. 3.1 . The upright resistances r_a and r_{ac} stand for the vertical turbulent transports, the others for the laminar transports at the surfaces of the plants (r_{ap}) and the soil surface (r_{as}). The resistance r_a accounts for the transport between the reference height z_r and the level of the main energy exchange inside the canopy while r_{ac} accounts for the transport between that level and the ground surface.

Fig. 3.1 The architecture of the aerodynamic resistances for the sensible and latent heat fluxes in the "no-microclimate" option

With specific latent heat of vaporization λ, the density ρ, and the specific heat c_p of the air, the densities of the sensible and latent heat fluxes to the plant are

$$H_{pl} = \rho\, c_p\, (T_r - T_{pl})/(r_{ap} + r_a) \tag{3.6}$$

and

$$V_{pl} = \lambda_{pl}\, (\rho_r - \rho_{s,pl})/(r_{ap} + r_a + r_{pl}) \qquad . \tag{3.7}$$

Here, T_r and ρ_r are the temperature and humidity at reference level, and $\rho_{s,pl}$ is the saturation humidity at leaf temperature. The saturation humidity will be used either in the case of transpiration, for the formation of dew, and the evaporation of dew, or intercepted rainfall. However, in the case of transpiration, the saturation humidity holds only for the vacuoles of the plant stomata (e.g. Thom, 1975, p. 87). Therefore in this case, the bulk stomatal resistance $r_{pl}=r_{st}$ (see Section 4.1) occurs in the transport equation; in the other cases $r_{pl}=0$ is used.

For the purpose of a straightforward solution of the equations, the saturation humidity is linearized by

$$\rho_{s,pl} = \rho_s(T_{pl}) \approx \rho_s(T_x) + \Delta_\rho\, (T_{pl} - T_x) \qquad , \tag{3.7a}$$

where T_x again is a suitable estimate for T_{pl}; $\rho_s(T_x)$ is the saturation humidity at T_x, and Δ_ρ is the slope of the saturation humidity function.

The aerodynamic heat flux densities at the soil surface are described by

$$H_{sa} = \rho \, c_p \, (T_r - T_{sa})/(r_a + r_{ac} + r_{as}) \tag{3.8}$$

and

$$V_{sa} = \lambda_{sa} \, (\rho_r - \rho_{sa})/(r_a + r_{ac} + r_{as}) \qquad . \tag{3.9}$$

For the soil surface temperature T_{sa} , the value calculated in the soil thermal section during the preceding time step is used for simplicity. The calculation of soil evaporation is described in detail in Section 5.6 .

The total vertical turbulent flux densities of sensible and latent heat are

$$H_{ca} = H_{pl} + H_{sa} \tag{3.10}$$

and

$$V_{ca} = V_{pl} + V_{sa} \qquad . \tag{3.11}$$

The flux densities of sensible and latent heat at the plants, H_{pl} and V_{pl} , and the plant temperature, T_{pl} , are calculated from Equations (3.1) to (3.7) as derived in Appendix A3.1.

3.3   The aerodynamic transports in the "microclimate" option

The arrangement of the resistances and aerodynamic fluxes used in this option are presented in Fig. 3.2. With the air temperature, T_{ca} , and humidity, ρ_{ca} , inside the canopy the transport equations for the aerodynamic heat flux densities at the plant are

$$H_{pl} = \rho \, c_p \, (T_{ca} - T_{pl})/r_{ap} \tag{3.12}$$

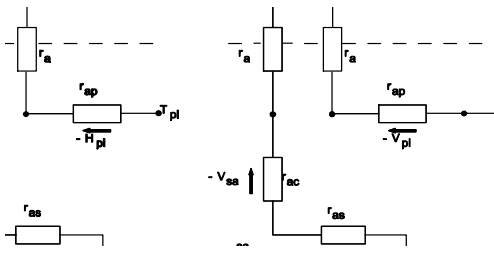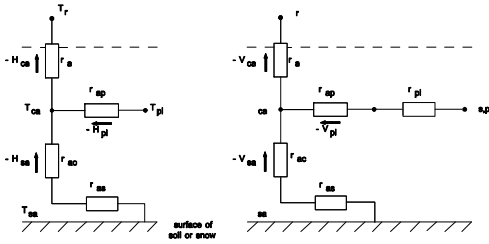**Fig. 3.2** The architecture of the aerodynamic resistances for the sensible and latent heat fluxes used in the "microclimate-option"

and

$$V_{pl} = \lambda_{pl}\,(\rho_{ca} - \rho_{s,pl})/(r_{ap} + r_{pl}) \qquad . \qquad (3.13)$$

The meaning of r_{pl} and the linearization of $\rho_{s,pl}$ is the same as described for Equation (3.7).
The aerodynamic heat fluxes at the soil surface are described by

$$H_{sa} = \rho\,c_p\,(T_{ca} - T_{sa})/(r_{ac}+r_{as}) \qquad\qquad (3.14)$$

and

$$V_{sa} = \lambda_{sa}\,(\rho_{ca} - \rho_{sa})/(r_{ac}+r_{as}) \qquad . \qquad (3.15)$$

For the soil surface temperature, T_{sa}, the remarks to (3.9) hold. The calculation of soil evaporation is described in Chapter 5.6 .
As can be seen from Fig. 3.2, the aerodynamical flux densities of the soil surface and the plants result in vertical turbulent flux densities for the whole canopy of sensible heat

$$H_{ca} = H_{pl} + H_{sa} = \rho\,c_p\,(T_r - T_{ca})/r_a \qquad\qquad (3.16)$$

and of latent heat

$$V_{ca} = V_{pl} + V_{sa} = \lambda \, (\rho_r - \rho_{ca})/r_a \qquad . \tag{3.17}$$

A simplification for the solution of the Equations 3.1 to 3.3, and 3.12 to 3.17, results from the division of the solution for one time step into two steps:

- At first, the fluxes and the temperature of the plants (H_{pl}, V_{pl} and T_{pl}), as well as the canopy climate T_{ca} and ρ_{ca}, are determined with the fluxes at the soil surface assumed to be known (taken from the last time step).

- Afterwards the calculations for the soil surface are carried out with the values for the temperature and humidity inside the canopy (T_{ca} and ρ_{ca}), just calculated.

This simplification will cause only minor errors, because

- the influence of the soil surface to the plants is small compared to the other exchange processes at the plants, and

- the temporal changes at the soil surface below a plant cover are relatively slow.

The flux densities of sensible and latent heat at the plants H_{pl} and V_{pl}, the plant temperature, T_{pl}, the temperature, T_{ca}, and humidity, ρ_{ca}, inside the canopy are calculated from Equations 3.1 to 3.3 and 3.12 to 3.17 as derived in appendix A3.2.

For the temporary calculation of the temperature and humidity in the lower part of the canopy, $T_{ca,u}$ and $\rho_{ca,u}$, the resistance r_{ac} is divided into $r_{ac,o}$ and $r_{ac,u}$ hereafter. The corresponding air temperature and humidity are determined from

$$T_{ca,u} = T_{ca} + (T_{sa} - T_{ca}) \, r_{ac,o}/(r_{ac} + r_{as}) \tag{3.18a}$$

and

$$\rho_{ca,u} = \rho_{ca} + (\rho_{sa} - \rho_{ca}) \, r_{ac,o}/(r_{ac} + r_{as}) \tag{3.18b}$$

The fraction $r_{ac,o}=0.85 \, r_{ac}$ has been determined empirically by comparing of the model results with corresponding measurements from the lower part of the canopy.

3.4   Additional remarks on the solution of the energy budget and transport equations (dew and evaporation of intercepted water)

In both options (3.2 and 3.3), two special cases have to be regarded:

1.)   If the plants are partly wet from dew or rain interception, the flux densities of the latent heat of evaporation from the plants V_{pl} is calculated with the resulting resistance r_{pl} for the combined diffusion through the stomata (r_{st}) on the one hand, and from the wet leaf surface (r_{int}) on the other hand

$$r_{pl} = r_{st}\, r_{int}\, /(r_{st} + r_{int}) \qquad\qquad . \tag{3.19}$$

The resistance r_{int} for the evaporation of water from the plant surfaces is calculated from

$$r_{int} = r_{im} \max\{\ 1 + f_J/2\ ,\ P_{im}/(2\,P_i) - 1\ \} \qquad\qquad , \tag{3.19a}$$

with r_{im}=40 s/m in the case of intercepted precipitation, and r_{im}=4 s/m in the case of dew. The resistance r_{int} accounts for plant senescens by f_J (4.2a) and for the amount of dew or intercepted water P_i (4.10, 4.11).

After this calculation according to Appendix A3.1 or A3.2, V_{pl} is divided into transpiration V_t and evaporation V_e of dew or interception according to

$$V_t = V_{pl}\, r_{st}\, (1 - P_i/P_{im})\, /\, r_{int} \qquad\qquad , \tag{3.20a}$$

$$V_e = V_{pl} - V_t \qquad . \tag{3.20b}$$

2.)   If $\rho_{s,pl} < \rho_r$ or $\rho_{s,pl} < \rho_{ca}$ in the "microclimate" option, r_{pl} is set equal to zero and dew can form. Since the stomatal resistance is related to the actual plant water potential (see Section 4.1), for each time step after the calculation of V_{pl} , it is tested whether the stomatal resistance used in the calculations is still in accordance with the actual water potential.

Once the energy balance and the aerodynamic flux densities H_{sa} and V_{sa} are determined at the soil surface (see Section 3.2 or 3.3), the microclimatic conditions, which are calculated for each time step, are adjusted to these fluxes with the help of (3.16) and (3.17):

$$T_{ca} = \{ \ [T_r \ r_{ap} + T_{pl} \ r_a](r_{ac} + r_{as}) + T_{sa} \ r_a \ r_{ap} \ \}/(r_a + r_{ac} + r_{as}) \tag{3.21a}$$

$$\rho_{ca} = \{ \ [\rho_r \ r_{ap} + \rho_{s,pl} \ r_a](r_{ac} + r_{as}) + \rho_{sa} \ r_a \ r_{ap} \ \}/(r_a + r_{ac} + r_{as}). \tag{3.21b}$$

3.5   The resistances for the aerodynamic transports

In this section, the resistances r_a and r_{ac} for the vertical turbulent transports of sensible and latent heat above and inside the canopy; as well as the resistances r_{ap} and r_{as} for the laminar transports at the surfaces of the plant elements and the soil surface (see Sections 3.2 and 3.3) are described. These are all calculated from the reference wind speed (input variable), from geometrical properties of the canopy, and from surface properties of the ground (surface of soil or snow). The stratification is taken into account in the calculation of the resistance for turbulent transport r_a .

To allow calculations for one canopy (or surface) with the input wind speed u_r from a nearby surface, the model offers the possibility of temporarily transforming the reference wind speed. The relation for the logarithmic wind profile (e.g. Thom, 1975, p. 63) is

$$u(z, d, z_0) = u_*/\kappa \ \ln[(z - d)/z_0] \tag{3.22}$$

with the friction velocity u_* and the von Karman constant κ (κ=0.4).

This relation is applied to both sites with the assumption that the wind speed at the height H (usually taken as H=20m) does not differ above both sites. This allows the conversion of the wind speed u_m , measured at a height z_u , into the reference input wind speed u_r at z_r by

$$u_r = u_m \ln[(H - d_u)/z_{0u}] \ \ln[(z_r - d)/z_0] / \{ \ \ln[(H - d)/z_0] \ \ln[(z_u - d_u)/z_{0u}] \ \}, \tag{3.23}$$

where stratification effects are omitted. Here d and z_0 are the zero plane displacements and the roughness lengths for momentum at the site of the application of the model and d_u and z_{0u} are the respective quantities at the site where the wind speed has been measured.

The zero plane displacement d, and the roughness length z_0 of the canopy, as well as the aerodynamic resistance r_{ac} for the turbulent transport inside the canopy are determined according to results of a discretized numerical model of the shear stress (Braden, 1982, p. 74). In that model, with the help of an estimate for the mixing length profile, depending on the structure and density of the canopy, the

downward decrease of the shear stress was related to the stress exerted on the plant elements. The profiles of wind speed and turbulent diffusivity resulting from that model have been evaluated for a variety of reference wind speeds, as well as structures and densities of the canopies. These results are introduced into the present model by means of numerical tables of F_d and F_r for d and r_{ac}, respectively. The displacement height d is determined as a portion of the canopy height z_c

$$d = F_d(l_a) z_c \quad , \tag{3.24}$$

where F_d is related to the leaf area index l_a as listed in Tab. 3.1.

Table 3.1   The relation between F_d and the leaf area index l_a

l_a	0.0	0.53	1.06	1.59	2.13	2.66	3.19	3.72	4.25	4.78	5.31	10.0
F_d "e"	0.0	0.120	0.176	0.251	0.310	0.362	0.406	0.445	0.489	0.518	0.544	0.560
F_d "p"	0.0	0.140	0.223	0.312	0.378	0.433	0.480	0.519	0.561	0.589	0.613	0.630

Two different relations are available for more or less upright leaves, referred to as "erectophil (e)" and "planophil (p)" (see Tab. 2.2). For intermediate values of the leaf area index the resulting values of F_d are interpolated with the help of third order polynoms.

The resistance r'_{ac} for adiabatic stratification is determined from

$$r'_{ac} = F_r(z_c) \, l_a \, 2.5/u_{20} \quad , \tag{3.25}$$

where u_{20} is the wind (in m/s) speed resulting from the logarithmic profile (3.22) at the height of 20m. As above, the relation of F_r to the canopy height z_c is available for more ("e") or less ("p") upright leaves (Tab. 3.2).

Table 3.2   The relation between F_r and the canopy height z_c

z_c	0.0	0.2	0.4	0.6	0.8	1.0	1.2	1.4	1.6	1.8	2.0	2.2
F_r "e"	65.0	80.0	93.4	102.4	107.0	113.6	121.6	132.0	149.4	166.3	186.6	200.0
F_r "p"	60.0	72.0	80.7	85.2	87.2	90.4	94.4	99.9	109.8	119.4	130.8	140.0

The roughness length of the canopy for the aerodynamic above the canopy is determined as

$$z_0 = F_z z_c \tag{3.26}$$

with F_z=0.16 for the more ("e") and F_z=0.12 for the less ("p") upright leaves.

The resistance for the turbulent transport from the reference height z_r to the top of the canopy is calculated from the integral

$$r'_a = \int K_m^{-1} \, dz \tag{3.27}$$

with the commonly used eddy diffusivity or eddy viscosity (see e.g. Thom, 1975, p. 70)

$$K_m(z) = u_* \, \kappa \, (z - d) \qquad . \tag{3.27a}$$

This results in the aerodynamic resistance for adiabatic lapse rate

$$r'_a = \ln[(z_r - d)/(z_c - d)]/(u_* \, \kappa) \qquad , \tag{3.28}$$

where the friction velocity u_* can be eliminated from (3.22) and (3.23).

In order to regard the transport from the upper part of the canopy, but not the top of the canopy, with the resistance r_a and with r_{ac} down from there, the two resistances for the adiabatic case are modified by

$$r_a^{(0)} = r'_a + 0.02 \, r'_{ac} \qquad , \tag{3.28a}$$

$$r_{ac}^{(0)} = 0.98 \, r'_{ac} \qquad . \tag{3.25a}$$

According to Campbell (1985, p. 67) the resistance r_{ap} (s m^{-1}) for the transport through the laminar layers of the plant elements (both sides of the leaves) is expressed as

$$r_{ap} = 90 \, (d_p/u_c)^{1/2} \qquad , \tag{3.29}$$

where d_p is a typical dimension of the plant elements taken as the leaf width, see also Braden (1982, p. 61). The wind speed u_c at the upper part of the canopy is estimated from (3.22) with $z=z_c$. The resistance r_{as} (s m^{-1}) for the laminar transport at the ground surface is calculated according to Campbell (1985, p. 67) from

$$r_{as} = 307 \, (d_s/u_s)^{1/2} \qquad . \tag{3.30}$$

Here d_s is an input parameter which is usually set to d_s=0.02 m as a characteristic length of the surface structure. For a snow cover d_s is set to 7.5 mm.

The wind speed u_s at d_s above the ground surface is determined from a logarithmic profile

$$u_s = u_{*s}/\kappa \, \ln(d_s/z_{0s}) \qquad , \tag{3.31}$$

with $z_{0s}=d_s/7.5$, according to Brutsaert (1982, p. 113). To obtain the required friction velocity u_{*s} at the ground surface, the two logarithmic wind profiles, one above the canopy and the other near the ground, are matched at the height $z_x=z_c$ giving

$$u_{*s} = u_* \, \ln[(z_x - d)/z_0] \, / \, \ln(z_x/z_{0s}) \qquad . \tag{3.31a}$$

Here u_* results from (3.22) with the boundary value $u_r=u(z_r)$ and d and z_0 from (3.24) and (3.26), respectively.

The influence of the stratification on the resistance r_a is regarded according to (Brutsaert, 1982, p. 66) by

$$r_a = r_a^{(0)} - \Psi(\zeta)/(\kappa \, u_*) \qquad , \tag{3.32}$$

using the logarithmic wind profile. For unstable stratification the function Ψ is determined according to Brutsaert (1982, p. 70) as

$$\Psi(\zeta) = 2 \, \ln[(1 + X_2)/(1 + X_1)] \tag{3.33a}$$

with the abbreviations

$$X_i = (1 - 16 \, \zeta_i)^{-1/2} \qquad . \tag{3.33b}$$

and

$$\zeta_1 = (z_x - d)/L_* \qquad , \tag{3.33c}$$

$$\zeta_2 = (z_r - d)/L_* \qquad\qquad . \tag{3.33d}$$

For stable stratification ($L_* > 0$) the function Ψ is determined from

$$\Psi = 7\,(\zeta_2 - \zeta_1) \qquad\qquad , \tag{3.33e}$$

which is limited to $\Psi \geq -0.85$, since the formulation does not hold for strongly stable situations. The Monin-Obukhov length L_* is calculated according to Brutsaert (1982, p. 65) and Thom (1975, p. 85)

$$L_* = \rho\, c_p\, T_r\, u_*^{3}/[\, g\, \kappa\, (H_{ca} + 0.61\, V_{ca}\, c_p\, T_r/\lambda)\,] \qquad\qquad , \tag{3.34a}$$

where g is the gravitational acceleration ($g \approx 9.81$ m s^{-2}).

In order to avoid recursions for H_{ca} and V_{ca} the Monin Obukhov length L_* for the actual time step is estimated from the one of the previous time step by the empirical relation

$$L_* = L_*^{(o)}\,(R_n'^{(o)}/R_n') \tag{3.34b}$$

with the "climatic net radiation"

$$R_n' = R_{ns} + R_l - \sigma\, T_r^4 \qquad , $$

including the net short-wave radiation $R_{ns} = R_{n\,s,pl} + R_{n\,s,g}$ according to Section 2.6. Here R_n', $R_n'^{(o)}$ are the climatic net radiation fluxes from the actual and the previous time step (marked with $^{(o)}$). The Monin Obukhov length $L_*^{(o)}$ has been determined from (3.34a) in the previous time step after the calculation of the aerodynamic fluxes H_{ca} and V_{ca}. With this relation, the expected impact of the change in shear stress and global radiation on buoyancy is temporarily estimated. Of course, this treatment of the turbulent vertical transport is not fully satisfying, but it seems to be acceptable for the purpose of this model.

3.6   Development, melting and insulation of a snow cover

The effects of a snow cover on the soil surface, for example, its insulation, have to be regarded in order to enable the proper calculation of the soil surface temperatures, and the temperatures above the surface, as well as the temperatures and the water contents of the soil layers. These are recommended for agrometeorological purposes like estimating survival conditions for insects at the soil surface, as well as for winter crops above the surface, and for infiltration and leakage during winter. Moreover, these are important for the reliable determination of the lower boundary in mesoscale applications.

In order to decide whether precipitation is frozen or not, the corresponding weather information, included in synoptic data, are evaluated. If these are not available, the reference air temperature, T_r, is used as an indicator. For $T_r < T_{sno}$ the precipitation is assumed to be frozen. From synoptic data of Braunschweig (1951 until 1980) it was found that the value $T_{sno}=1.5$ °C gives the best agreement with the observed types of precipitation. Of course, erratic decisions at this point may cause severe deviations in the succeeding simulations.

In the case of frozen precipitation, the additional amount of water is added to the water content w_{sn} of the snow cover. The height of the snow cover d_{sn} is defined by w_{sn} and the snow density w_{sn}/d_{sn}, which is initially set equal to $w_{sn}/d_{sn}=100$ kg m^{-3} of water for fresh snow. Afterwards the snow density is increased in the cases of rainfall or temporary melting up to the value of 500 kg m^{-3}.

The existence of a snow cover is accounted for by the modification of various surface properties:

-       The roughness length is diminished (see Section 3.5).
-       The emissivity for long-wave radiation ε_g is changed (see Chapter 2.5).
-       The reflectivities of the short-wave components of radiation are raised remarkably (see Chapter 2.5).
-       The resulting net short-wave radiation is considered to penetrate into the snow cover with and the extinction 0.30 w_{sn} (w_{sn} in mm$_{(H2O)}$). This extinction coefficient has been estimated from data of Dirmhirn (1964, p.160) and Thomas (1963), who only gave results for visible radiation. Thus, a thin snow cover with $w_{sn}=2.31$ kg m^{-2} only absorbs half the incident radiation, while the other half is transmitted to the soil surface.

The most important effect, however, results from the insulation by the snow cover. The lower boundary condition for the aerodynamic transports, T_{sa}, no longer coincides with the soil surface temperature T_{s0}. The heat transport between the top and the bottom of the snow cover due to conduction is

$$G_{sa} = \lambda_{sn} (T_{sa} - T_{ss})/d_{sn} \qquad , \tag{3.35}$$

where T_{ss} is the temperature at the lower boundary of the snow cover. The heat conductivity of the snow cover is linearly varied between the values $\lambda_{sn} = 0.08$ W m^{-1} K^{-1} for fresh snow (w_{sn}/d_{sn}=100 kg m^{-3} of water) and $\lambda_{sn} = 0.42$ W m^{-1} K^{-1} for old snow (w_{sn}/d_{sn}=500 kg m^{-3} of water) given by Oke (1978, p. 38).

In a first step, from the preliminary energy balances of the top and the bottom of the snow cover, the internal time step is determined for the subsequent calculations of soil and snow heat budgets. The latent heat of snow or rain in the case of precipitation and the heat capacity of the snow are included. The resulting time step is limited in order to avoid phase transitions between the stages "frozen" ↔ "melting" or "melting" → "liquid" during one internal time step (see also Section 5.2). The soil surface heat flux is determined from the energy balance of the soil surface, including the transmitted short-wave radiation, as well as the fluxes of sensible and latent heat (molecular diffusivity $\triangle z$=1mm). Doing this, spotted melting is accounted for, for thin layers of snow (d_{sn}<17 mm) considering an increasing portion of the soil surface to be already free of snow.

The soil heat budgets are calculated with the internal time step according to Sections 5.1 and 5.2 using the soil surface heat flux as a boundary condition.

The heat budgets of the upper and the lower parts of the snow cover are calculated separately on the basis of the resulting surface temperature. As far as possible, the changes in the heat capacities and the latent heats of freezing (see Chapters 5.2 and 5.3), are restricted to the upper and lower parts.

From a physical point of view this part of the model is simple, but controls (not explained in detail here) are recommended at the freezing point in order to enable proper operation in all situations. The treatment of the phase transitions is reported in more detail for soil chill in Section 5.2.

The balance equation (3.4) is generalized to the energy budget equation of the upper part of the snow cover

$$R_{n s,g} + H_{sa} + V_{sa} + G_{sa} = w_{sn} C_w (T_{sa} - T_{sa,o})/2 + Q_{ph,s} + Q_{ph,p}, \tag{3.36}$$

where $T_{sa,o}$ is the surface temperature of the previous time step, and C_w is the heat capacity of frozen water (see Tab. 5.1). The term $Q_{ph,p}$ accounts for the freezing heat of precipitation and occurs if its phase state differs from that of the snow cover. The freezing heat of the snow cover $Q_{ph,s}$ has to be overcome in the case of melting. The different cases are carefully distinguished in the model to ensure its proper operation.

4   Plant-water interactions

The stomatal resistance is the control mechanism for the plant heat and water budgets. In contrast to the passive role of the plants in the transmission and reflection of radiation, the stomata are involved in complex physiological mechanisms, which will not be considered here (see Larcher, 1976; Ziegler, 1978 or Zelitch, 1971). The combined effect of all the stomata in the canopy is considered to be unified in the so-called bulk stomatal resistance. In order to account for its most important reactions, these are empirically related to the significant quantities of influence, as described in Section 4.1. This part of the model is the only element that needs calibration using the whole model. Water transport through the plant roots, stems and leaves is considered (Section 4.2), because it enables a realistic presentation of the extraction term for the soil water as well as for the plant water stress, that remarkably influences the stomatal resistance. In addition to the water fluxes inside the plants, the passive impact of the plants on the water budget by interception of precipitation is empirically simulated, as described in Section 4.3.

4.1   The bulk stomatal resistance and its calibration

The bulk stomatal resistance, r_{st}, is calculated from the visible radiation $R_{n\,vi,pl}$ absorbed by the plants, the leaf area index, l_a, and the plant water potential, ψ_{pl},

$$r_{st} = \{\, r_{smi} + r_{se}(\text{plant age}) + r_R(R_{n\,vi,pl}, l_a)\} \,/ f_1(l_a) + r_{pw}(\psi_{pl}) \tag{4.1}$$

The minimum stomatal resistance, r_{smi}, is an important quantity, which must be specifically be calibrated to the respective crop. The additional resistance, r_{se}, accounts for the fact that older crops are unable to transpire as much as they can in younger stages, because the stomata can no longer fully be opened or because they dry out, as in the case of cereals. For young, fully transpiring crops r_{se} is equal to zero. Similar to Thompson et al. (1981, p. 24), this senescence resistance is related to the plant age by

$$r_{se} = r_{s1}f_J + r_{s2}f_J^3 \qquad , \tag{4.2}$$

with

$$f_J = (J - J_b)/(J_e - J_b) \qquad \text{for } J_b \leq J \leq J_e \qquad . \tag{4.2a}$$

The resistances r_{s1} and r_{s2} have to be calibrated. The value of the senescence resistance r_{se} depends on the days of year (J_b and J_e) of the two corresponding phenological stages of the crop (see Zadoks et al. 1974; Biologische Bundesanstalt, 1979; Hack et al., 1992). For days of the year $J \leq J_b$ the resistance r_{se} is equal to zero and for $J \geq J_e$ it equals $r_{s1} + r_{s2}$.

For intermediate days r_{se} rises from zero to its maximum value. A typical shape of r_{se} is presented in Fig. 4.1. The phenological stages,

Fig. 4.1   The senescence resistance r_{se}

that have turned out to be relevant for J_b and J_e of the different crops according to Schrödter (1981) and Löpmeier (1991), are listed in Tab. 4.1.
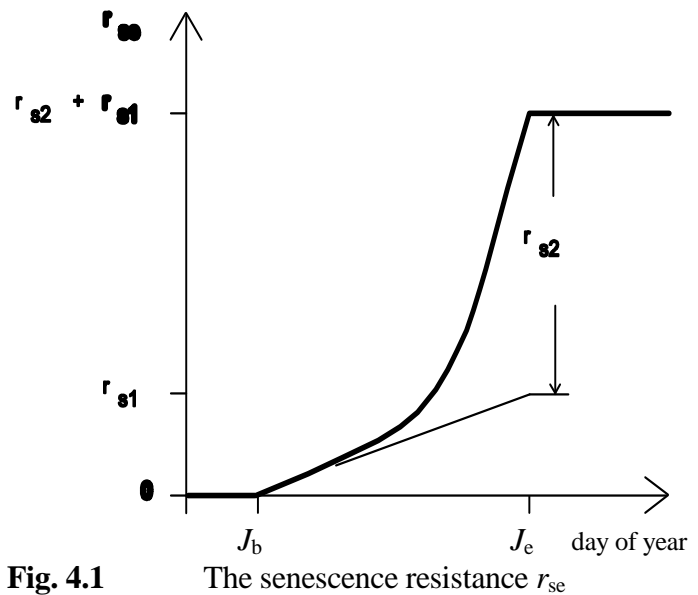
Table 4.1   The phenological stages for the beginning (J_b) and the end (J_e) of senescence according to Löpmeier (1991)

crop	J_b	J_e
winter wheat	heading + 10	fully ripe
spring wheat	heading + 5	fully ripe
winter barley	heading + 10	fully ripe
spring barley	heading + 10	fully ripe
oats	heading	fully ripe
winter rye	heading + 10	fully ripe
maize	flowering	dough stage
sugar beet	crop cover complete + 10	full maturity
potatoes	crop cover complete + 5	crop cover complete + 110
rape	begin of flowering	fully ripe

For the reaction on the absorbed visible or photosynthetically active radiation a corresponding relation, given by Feddes et al. (1978, p. 27) has been converted and listed in Tab. 4.2.

Table 4.2   The relation between the resistance r_R and the absorbed visible radiation R'_{nvpl}, modified according to Feddes et al. (1978, p. 27)

R'_{nvpl}	0	40	60	80	100	110	500
r_R	2800	237	141	69	10	0	0

For leaf area indices $l_a > 1$ the input quantity R'_{nvpl} is equal to the absorbed visible radiation $R_{n\,vi,pl}$ calculated according to Section 2.6, else $R'_{n\,vi,pl} = R_{n\,vi,pl}/l_a$ is used. Intermediate quantities are interpolated from Tab. 4.2 with the help of third order polynoms.

The function $f_1(l_a)$ in (4.1) reflects the main impact of the leaf area index on the bulk stomatal resistance: Since transpiration for $l_a \to 0$ becomes zero, $f_1(l_a=0)$ is zero. On the other hand, transpiration is limited even for an unlimited increase of l_a . This is due to the fact, that, in contrast to the simplifying network for the aerodynamic resistances (Fig. 3.1 and 3.2), the aerodynamic transports from the deeper canopy layers have to overcome supplementary resistances up to r_{ac} additional to r_a . For this reason, f_1 is limited to 1 for $l_a \geq 2.15$ resulting in

$$f_1(l_a) = \min\{1,\ 1.2\ [1 - \exp(-l_a/1.2)]\} \qquad\qquad . \qquad\qquad\qquad\qquad (4.3)$$

The resistance r_{pw} for the water stress reaction, is zero if no water stress occurs. This is assumed to be provided as long as the plant water potential, ψ_{pl} , (see Section 4.2) exceeds ψ_{pl0} ($|\psi_{pl}| < |\psi_{pl0}|$). Otherwise, for $|\psi_{pl}| < 2|\psi_{cr}|$, the resistance r_{pw} increases linearly up to r_{pm} , as shown in Fig. 4.2. The water potentials ψ_{pl0} and ψ_{cr} are determined during the calibration and the resistance r_{pm} is assigned to 8000 s/m, a typical value for the transport through the cuticular, that remains possible even if the stomata are totally closed.
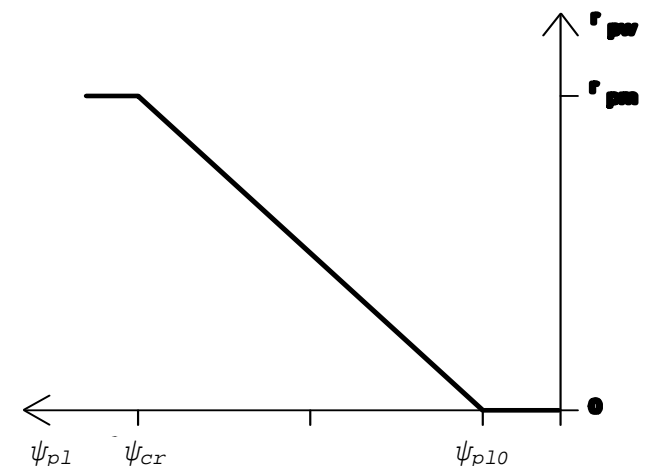

Fig. 4.2   The resistance for plant water stress

This parameterization of the (bulk) stomatal resistance certainly is not satisfying from a plant physiological point of view. However, it seems to be acceptable for the purpose of this

agrometeorological model.

In summation, the parameterization of the bulk stomatal resistance consists of five quantities, that have to be calibrated for each different crop (see Tab. 4.4 at the end of this Section). These are

-        the minimum resistance r_{smi},

-        the resistances r_{s1} and r_{s2}, that are responsible for the shape of the increase of the senescence effect and

-        the water potentials ψ_{pl0} and ψ_{cr}, that determine the reaction on water stress.

The **calibration** parameters have been determined by comparing the evapotranspiration courses, resulting from the model AMBETI, with corresponding measured courses of evapotranspiration. The five calibration parameters have been adjusted repeatedly according to the preceding model runs until there was a good agreement between the simulated and the measured course of evapotranspiration.

This procedure implies the impact of other elements of the model on the parameters determined during the calibration. Especially the choice of soil-hydraulic properties - the retention functions and conductivity functions - might remarkably influence the calibration potentials ψ_{pl0} and ψ_{cr} (see below). Since the model properly describes all the processes relevant for the water and heat budgets of the system, the calibration parameters will represent only the properties of the crops themselves. This gives justification for the hypothesis of the transferability of the calibration to soil types other than the sandy loam that had been used in the calibration (see Tab. 4.3).

For the purpose of calibration the evapotranspiration has been determined from the mass balances of two weighing lysimeters. Each has a depth of 1.5 m, is drained with the suction of 1m column of water at the bottom and has a surface of 1.7 m by 1.7 m (see von Hoyningen-Huene and Bramm, 1978). For the evaporation experiments, the crops were cultivated on

Table 4.3   The composition and properties of the sandy loam used with the calibrations

depth cm	m_c %	m_u %	m_o %	ρ_b g cm^{-3}	K_s cm/day
0-15	10	42	1.5	1.50	30
15-25	10	42	1.1	1.50	20
25-70	10	42	0.4	1.51	20
> 70	10	42	0.4	1.60	2

the lysimeters, in as similar a manner as possible to the surrounding fields of about 45 m by 45 m. Starting in winter, the corresponding model runs have been realized with the respective measured meteorological boundary conditions and with the plant development (z_c, l_a). For the root distributions and densities measurements of Westing and Söchtig (1985) and Kücke and Löffler (1990) from com-

parable soils have been considered. Additionally, for young crops root densities had to be augmented occasionally in order to avoid severe water stress which did not in reality occur.

In general, the need of the model for courses of root density profiles as input quantities appears to obstruct its application. On the other hand, the advantages of the implementation of the plant water conduction are described in Section 4.2. Fortunately, at least in the case of agricultural crops in humid climates, the requirements of root distribution (root depth), and root densities as input parameters seem to be a minor problem. With a certain experience in the use of the model, the knowledge of root densities can be adjusted from the demand to give no severe water stress under normal conditions. However, the supply with the input quantity "rooting depth" still is a disadvantage, since it may depend on the individual crop, on the stratification of soil types, and even on the previous development of the water distribution in the soil. Eventually, this problem can be solved in the future by the implementation of a sub-model for the root growth (Richter and Kücke, 1994).

Calibrations had been carried out with an earlier version of the model for

-       winter wheat from the vegetation period of the year 1985,

-       for winter barley from the vegetation periods of 1983 and 1986 and

-       for sugar beet from the vegetation periods of 1983 and 1984.

The resulting calibration coefficients are listed in Tab. 4.4.

The time courses of evapotranspiration resulting from the calibrated model are cumulatively plotted in Figs. 4.4a-4.4e together with the measured courses of evapotranspiration. In the cases of two vegetation periods available for one crop, the model runs have been calculated with identical calibration parameters.

For the calibration the model has been run with van Genuchten retention functions (5.23) and conductivities

Fig. 4.3   Retention functions used in the calibrations:
_____: after Vereecken (1989)
------: fitted to measured retention (x,o) (two dephts)

(5.25a) with the coefficients fitted to the measured retention curves (see Fig. 4.3). This has the advan-

tage that deviations of the pedo-transfer functions (see Section 5.5) for the sandy loam used do not effect the calibration. In accordance with infiltration experiments the hydraulic saturation conductivities have been set to the values given in Tab. 4.3 . Figures 4.4a and 4.4b show the results for the two vegetation periods available for winter barley. With the calibration, a good agreement of the measured and simulated courses of evapotranspiration was achieved for both vegetation periods.
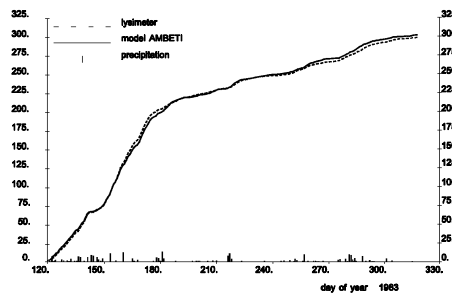
Fig. 4.4a   Comparison of the courses of cumulative evapotranspiration for winter barley (harvest 189th day of year)

Remarkable deviations occurring after harvest in 1986 are probably caused by shortages in the soil evaporation sub-model used in this earlier version of the model AMBETI.
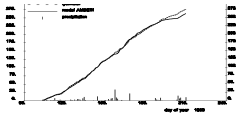
Fig. 4.4b   Comparison of the courses of cumulative evapotranspiration for winter barley (harvest: 195th day of year 1986)
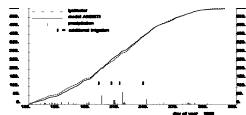
Fig. 4.4c   Comparison of the courses of cumulative evapotranspiration for sugar beet (vegetation period: 122nd to 293rd day of year)

Also for the calibration of sugar beet, two vegetation periods have been available (see
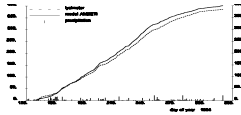
Fig. 4.4d   Comparison of the courses of cumulative evapotranspiration for sugar beet
                        (vegetation period: 120th to 290th day of year 1984)

Figs. 4.4c and 4.4d). During 1983, the sugar beets were irrigated on the 194th, 206th-207th, 215th and
239th days of the year. The calibration for sugar beets did not succeed in giving totally satisfying
agreement for both vegetation periods. During 1984, the simulated cumulative evapotranspiration
exceeded the measured one by about 4%.

Fig. 4.4e   Comparison of the courses of cumulative evapotranspiration for winter wheat
                        (harvest 240th day of year 1985)
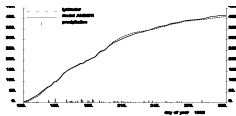
The results of the calibration for winter wheat are presented in Fig. 4.4e.

With the new version of the model up to now calibrations for spring barley, winter rye, winter wheat and potatoes have been realized by Blanke (pers. communication). For these simulations pedotransfer functions according to Vereecken et al. (1989, 1990) have been used for the sandy loam (with m_o=1% in Fig. 4.3). Fig.
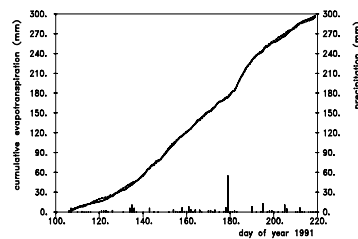
Fig. 4.5a   Simulated (____) and measured (----) courses of cumulative evapotranspiration for summer barley (harvest: 219th day of year 1991); PTF after Vereecken; |= precipitation; (see text)

4.5a shows one example for spring barley during the vegetation period of 1991.

In order to test the impact of the retention functions and hydraulic conductivities (see Section 5.5) on the calibration, the simulation was repeated with the soil hydraulic functions used in the old calibrations of Figs. 4.4. The resulting cumulative courses of evapotranspiration are presented in Fig. 4.5b. All the other
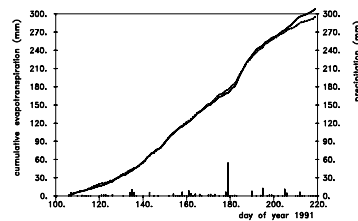
Fig. 4.5b   Simulated (____) and measured (----) courses of cumulative evapotranspiration for summer barley (harvest: 219th day of year 1991); fitted retention functions; |=precipitation

input parameters, namely the calibration coefficients and the starting conditions at the first day of January 1991 had been identical in both simulations. Obviously the influence of the deviations between the two sets of soil-hydraulic functions does not require modifications of the calibration. For this reason, the old calibration coefficients (Figs. 4.4) are used even for the new version of the model AMBETI with the pedo-transfer functions according to Vereecken et al. (1989, 1990). The results of the new calibrations are listed in Tab. 4.4 together with the old ones.

Table 4.4   The results of the calibration procedure

crop	r_{smi} (s/m)	r_{s1} (s/m)	r_{s2} (s/m)	ψ_{p10} (kJ/kg)	ψ_{cr} (kJ/kg)	vegetation periods
winter barley	70	400	200	-0.4	-1.9	1983,1986
sugar beet	45	20	0	-0.5	-0.9	1983,1984
winter wheat	55	30	2370	-0.3	-1.5	1985,1989
spring barley	37	10	70	-0.4	-1.9	1990,1991
winter rye	40	10	480	-0.4	-1.5	1989,1990
potatoes	50	10	70	-0.3	-0.9	1988,1991

4.2   Plant water conduction

The transport of liquid water from the soil through the roots and stems into the leaves is treated in a mechanistic manner. The fluxes are calculated with the help of a resistance network with differences of water potentials between the soil layers and the upper part of the plant as the driving forces. In spite of the difficulties of properly defining the resistances from the distribution of the roots, this method implies two advantages:

-       The extraction terms for the soil water (see Section 5.4) are easily determined.

Fig. 4.6   The resistance network for the plant water transport

-       In the case of water stress the plant realistically reacts on both soil water potential and transpiration demand.

In simpler models, plant water stress usually is directly related to soil water content. The additional dependence on transpiration demand has to be considered empirically (see e.g. Slabbers, 1980).

In the resistance network (Fig. 4.6) the resistances $r_{so,i}$ for the water transport from the surrounding soil in layer i to the root elements are regarded as well as the resistances $r_{ro,i}$ for the following transport
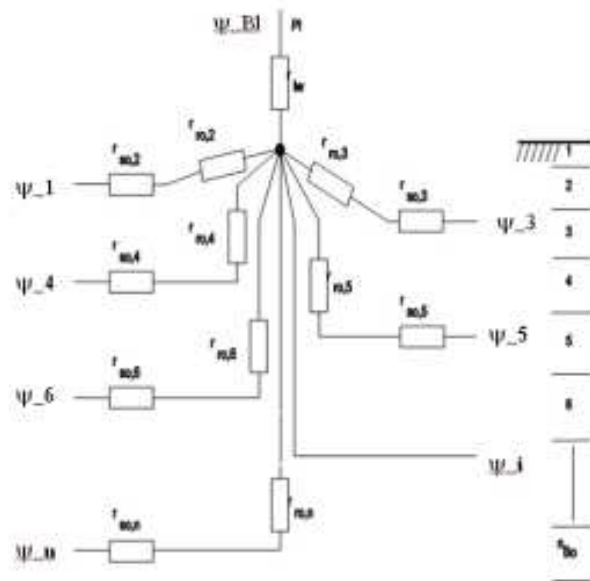
through the corresponding roots to the central root. The resistance r_{pl} accounts for the transport from the central root to the upper part of the plant (regarded as the "bulk stomata").

According to literature the resistance r_{pl} is set to 0.01 $m^3_{(H2O)}$ m^{-2} s^{-1}/(J kg^{-1} m^{-1}) (Denmead and Millar, 1975; Hansen, 1974). The root resistances $r_{ro,i}$ are set inversely proportional to the respective root length densities $d_{ro,i}$ (m m^{-3})

$$r_{ro,i} = [\ c_2\ (c_3 + c_4\ T_{so,i})\ d_{ro,i}\ \Delta z_i\ ]^{-1} \qquad , \qquad\qquad (4.4)$$

with the thickness of the soil layer Δz_i . The observed temperature dependence (Slatyer, 1967, p. 204) is obtained by c_3=0.1 and c_4=0.045 K^{-1}. The constant c_2 takes the value 2.8 $_{10}$$^{-14}$ $m^3_{(H2O)}$ m^{-2} s^{-1}/(J kg^{-1} m^{-1}) in accordance with Busscher and Fritton (1978), Hansen (1974), Denmead and Millar (1975) and Slatyer (1967, p. 207).

According to Hullugalle and Willatt (1983) and Gardner (1960) the resistances $r_{so,i}$ for the transport along the cylindric geometry through the soil to each single root element are

$$r_{so,i} = \ln\{\ (\pi\ d_{ro,i}\ R_{ro}^2\ )^{-1}\ \}/(\ 4\ \pi\ d_{ro,i}\ K_{u,i}\ \Delta z_i\ ) \qquad . \qquad\qquad (4.5)$$

The radius of the root elements R_{ro} is usually taken as 0.5 mm, and $K_{u,i}$ is the hydraulic conductivity in the respective soil layer (see Sections 5.4 and 5.5). In order to account for the reaction on the lack of oxygen available to the roots (Hoogland et al., 1981), the resistance $r_{g,i}$ between the water potentials $\psi_{t,i}$ [*] inside the soil layers i and at the central root ψ_c is raised for nearly saturated soil layers:

$$r_{g,i} = (r_{ro,i} + r_{so,i})/b \qquad . \qquad\qquad (4.6)$$

If the air filled portion of the soil layer $\varphi_{a,i}$ exceeds 0.05, then b=1, otherwise b linearly approaches zero for $\varphi_{a,i} \to 0$.

From the resistance network presented in Fig. 4.6 with Eq. (4.6), the resulting fluxes can be calculated from Kirchhoff's and Ohm's laws. From the demand for equilibrium between the liquid stem flow and the transpiration $f_{vz,0}=V_{pl}/\lambda$ (see (3.7 and 3.13)), the plant water potential ψ_{pl} is determined as

$$\psi_{pl} = [\ f_{vz,0}\ (1 + r_{pl}\ S_{ru}\ ) + S_{rp}\ ]/S_{ru} \qquad , \qquad\qquad (4.7a)$$

---

[*] sum of matric and gravitational potentials (see section 5.4)

with the abbreviations

$$S_{ru} = \Sigma \; r_{g,i}^{-1} \quad , \tag{4.7b}$$

$$S_{rp} = \Sigma \; \psi_{t,i}/r_{g,i} \quad . \tag{4.7c}$$

In solving Eq. (4.7), care is taken to restrict the summations to the fluxes out of the respective soil layers. The evaluations of the stomatal resistance (4.1), the transpiration (3.7 and 3.13) and the plant water potential (4.7) are carried out recursively until the water potential, as control variable (4.1 and 4.7), is stable. The resulting root extraction terms ($q_{ro,i} < 0$) for transpiration, $f_{vz,0} < 0$, are determined from

$$q_{ro,i} = (\psi_c - \psi_{t,i})/r_{g,i} \quad , \tag{4.8}$$

if the water potential

$$\psi_c = (S_{rp} + f_{vz,0})/S_{ru} \tag{4.9}$$

in the central root is exceeded by $\psi_{t,i}$ ($|\psi_c| > |\psi_{t,i}|$).

The reaction of the plant on water deficit described above, works as a control circuit: The plant water potential controls the transpiration via the bulk stomatal resistance (4.1 and 4.4).

4.3   The interception of precipitation

The interception of precipitation by the plants, P_i', is empirically related to the leaf area index, l_a, the portion of soil covered by plants, b_o, and the amount of precipitation, P_r, by the formula

$$P_i' = P_{im} [1 - (1 + b_o P_r/P_{im})^{-1}] \qquad (4.10)$$

presented by Braden (1985). The limiting interception P_{im} is estimated as $P_{im}=a\ l_a$, where the factor a is increased from $a=0.3$ up to $a=0.6$ during senescence according to

$$a = 0.3\ (1 + f_J) \qquad (4.10a)$$

with the function f_J (4.2a). This accounts for the fact that leaves gradually become able to hold more water at the surface during senescence. The reason is that the surface becomes cracked and less slippery. The portion of soil covered by vegetation, b_o, is related to the leaf area index by

$$b_o = 1 - \exp(- 0.5\ l_a) \qquad . \qquad (4.10b)$$

According to (4.10) small amounts of precipitation are almost totally intercepted by dense crops ($b_o \approx 1$). Since more and more of the intercepted water falls to the ground, P_i' asymptotically approaches P_{im} for increasing amounts of precipitation (Fig. 4.7). In the case of interception present from previous time steps or rests from preceding precipitation events, this water is regarded cumulatively according to (4.10).

Fig. 4.7   The relative interception P_i'/P_{im} for $b_o=0.9$
-----: slope at the origin

Additionally, higher amounts of interception are allowed to drop due to wind effects by limiting the interception to

$$P_i = P_i'\ \exp\{-(P_i'/P_{im} - 0.1)(u_* - 0.2)\} \qquad (4.11)$$

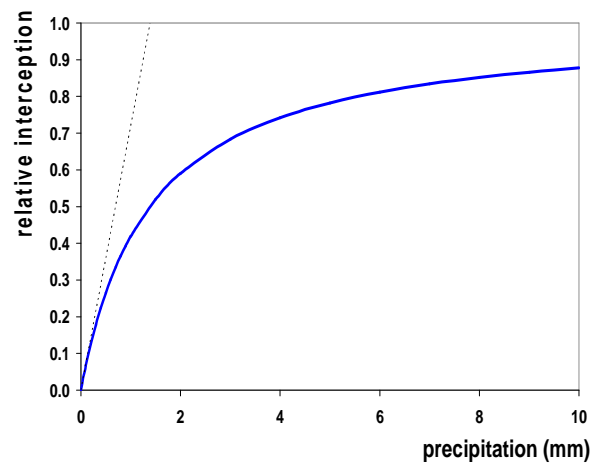for $P_i^{'}$>0.1 P_{im} and friction velocities u_*>0.2 m/s (see Section 3.5). The intercepted water is allowed to evaporate (see Section 3.4). The through-falling portion (P_r-P_i) of the precipitation is regarded in the upper boundary for the soil water (Section 5.4).

5   Soil heat and water transport

5.1   Soil heat transport: basic equations and solution
5.2   The treatment of soil chill
5.3   Thermal soil properties and soil composition
5.4   Liquid soil water transport: basic equations and solution
5.5   The hydraulic soil properties; Pedo-transfer functions
5.6   Water vapour transport in the soil and at the soil surface

Soil heat and water transport are incorporated into the model AMBETI because of their important influence on evaporation and transpiration. Moreover, they are a requirement for the proper calculation of the microclimate. The coupling of evaporation and transpiration with the soil water content results in a stabilization of long-time evaporation values during drying periods, which works by the following feed-back mechanism: If evaporation is "too" high for one or more days, the resulting reduction in soil water leads to a decrease of the further evaporation. In consequence, the deviation of the calculated cumulative evaporation from the actual one is reduced, and vice versa.

The calculation of soil heat transport is described in Section 5.1 including the solution method, that is used also for the liquid water and the vapour transport in the soil. The treatment of soil chill is explained in Section 5.2 . Section 5.3 deals with the thermal soil properties which are related to some basic soil properties describing the soil composition. The treatment of liquid soil water transport used in the model is described in Section 5.4. The mathematical formulations of the required hydraulic soil properties as well as their relation to basic soil properties - the so-called pedo-transfer functions - are presented in Section 5.5 and Appendix A5.1. Vapour flux from the uppermost soil layers must be treated carefully for the proper calculation of evaporation. Moreover, vapour flux in the soil may exceed liquid water flux for low water contents. The calculation of these vapour fluxes is described in Section 5.6.

Both soil heat and soil water vapour transports are calculated alternatingly with the global time step of about 900 to 3600 s. In both cases, the global time step is divided into smaller time steps according to the corresponding changes of the upper boundary conditions. This creates the possibility of some simplifications like linearizations, steady state treatment, and the decoupling of the calculation of heat and water movement. The liquid water transport caused by temperature gradients is not implemented in the model. It is relevant only for high water contents and strong gradients (Campbell, 1985, p. 102), as in subterranean systems for transport of heat or gas (pipelines).

5.1   Soil heat transport: basic equations and solution

Soil heat transport is determined most of all by the upper boundary soil heat flux G (see Section 3.1). Inside the soil, the vertical heat flux f_h is proportional to the temperature gradient and the thermal conductivity λ_h

$$f_h = -\lambda_h\, \partial T/\partial z \qquad . \tag{5.1}$$

As temporal changes of the volumetric soil heat capacity ($C_h\, T$) are caused by divergences of the soil heat flux, the one-dimensional heat budget equation is

$$\partial(C_h\, T)/\partial t = \partial/\partial z\, (\,\lambda_h\, \partial T/\partial z + f_x\,) + q_h + q_{ph} \qquad . \tag{5.2}$$

Here C_h is the volumetric specific heat of the soil (see below), q_h is an extraction term ($q_h<0$) and f_x will be used for the heat transport that is connected with the soil water transport. The term q_{ph} accounts for the latent heat that is coupled with melting and freezing of water (see Section 5.2). The specific heat C_h can be taken as constant during the time step Δt, since f_x accounts for these changes connected with the transport of liquid water. So the discretization of the parabolic differential Equation (5.2) according to Crank and Nicolson (see Marsal, 1976, p. 130) for soil layer i gives

$$C_{h,i}\,(T_i^j - T_i^{j-1})/\Delta t = \quad \{\,\lambda_{h,i}\,[(T_{i+1}^j + T_{i+1}^{j-1}) - (T_i^j + T_i^{j-1})]/(\Delta z_{i+1} + \Delta z_i)$$

$$- \lambda_{h,i-1}\,[(T_i^j + T_i^{j-1}) - (T_{i-1}^j + T_{i-1}^{j-1})]/(\Delta z_i + \Delta z_{i-1}) + f_{x,i} - f_{x,i-1}\,\}/\Delta z_i$$

$$+ q_{h,i} \quad + q_{ph,i} \qquad , \qquad i=1,...,n_h \qquad . \tag{5.3}$$

Here the specification of Fig. 5.1 is used, with temperature T_i and thickness Δz_i of layer i and fluxes $f_{x,i}$ and $f_{x,i-1}$, respectively, at the upper and lower border of that layer. The upper index j stands for the actual time step, for which the calculations are carried out. A non-equidistant vertical discretization is used with small Δz_i at the top and thick layers in the deeper soil. For sake of simplicity, the calculations are usually expanded down to a depth of about 12 m, since the lower boundary condition can be taken as constant there.

$$\begin{array}{ll}
\underline{\hspace{4cm}} & \downarrow f_{h,0}, \;\; f_{w,0}, \;\; f_{v,0} \\
\Delta z_1, \quad T_1, w_1, \rho_{v,1} & \\
\text{-----------------------} & \downarrow f_{h,1}, \;\; f_{w,1}, \;\; f_{v,1} \\
\Delta z_2, \quad T_2, w_2, \rho_{v2} & \\
\text{-----------------------} & \downarrow f_{h,2}, \;\; f_{w,2}, \;\; f_{v,2} \\
\quad\quad .... & \quad\quad .... \\
\text{-----------------------} & \downarrow f_{h,i-1}, f_{w,i-1}, f_{v,i-1} \\
\Delta z_i, \quad T_i, w_i, \rho_{v,i} & \\
\text{-----------------------} & \downarrow f_{h,i}, \;\; f_{w,i}, \;\; f_{v,i} \\
\Delta z_{i+1}, \quad T_{i+1}, w_{i+1}, \rho_{v,i+1} & \\
\text{-----------------------} & \downarrow f_{h,i+1}, f_{w,i+1}, f_{v,i+1}
\end{array}$$

Fig. 5.1   The discretization scheme for soil heat and water transport

The Equations (5.3) can easily be rearranged to the tri-diagonal form

$$A^*_i \, T_{i-1} + B^*_i \, T_i + C^*_i \, T_{i+1} = D^*_i \qquad , \qquad i=1,...,n_h \qquad , \tag{5.4}$$

where A^*_i, B^*_i and C^*_i form the tri-diagonal matrix and D^*_i is the right-hand side vector with the known components. The temporal index j of each unknown T is omitted in (5.4) for sake of clarity. For the solution of (5.4) a recursive procedure is used (see Marsal, 1976, p. 116)

$$T_i = a_i - b_i \, T_{i+1} \qquad , \tag{5.5a}$$

with

$$a_i = (D^*_i - A^*_i \, a_{i-1})/(B^*_i - A^*_i \, b_{i-1}) \tag{5.5b}$$

and

$$b_i = C^*_i/(B^*_i - A^*_i \, b_{i-1}) \qquad . \tag{5.5c}$$

At the upper boundary, the soil heat flux G, calculated according to Section 3.1, is given and $A^*_0 = 0$ is used in the recursion. At the lower boundary a constant temperature (of about 9 °C) below the lowest layer in the calculation and therefore $C^*_{nh} = 0$ is used.

The time step Δt initially is set equal to half the time constant

$$\Delta t_c = (\Delta z_1)^2 \, C_{h,1}/\lambda_i \qquad\qquad\qquad\qquad\qquad\qquad\qquad\qquad (5.5d)$$

of the uppermost soil layer. Then the expected change of the surface temperature ΔT_{sa} is calculated from the energy balance of the soil surface (3.4) and its heat capacity. The initial time step is doubled whenever one of the following conditions holds:

-       if the temperature change ΔT_{sa} is less than 0.2 K,
-       if the change of the soil heat flux is less than 20 W m^{-2} and
-       if the soil heat flux does not exceed 50 W m^{-2}.

In this way some few cycles are calculated until the time steps sum up to the global time step Δt_g, which is commonly set to 900 s or 3600 s depending on the temporal resolution of the boundary conditions.

5.2   The treatment of soil chill

In the calculation of the soil heat budgets, the heat for melting and freezing of water in the soil layers is taken into account in the following way. For each soil layer three states are distinguished: liquid, freezing/melting ("f/m") and frozen.

The melting or freezing heat is added or extracted, until the whole freezing heat

$$Q_{ph,i} = \rho_w \, C_{ph} \, w_i \, \Delta z_i \qquad\qquad\qquad\qquad\qquad\qquad\qquad\qquad (5.6)$$

of the soil layer is achieved ($C_{ph} = 332 \cdot 10^3$ J/kg specific latent heat of melting, w_i volumetric soil water content, $\rho_w = 10^3$ kg/m^3 density of liquid water). In this state, the soil temperature T_i is kept constant at the level of the freezing temperature T_{ph}, usually taken as $T_{ph} = 0$ °C.

The fixing of the soil temperature T_i at T_{ph} is achieved by defining the coefficients $A^*_i = C^*_i = 0$, $B^*_i = 1$ and $D^*_i = T_{ph}$ in (5.4). The latent heats of freezing ($q_{ph,i} > 0$) and melting ($q_{ph,i} < 0$), respectively, are calculated from

$$q_{ph,i} = (f_{h,i} - f_{h,i-1}) \, \Delta t \qquad\qquad\qquad\qquad\qquad\qquad\qquad\qquad (5.7)$$

and cumulated until the maximum possible amount of freezing heat $Q_{ph,i}$ is obtained. The proper

transitions between the three states of water - liquid, freezing/melting and frozen - in each soil layer i are managed with the help of the following controls:

- If in the liquid ($q_{ph,i}=0$) or frozen state ($q_{ph,i}=Q_{ph,i}$) the temperature T_i^j calculated from (5.5) deviate from T_{ph} by more than 0.05 K, then the soil heat budget calculation is interrupted and repeated with a smaller time step, in order to avoid the phase transition. For the marginal transitions, the excess heat capacity density

$$Q_{e,i} = C_{h,i} \, (T_{ph} - T_i^j) \, \Delta z_i \tag{5.8a}$$

is added to the freezing heat density

$$q_{ph,i}{}^j = q_{ph,i} + Q_{e,i} \qquad , \tag{5.8b}$$

where $C_{h,i}$ is the volumetric specific heat (see Section 5.3) and T_i^j is set to T_{ph}.

- If the cumulated latent heat of freezing $q_{ph,i}$ (5.7) exceeds $Q_{ph,i}$ during freezing, then the excess is converted into latent heat, giving

$$T_i^j = T_{ph} - (q_{ph,i} - Q_{ph,i})/(\Delta z_i \, C_{h,i}) \qquad , \tag{5.9a}$$

and $q_{ph,i}$ is set to $Q_{ph,i}$.

- If the cumulated heat of freezing $q_{ph,i}$ goes beyond zero during melting, then the excess is converted into latent heat, giving

$$T_i^j = T_{ph} - q_{ph,i}/(\Delta z_i \, C_{h,i}) \qquad , \tag{5.9b}$$

and $q_{ph,i}$ is set to zero.

This procedure involves a simplification since soil water usually is not pure but consists of solutes, which lead to a reduction of freezing temperature. Moreover, most of the soil water is more or less bound to the soil particles, which leads to an additional reduction of freezing temperature for parts of the soil water. However, in spite of this simplification, under humid conditions in "normal agricultural situations", freezing is satisfactorily modeled (see Section 6.3).

5.3   Thermal soil properties and soil composition

The thermal properties of the individual soil layers depend on the composition of the soil, namely, the quantities of different mineral and organic matter and of water. Though the specific heat and the thermal conductivity are calculated for each individual soil layer, the index of the individual layer is omitted hereafter for clarity. The volumetric specific heat C_h (see Equation 5.2) is the sum of the specific heats C_q, C_m, C_o and C_w of the constituents

$$C_h = C_q \; \varphi_q + C_m \; \varphi_m + C_o \; \varphi_o + C_w \; w \qquad\qquad , \qquad\qquad\qquad (5.10)$$

where w, φ_q, φ_m and φ_o are the volume fractions of **w**ater, **q**uartz, other **m**inerals, and organic matter, respectively. According to de Vries (1963) for the specific heats of the individual constituents the quantities listed in Tab. 5.1 are used in the model (see Campbell, 1985).

Table 5.1   The specific heats and densities of the main soil constituents

material	quartz	clay minerals	organic matter	water	ice	
volumetric specific heat	C_q=2.13	C_m=2.39	C_o=2.50	C_w=4.18	1.73	MJ/(m^3 K)
density	ρ_q=2.66	ρ_m=2.65	ρ_o=1.30	ρ_w=1.00	0.92	g cm^{-3}

Because of the low density, the specific heat of air is more than three orders of magnitude smaller and is neglected.

For the calculation of thermal conductivity λ_h a method given by Campbell (1985, p. 32) is used based on results of de Vries (1963) and Mc Innes (1981).

$$\lambda_h = A + B \, w + (D - A) \, \exp[-(Cw)^E] \qquad\qquad\qquad\qquad (5.11)$$

The coefficients A, B, C and D are related to soil properties more or less empirically, and E=4 is used. With the volume fraction of solids

$$\varphi_s = \varphi_q + \varphi_m + \varphi_o$$

$$(5.12a)$$

the coefficients are calculated from

$$A = (0.57 + 1.73\,\varphi_q + 0.93\,\varphi_m)/(1 - 0.74\,\varphi_q - 0.49\,\varphi_m) - 2.8\,\varphi_s(1 - \varphi_s) \qquad (5.12b)$$

$$B = 2.8\ \varphi_s \qquad , \qquad\qquad\qquad\qquad\qquad\qquad\qquad\qquad\qquad (5.12c)$$

and

$$D = 0.03 + 0.7\varphi_s{}^2 \qquad . \qquad\qquad\qquad\qquad\qquad\qquad\qquad (5.12d)$$

With the mass fraction m_c of clay (particle size diameter $< 2\ \mu$m)

$$C = 1 + 2.6\ (m_c)^{-1/2} \qquad\qquad\qquad\qquad\qquad\qquad\qquad\qquad (5.12e)$$

is used.

Some examples of the shapes of thermal conductivities $\lambda_h(w)$ are given in Fig. 5.2 for sandy loam (φ_q=0.45, φ_m=0.15 and m_c=0.01, 0.02 and 0.03) and clay loam (φ_q=0.25, φ_m=0.25 and m_c=0.30). For low clay contents, a marked increase of the conductivities for low water contents is due to the formation of heat conducting bridges by water films between neighbouring soil particles (see de Vries, 1975). Since the thermal conductivity $\lambda_{h,i}$ (in Equation 5.3) refers to heat transport between the layers i and i+1, the results of (5.11) are weighted for i≥1 with the corresponding thicknesses Δz_i and Δz_{i+1} of the layers to give $\lambda_{h,i}$.

Thermal soil conductivity after Campbell (1985)
(————): sandy loam (q=.45;m=.15;t=.01,.02,.03)
(------): silt loam (q=.25;m=.25;t=.30)

Fig. 5.2   Thermal soil conductivities after Campbell (1985)
_____: sandy loam
-----------: clay loam

Different representations characterizing soil composition have to be converted because the thermal properties are related to the mineral composition, and the hydraulic properties depend on the particle size distribution. Moreover, soil compositions may be given in different forms, either as mass or volume fractions φ_i of materials, or as masses of particle size

fractions m_i . The main particle size fractions considered in the model are listed in Tab. 5.2 according to the German classification. The conversion to the U.S.D.A. classification, that uses d=0.05mm as the boundary between silt and sand, is performed with $m_{s,US} = m_{s,G} + 0.0666 \, m_{u,G}$ (Diekkrüger, pers. communication).

Table 5.2   The main particle size classes (German classification)

fraction	particle size diameter	arithmetic mean	mass fraction
clay	$d < 0.002$ mm	$d_c = 0.001$ mm	m_c
silt	$0.002 \leq d < 0.063$ mm	$d_u = 0.0325$ mm	m_u
sand	$0.063 \leq d \leq 2$ mm	$d_s = 1.0315$ mm	m_s

The solid materials considered in the model are organic matter $(m_o , \varphi_o)^{*)}$, quartz (m_q , φ_q) and other minerals (m_m , φ_m) including clay minerals and feldspar, see Tab. 5.1. The three representations of input compositions are listed in Tab. 5.3, where

$$\rho_b = \rho_q \, \varphi_q + \rho_m \, \varphi_m + \rho_o \, \varphi_o \qquad\qquad (5.13)$$

is the dry bulk density. For these quantities the relationships

$$m_s + m_u + m_c = 1 \qquad\qquad (5.14a)$$

for the masses of particle sizes fractions (sand, silt and clay) and

$$m_q + m_m + m_o = 1 \qquad\qquad (5.14b)$$

for the mass fractions $m_i = \rho_i \, \varphi_i$ (i=q,m,o) of the minerals (**q**uartz, other **m**inerals and **o**rganic matter) hold. Moreover, a link between particle sizes and minerals is recommended for the conversion. This is taken from Scheffer und Schachtschabel (1992, Fig. 32), where the average mass fractions of minerals is related to the particle size fractions for soil under moderate humid climates. From that figure the relationship

---

*)   Instead of organic matter contents m_o often organic carbon content C_{org} is given as input
      parameter. For conversion $m_o = 1.72 \, C_{org}$ is used.

$$m_q/(m_q + m_m) = 0.84\, m_s + 0.56\, m_u + 0.08\, m_c \qquad (5.14c)$$

is evaluated. With the help of (5.13) and (5.14) the input representations for the composition (Tab. 5.3) of each soil layer are converted into the recommended other variables. In the third case m_c has to be chosen in consistence with (5.14c).

Table 5.3   The three possible input representations of soil compositions

1.)	m_u, m_c, m_o or φ_o, ρ_b
2.)	m_q, m_c, m_o or φ_o, ρ_b
3.)	φ_q, m_c, φ_o, φ_m

5.4   Liquid soil water transport: basic equations and solution

The driving force for the liquid water transport in the soil is the gradient of the total water potential ψ_t. The total water potential is the potential energy per unit mass (or volume) of water compared to that of free water and will be expressed in J/kg. Since the dimension is equal to that of a pressure, it is frequently expressed in pressure units Pa, bar or even as the equivalent height of a water column[*]. The total water potential ψ_t consists mainly of the matric potential ψ, the pressure potential ψ_p and the gravitational potential ψ_g, which is a function of depth z only (gravitational acceleration $g \approx 9.81$ m/s^2).

$$\psi_t = \psi + \psi_p - \psi_g = \psi + \psi_p - g\, z \qquad , \qquad (5.15)$$

Further components like the osmotic potential are neglected in this context. The matric potential arises from adhesive and cohesive forces binding the water to the soil particles and therefore depends strongly on the soil water content and the particle size distribution.

The liquid water flux density f_w can be written as

$$f_w = - K_u\, \mathrm{grad}(\psi_t) = - K_u\, \partial\, \psi_t/\partial z = - K_u\, [\partial(\psi + \psi_p)/\partial z - g] \qquad . \qquad (5.16)$$

The hydraulic conductivity K_u[**] is strongly dependent on matric potential ψ.
With the density of liquid water ρ_w (≈ 1000 kg m^{-3}), the mass-conservation for water gives

$$\rho_w\, \partial w/\partial t = - \mathrm{div}(f_w) + q_e \qquad , \qquad (5.17)$$

---

[*]   With the density $\rho_w = 10^3$ kg/m^3 of water and the gravitational acceleration $g \approx 9.81$ m/s^2 the conversion for the water potential is 1 J/kg = 1 kPa = 0.01 bar ≈ 9.81 cm of water. In the equations the units J/kg=m^2/s^2 are used.

[**]   With the flux density f_w in (kg(water) m^{-2} s^{-1}) and the water potential in (J/kg)=(m^2 s^{-2}) the hydraulic conductivity has to be expressed in (kg(water) m^{-3} s).

The combination of (5.16) and (5.17) gives a partial differential equation known as Fokker-Planck-equation. Similar to the heat budget equation, the one-dimensional water budget equation is (see Hillel, 1971, p. 110)

$$\rho_w \, \partial w/\partial t = \partial/\partial z \, \{ \, K_u(\psi) \, \partial \, \psi_t/\partial z \, \} + q_e = \partial/\partial z \, \{ \, K_u(\psi) \, [\, \partial(\, \psi + \psi_p \,)/\partial z - g \,] \, \} + q_e, \tag{5.17a}$$

where q_e (≤ 0) is an extraction term, that represents root-water uptake. With the specific water content

$$C(\psi) = \partial w(\psi)/\partial \psi \tag{5.18}$$

the variable w in (5.17a) can be eliminated if no pressure potential exists ($\psi_p = 0$) and ψ and w are uniquely related to each other, which is only is only valid in unsaturated situations (neglecting hysteresis):

$$\rho_w \, \partial w/\partial t = \rho_w \, C(\psi) \, \partial \, \psi \, /\partial t = \partial/\partial z \, \{ \, K_u(\psi) \, [\, \partial(\, \psi + \psi_p \,)/\partial z - g \,] \, \} + q_e. \tag{5.19}$$

This is the one-dimensional form of the Richards equation.

The non-explicit discretisation of (5.19) results in a tri-diagonal equation.
According to Diekkrüger (1992, p.40; see also Hornung und Messing, 1984, p...) a better consistence with the water balances is achieved by using a "Quasi-Newton"-approximation during the iterative solution of (5.19). This is done by replacing the left side of (5.19) by

$$\rho_w \, (w_i^{j,k+1} - w_i^{j-1})/\Delta t = \rho_w \, \{ \, w_i^{j,k} + C(\psi_i^{j,k})(\, \psi_i^{j,k+1} - \psi_i^{j,k})- w_i^{j-1} \, \}/\Delta t \qquad , \tag{5.19a}$$

$$= \rho_w \, \{ \, w_i^{j-1} + C(\psi_i^{j,k})(\, \psi_i^{j,k+1} - \psi_i^{j-1})- w_i^{j-1} \, \}/\Delta t$$

$$= \rho_w \, \{ \, C(\psi_i^{j,k})(\, \psi_i^{j,k+1} - \psi_i^{j-1}) \, \}/\Delta t \qquad , \tag{5.19b}$$

where the index k stands for the iteration step. Similar to the heat budget Equation (5.2), the partial differential equation (5.19) is discretized for non-equidistant soil layers according to Crank and Nicolson (implicit/explicit) using (5.19b):

$$\rho_w \, \{ \, C(\psi_i^{j,k})(\, \psi_i^{j,k+1} - \psi_i^{j-1}) \, \}/\Delta t \, =$$

$$\{ \, K_{u \, i}' \, [(\psi_{i+1}'^{j} + \psi_{i+1}'^{j-1}) - (\psi_i'^{j} + \psi_i'^{j-1})]/(\Delta z_{i+1}+\Delta z_i)$$

$$- K_{u \, i-1}' \, [(\psi_i'^{j} + \psi_i'^{j-1}) - (\psi_{i-1}'^{j} + \psi_{i-1}'^{j-1})]/(\Delta z_i+\Delta z_{i-1})$$

$$- g \, (K_{u \, i}' + K_{u \, i-1}') \, \}/\Delta z_i + q_{e,i}^{j-1} \qquad . \tag{5.20}$$

Here, Δz_i is the thickness of the layer i and j stands for the time step. Because of its strong variation the hydraulic conductivity $K_{u \, i}'$ in Eq. (5.20) is determined by geometrical averaging

$$K_{u \, i}' = (K_{u,i} \, K_{u,i+1})^{1/2} \qquad . \tag{5.21}$$

The tri-diagonal system of linear equations resulting for the layers $i=1,...,n_w$ is solved by recursion similar to (5.5). Because of the non-linearities of $K_u(w)$ and $C(\psi)$ (see Section 5.5), an iteration has to

be carried out:

> At first, $K_{u,i}$ and $C(\psi_i)$ are calculated at $\psi_i^{j,k=0} = \psi_i^{j-1}$ from the preceding time step. The solution of (5.20) is repeated with $K_{u,i}(\psi_i^{j,k})$ and $C(\psi_i^{j,k})$ at

$$\psi_i^{*j,k} = [\psi_i^{j-1} + (\psi_i^{j,k-1} + \psi_i^{*j,k-1})/2]/2$$

> until any successive iterative estimates of $\psi_i^{j,k}$ and $w_i^{j,k}$ from the last iteration ($\psi_i^{j,k-1}$, $w_i^{j,k-1}$) do not deviate by more than $\triangle\psi_{it}=0.1$ J/kg and $\triangle w_{it}=0.001$, respectively.

Since the hydraulic properties $K_u(w)$ and $\psi(w)$ are not sufficient to restrict matric potentials below saturation, the matric potentials are explicitly forced to that limit. In case of infiltration saturation can occur in the upper soil layers, which is solved separately. For the unsaturated layers below (5.20) is used.

In contrast to (5.21) the hydraulic conductivities now are calculated as arithmetic mean values

$$K_{u\,i}' = (K_{u\,i}^*(\psi_i^{j-1}) + K_{u\,i}^*(\psi_i^{j,k+1}))/2 \tag{5.21b}$$

with $K_{u\,i}^*$ calculated from the sum of the corresponding resistances in series

$$K_{u\,i}^* = (\triangle z_{i+1}+\triangle z_i)/(\triangle z_{i+1}/K_{u\,i+1} + \triangle z_i/K_{u\,i}) \qquad . \tag{5.21c}$$

At the lower boundary, a constant water content has to be given below z_{nw}. At the upper boundary, water contents are modified externally: augmented by precipitation or diminished by soil evaporation (see Section 3.6). The amount of precipitation that cannot infiltrate at the moment remains on the soil surface and the model attempts to infiltrate during subsequent time steps. To allow for surface runoff a very simple approach is used: Water runs off from the surface, if

$$w_{su} > d_g/2 \cos (2\lambda) \qquad , \tag{5.22a}$$

where w_{su} is the quantity of water (in kg m^{-2} = mm$_{(H2O)}$) standing at the surface with the slope λ and the characteristic length (in mm) of the surface structure (see Eq. 3.30f).

The time step used in the soil water calculation is determined according to the actual amount of change at the upper boundary. If this time step is less than the global model-time step, the whole calculations are repeated step by step, until the single time steps of the water sub-model cumulate to the global time step.

5.5   The hydraulic soil properties; Pedo-transfer functions

The hydraulic properties - matric potential and hydraulic conductivity - depend most of all on the particle size distribution of the soil and on the (volumetric) water content. For the retention functions $\psi(\theta)$ the parameterization

$$\psi(\theta) = (\theta^{-1/m} - 1)^{1/n}/\alpha \tag{5.23}$$

can be used (van Genuchten, 1980), where α, m and n are constants and

$$\theta = (w - w_r)/(w_s - w_r) \tag{5.24}$$

is the relative water content with the residual water content w_r and the saturated water content w_s. From theoretical considerations Mualem (1976) related the hydraulic conductivity K_u to an integral of the retention function by

$$\tag{5.25}$$

that can be solved analytically for integer values m-1+$1/n$ (van Genuchten, 1980), giving

$$K_u(\theta) = K_s\, \theta^{\frac{1}{2}} \left[1 - (1 - \theta^{1/m})^m \right]^2 \tag{5.25a}$$

The saturated hydraulic conductivity K_s as well as the coefficients of (5.23) and (5.24) have to be determined empirically.

A simpler parameterization for the matric potential has been proposed by Brooks and Corey (1966)

$$\psi(\theta) = \psi_b\, \theta^{-b} \qquad \text{for} \qquad 0 < \theta \leq 1 \tag{5.26}$$

where ψ_b is the "bubbling pressure", the water potential at which the largest water filled pores in the soil begin to drain. For $\psi \leq \psi_b$ the soil is assumed to be saturated (θ=1). This discontinuity of the derivate of ψ at θ =1 was overcome by Smith (1992) using (5.23) instead of (5.26) with m =1/(5b), n=5 and α =$1/\psi_b$.

For the hydraulic conductivity the alternative relation

$$K_u(\theta) = K_s \, \theta^a \tag{5.27}$$

has been proposed by Brooks and Corey (1964) and by Campbell (1974).

Another form of the hydraulic conductivity relation, expressed by the water potential, has already been proposed by Gardner (1958).

$$K_u(\psi) = K_s \, / [b \, (|\psi|^v + b)] \tag{5.28}$$

Several methods have been proposed for the relation of hydraulic properties to soil properties that can be more easily obtained: The so-called pedo-transfer functions give parameterizations for the determination of the coefficients used in the above relations from basic soil properties (Tietje and Tapkenhinrichs, 1993). Whereas most of the methods are empirical, Campbell's method (1985, p. 45) is physically-based. Using (5.24) with the residual water content $w_r=0$ and the saturation water content

$$w_s = 0.93 \, (1 - \rho_b/\rho_s) \tag{5.29}$$

with the particle density ρ_s of solids[*], Campbell (1985, p. 45) relates the coefficients of (5.26 and 5.27) to the dry bulk density ρ_b (5.13, given in g cm^{-3}) and the particle size distribution (Tab. 5.2). The "bubbling pressure" ψ_b is set to

$$\psi_b = \psi_{es} \, (\rho_b/1.3)^{0.67 \, b} \tag{5.30a}$$

with

$$\psi_{es} = -0.5 \, d_g^{-1/2} \tag{5.30b}$$

where d_g is in mm, ψ_{es} in J/kg and for b in (5.26) and (5.30) the following expression is used

$$b = -2 \, \psi_{es} + 0.2 \, \sigma_g \quad . \tag{5.30c}$$

---

[*] As usual the particle density of solids is assigned to $\rho_s=\rho_m=2.65$ g cm^{-3}, see Tab. 5.1.

For the exponent in (5.27) Campbell (1974) gives $a = 2\,b + 3$.

Here d_g and σ_g are the geometric mean and standard deviation of the particle size diameters

$$d_g = \exp(d') \tag{5.31a}$$

and

$$\sigma_g = \exp(\sigma') \tag{5.31b}$$

with the abbreviations

$$d' = \Sigma\; m_i \ln^2(d_i) \tag{5.31c}$$

and

$$\sigma' = [\; \Sigma\; m_i \ln^2 (d_i) - d'^2 \;]^{1/2} \qquad . \tag{5.31d}$$

The summations include all regarded classes of particle sizes, in this case i=c,u,s (see Tab. 5.2).

Campbell's physically-based method (1985) has already been implemented in preliminary versions of the model AMBETI. To date the model offers the optional choice of the pedo-transfer functions of Vereecken et al. (1989), Vereecken et al. (1990) and of Rawls and Brakensiek (1985), which have proven to be the most suitable methods (Tietje und Hennings, 1993; Tietje and Tapkenhinrichs, 1993). In all cases, the demand of input parameters is restricted to the main soil texture classes since finer classifications are generally not available.

Rawls and Brakensiek (1985) give empirical relations for coefficients used in the retention functions (5.23) and (5.26) as well as for the hydraulic conductivities (5.25a) and (5.27) proposed by van Genuchten (1980) and Brooks and Corey (1966, 1964), respectively. For these relations clay and sand contents and total porosity are needed as input data.

Vereecken et al. (1989) and Vereecken et al. (1990) use the van Genuchten functions (5.23) with m=1 and relates the remaining coefficients to the same soil properties and organic matter content. From these input parameters the coefficients of the hydraulic conductivity (5.28) are derived according to Vereecken et al. (1990) (see Appendix A 5.1). In the corresponding method No.3 (see Tab. 5.4) K_u is

log-linearly interpolated in the region of high water contents for $0.10 < |\psi| < 1.0$ J/kg between K_s and the value resulting from (5.28) for $\psi_x = 1$ J/kg.

$$K_u(\psi) = K_s \exp\{ \log_{10}(|\psi|) [\ln(K_u(\psi_x)) - \ln(K_s)] \} . \qquad (5.28a)$$

Including the modification of the Brooks and Corey function proposed by Smith (1992), five different sets of pedo-transfer functions are available in the model AMBETI (see Tab. 5.4).

Table 5.4   The available methods and pedo-transfer functions

no.	method	retention	conductivity	recommended input
1	Campbell	(5.26), $w_r = 0$	(5.27)	m_c, m_u, ρ_b
2	R.-B./v.Gen.	(5.23)	(5.27)	m_c, m_u, ρ_b
3	Vereecken	(5.23), $m = 1$	(5.28)	m_c, m_u, ρ_b, m_o
4	R.-B./Br.-Cor.	(5.26)	(5.27)	m_c, m_u, ρ_b
5	R.-B./Smith	(5.23)	(5.27)	m_c, m_u, ρ_b
		$(n=5, m = (5b)^{-1})$		

Since the retention functions of Vereecken et al. (1989) are the most reliable (see Tietje and Hennings, 1993), this method is the best choice if the organic matter contents[*] m_o seem to be given sufficiently accurate. In Fig. 5.3, the Vereecken functions are presented for three different values of m_o (0.5, 1.0 and 1.5%). Obviously the influence of the organic matter content is not strong.

The relations given by Rawls and Brakensiek (1985) and by Vereecken et al. (1989, 1990) for the pedo-transfer coefficients can be found in Appendix A 5.1.

The retention functions in general show realistic behaviour only for water contents below the wilting point. For the calculation of soil water vapour transport, including evaporation, it is important that the retention functions reach matric potentials ψ_0 of about 10^6 J/kg (= pF7[**]) for $w \le w_{WP}$ (see Section 5.6). For this reason the retention functions are log-linearly interpolated beyond wilting point (ψ_{WP}, w_{WP}) according to

---

[*]   Organic matter contents are also recommended for the relations of the thermal soil properties (see section 5.3).

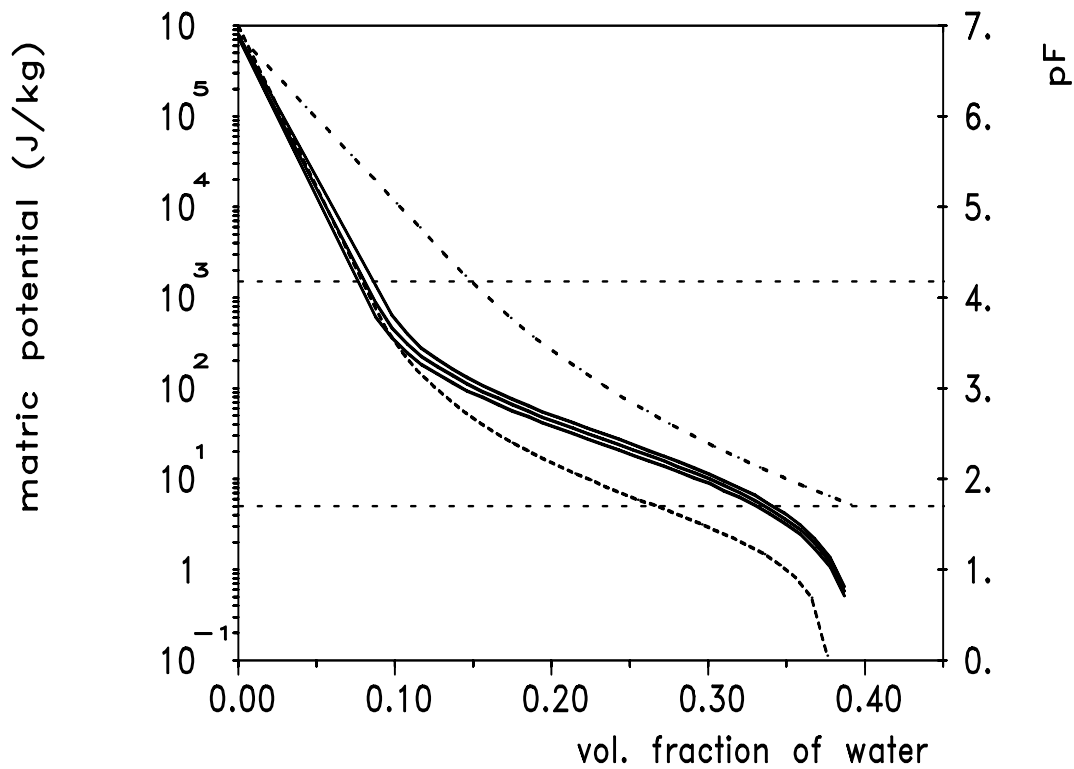[**]   pF is the decadic logarithm of the absolute water potential expressed in cm of water.

Fig. 5.3   Retention functions after van Genuchten (------); Campbell (- - - -);
                   Vereecken (_____) , dashed lines: ψ_{FK} (pF1.7), ψ_{WP} (pF4.2)

$$\psi(w) = \psi_0 \exp\{ \, [\, \ln(-\psi_{WP}) - \ln(-\psi_0) \,] \, w/w_{WP} \, \} \qquad . \qquad\qquad (5.32)$$

The influence of temperature on the hydraulic conductivities is subsequently described by a decrease
with **absolute** temperature for temperatures above freezing point

$$K_u(T,w) = K_u(w) \, (T/T^*)^6 \approx K_u(w) \, [\, 1 - 6 \, (\, 1 - T/T^*) \,] \qquad , \qquad\qquad (5.32a)$$

which reveals the predominant influence of viscosity (Campbell, 1985, p. 54). The value T^*=283 K is
assumed as reference temperature for K_u . Below freezing point the previously easily moveable water
is assumed to be frozen and therefore hydraulic conductivities are set to an extremely low value

$$K_u(T,w) = 10^{-13} \, \text{m}^3 \, \text{m}^{-2} \, \text{s}^{-1} = 1.16 \, {}_{10}{}^{-20} \, \text{cm/day} \qquad , \qquad\qquad (5.32b)$$

which effectively stops any water movement.

5.6   Water vapour transport in the soil and at the soil surface

Besides liquid water transport described above, the model AMBETI also accounts for the water vapour transport in the soil. This is an important prerequisite for the proper determination of soil evaporation and the drying of the uppermost soil layers. The vertical vapour transport in the soil layers is driven by the gradient of vapour concentration in the air-filled pore space $\varphi_a = 1 - \varphi_s - w$ of the soil. The saturation water vapour content for water under potential $\psi < 0$ is

$$\rho_{vs}(T, \psi) = \rho_{vs}(T)\, h_r(T, \psi) \tag{5.34a}$$

with the saturated water content $\rho_{vs}(T)$ of unstressed water and the reduction function (Slavik, 1974, p. 10)

$$h_r(T, \psi) = \exp\{\ \psi/(R_w\, T_{abs})\ \} \qquad\qquad , \tag{5.34b}$$

where $R_w = 461.5$ J kg^{-1} K^{-1} is the gas constant for water. This function remarkably reduces the vapour content only below wilting point ($\psi = -1.5$ kJ/kg), as can be seen from Fig. 5.4.

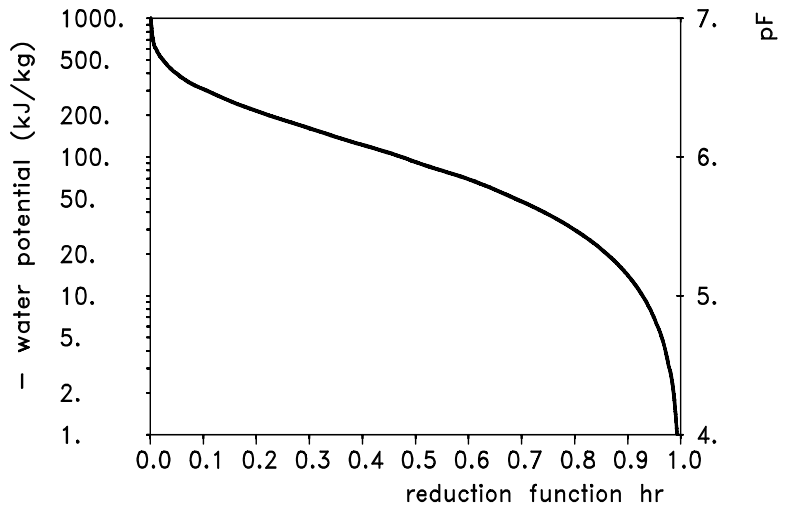The vertical vapour flux density is taken as proportional to the gradient of the vapour content

Fig. 5.4   The reduction function h_r for stressed water (T=17 °C)

$$f_v = -\, D_{vs}\, \partial \rho_v / \partial z \qquad\qquad . \tag{5.35}$$

According to Campbell (1985, p. 100) the vapour diffusivity D_{vs} in the soil is taken as

$$D_{vs} = 0.66\ \varphi_a\, D_v \qquad\qquad , \tag{5.35a}$$

where D_v is the water vapour diffusivity in air ($D_v = 2.12 \times 10^{-5}$ m^2/s at normal temperature and pressure).

The temperature dependence is the same as in (5.32a).

The diffusivities for the thermally induced soil vapour transport have long been known to exceed D_{vs} (Philip and de Vries, 1957). The reasons are local microscopic temperature gradients exceeding the macroscopic ones, as well as multiple condensation and evaporation of vapour at liquid islands between the pores. These enhanced thermal diffusivities will be accounted for by an enhancement factor η, which is inserted into the flux equation (5.35) after the expression of ρ as total differential

$$f_v = f_{vT} + f_{v\psi} = -\eta\, D_{vs}\, (\partial\rho_v/\partial T)(\partial T/\partial z) - D_{vs}\, (\partial\rho_v/\partial\psi)(\partial\psi/\partial z). \tag{5.36}$$

Since the temperature dependence of the reduction function can be neglected for $h_r > 0.1$ ($|\psi| < 300$ kJ/kg), the flux densities simplify to

$$f_{vT} = -\eta\, D_{vs}\, h_r\, (\partial\rho_{vs}/\partial T)(\partial T/\partial z) = -\eta\, D_{vs}\, h_r\, (\partial\rho_{vs}/\partial z) \qquad , \tag{5.37a}$$

$$f_{v\psi} = -\, D_{vs}\, \rho_{vs}\, (\partial h_r/\partial\psi)(\partial\psi/\partial z) = -\, D_{vs}\, \rho_{vs}\, (\partial h_r/\partial z) \qquad . \tag{5.37b}$$

With the help of heat conductivity measurements Cass et al. (1984) determined the enhancement factor η as a function of the water content w in m^3/m^3 and the clay content m_c in kg/kg

$$\eta = 9.5 + 6\, w - 8.5\, \exp\{-(C\, w/w_s)^4\} \tag{5.38}$$

with

$$C = 1 + 2.6\, (m_c)^{-1/2} \qquad . \tag{5.38a}$$

Due to similar physical mechanisms, the enhancement factor η has a shape similar to the thermal conductivity (Fig. 5.2). The water vapour flux densities are calculated from the discretized form of (5.37) and considered in the water budgets.

In the above treatment, the vapour contents inside the pore spaces of each layer are assumed to be in equilibrium with the respective saturation contents of the stressed water according to (5.34a).

In contrast, evaporation results in a reduction of top soil vapour contents $\rho_{v,i}$ relative to the saturated

values. The evaporative flux at the surface is calculated in a second step without the enhancement factor and without allowing for vapour condensing from other layers.
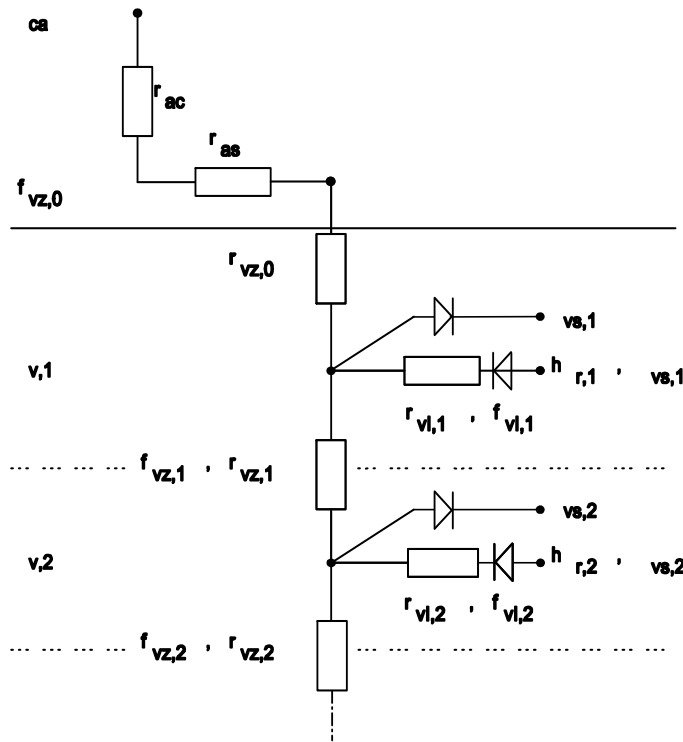

Dew is calculated with the help of (5.35) and the aerodynamic surface resistance, if the dew point above the soil surface exceeds the dew point of one layer and vapour content above the soil surface is lower than the saturated water content ρ_{vs} h_r (5.34a) of the layers above.

Evaporation is calculated, if the vapour content inside the canopy or at the reference height (see Sections 3.2, 3.3), is lower than the actual vapour content in one of the upper soil layers.

Fig. 5.5   The resistance network used for the calculation of soil vapour transport

This is done with the help of the resistance network shown in Fig. 5.5. The entities r_{ac} and r_{as} are the resistances for the turbulent and laminar transport above the soil surface, see Figs. 3.1 and 3.2. The vertical vapour transport between adjacent soil layers is described by the resistances $r_{vz,i}$. The resistances $r_{vl,i}$ describe the vapour flux inside layer i between the liquid and the gaseous phase, where the small resistance of the diodes in parallel accounts for the condensation in the case of $\rho_{v,i} > \rho_{vs,i}$. For the flux densities

$$f_{vz,i} = (\rho_{v,i} - \rho_{v,i+1})/r_{vz,i} \tag{5.39a}$$

the resistances r_{vz} are calculated from the distances of the centers of the layers and the respective diffusivities

$$r_{vz,i} = (\Delta z_i/D_{vs,i} + \Delta z_{i+1}/D_{vs,i+1})/2 \qquad . \tag{5.39b}$$

At the top layer

$$f_{vz,0} = (\rho_{ca} - \rho_{v,1})/(\Delta z_1/(2\,D_{vs,1}) + r_{ac} + r_{as}) \tag{5.39c}$$

is the evaporative flux in the "microclimate" option (see Section 3.3). For the vapour transport out of layer i

$$-f_{vI,i} = -(\rho_{v,i} - \rho_{vs,i}\, h_{r,i})/r_{vI,i} \qquad , \tag{5.40a}$$

the resistance

$$r_{vI,i} = 0.1\ \Delta z_i/D_{vs,i} \tag{5.40b}$$

is used. Repeated consideration of a vapour flux into a layer, that has already been taken into account with (5.37), is prevented by setting $r_{vI,i}$ to infinity, if $\rho_{v,i}$ is going to exceed $\rho_{vs,i}\, h_{r,i}$. This is represented in Fig. 5.5 by the diodes in series with the resistance.

With the balance equation

$$f_{vz,i-1} = f_{vz,i} + f_{vI,i} \tag{5.40c}$$

a tri-diagonal equation system results, which is solved as described in Section 5.1.

The evaluations of (5.39) and (5.40) are restricted down to the depth where evaporation still reduces $\rho_{v,i}$ relative to $\rho_{vs,i}\, h_{r,i}$. This procedure guarantees that the fluxes induced by temperature and water potential gradients f_{vT} and $f_{v\psi}$ (5.37), respectively, are not taken into account twice.

The method described is an elaborated model of the complex phenomena in the top soil that govern evaporation.

6   The use of the model AMBETI

In addition to the description of the model AMBETI given in the previous chapters, this chapter gives some information important for the use of the model. In Section 6.1, the different types of input quantities are discussed. Two different versions for the supply with these input quantities exist. One has been developed especially for the purpose of agrometeorological advice in the environment of the program system AMBER (Löpmeier, 1990). This version is called BEKLIMA[*], since it is used for the calculation of the microclimatic conditions inside the canopy and the soil. It is usually run with synoptic or forecast data as meteorological boundary conditions. The data structure for BEKLIMA is consistent to the one used in the AMBER system. The other version (AMBETI) yields some more possibilities for modifications of model parameters, that are set to fixed values in the BEKLIMA version. For both versions, the recommended file structure is described in Section 6.2. Finally, Section 6.3 gives some examples of the results of the model. These results are usually time courses of the respective quantities from several days or even weeks. Additionally, the model runs had normally been started some days or even weeks before the presented period. For this reason, the computing needs are of interest.

The typical computing time for the simulation of one day with the global time step Δt_g=15 minutes is 0.35 s on a HP9000/735 workstation and with Δt_g=1 h about 2 s on a 486DX computer with 40 MHz.

6.1   The recommended input quantities

The model AMBETI requires a variety of different input quantities, which may be divided into

-        parameters controlling the model run,

-        parameter describing the site (soil and canopy),

-        starting values and

-        meteorological boundary conditions.

Besides the names of the files to be read, the dates for the start and stop of the model run belong to the

---

[*] for canopy climate (in German 'Bestandsklima')

first class of input parameters. Since the other control parameters are fixed in the BEKLIMA version (see Section 6.2), the following options refer only to the original AMBETI version. The global time step of the model is normally taken as the time step of the boundary conditions and read from the corresponding data. The number of soil layers used in the simulations and their individual dimensions have to be given, if the standard division of n_w=13 layers with Δz_1=0.5 cm for the uppermost layer, reaching down to 12 m is not accepted. For the simulations of the soil water, the same division of the top soil is used, usually with a restriction to a given number of layers. Finally, the method to be used in the derivation of the soil hydraulic functions from the soil composition (pedo-transfer functions, see Section 5.5) has to be chosen.

Additional input files can be given to account for irrigation, that may be supplied from above the canopy or from just above the soil surface, without considering interception. Chosen by control parameters, different forms of the model output is available: standard lists with hourly or daily data, as well as optional output of selected quantities to additional files. These are in detail:

- evaporation and transpiration,

- apparent surface temperatures (see Section 2.7) for the comparison with the corresponding remote sensing measurements,

- microclimatic conditions like leaf temperatures, air temperatures and humidities inside the canopy as well as dew and interception on the leaves and

- temperatures or water contents in the soil layers.

The recommended **parameters describing the site** (canopy and soil) are

- the height of the boundary quantities wind speed as well as air temperature and humidity,

- the zero-plane displacement and roughness length of the surface corresponding to the wind speed in case this differs from the site considered in the simulations (see Section 3.5) and

- the dry bulk densities and soil types or soil compositions (see Section 5.3) of the soil layers.

For the German soil classification the fractions of the main classes of particle sizes are given in Appendix A6.1.

If the considered surface is vegetated, the type of the vegetation, its height z_c, the number of stems/m^2, the leaf area index l_a, the distribution of the leaf inclinations, the phenological age of the plants as well as the rooting density and distribution have to be given. In the BEKLIMA version these quantities describing the vegetation can be supplied by other elements of the AMBER system.

As **starting values** the temperatures and water contents of the soil layers have to be given. If these are

not known with satisfying accuracy, it is advisable to start the simulations a sufficient number of days before the period of interest. This allows accommodation of the temperatures and water contents of the soil. In many cases it is possible to start with early spring time, assuming that the soil water is at field capacity[*]. The starting values for the soil water contents can be given either in absolute values or in portions of plant available water (the water between field capacity and wilting point $\psi=1.5$ kJ/kg corresponding to pF 4.2).

In the case of a start with soil layers or the snow cover during freezing, the respective amounts of latent heat of freezing have to be given. Moreover, dew or intercepted water on the plant elements and water standing at the soil surface can be given as starting values.

The recommended **meteorological boundary conditions** are

-        air temperature and humidity from a reference height (usually 2 m),
-        wind speed from a reference height measured above the considered surface or above a nearby
         surface (see Section 3.5),
-        precipitation and
-        global radiation.

If available, long-wave radiation can be given additionally. The other case it is parameterized from air temperature and cloud information.

Of course, the use of the parameterizations instead of measured radiation components introduces a source of inaccuracy to the model results. The same has to be kept in mind for forecast boundary conditions which are frequently used for the BEKLIMA version in the AMBER environment.

---

[*]   The field capacity is defined as the water content that cannot be drained by gravity. For most
        soils the corresponding matrix potential lies near 5 J/kg (pF 1.7, see Section 5.4).

6.2   The file structure for model runs

The supply of the model with the data described in the previous section as well as the storage of the model results are organized in different ways for the AMBETI and the BEKLIMA versions of the model. In the **AMBETI version**, which is runnable under MS-DOS as well as under UNIX systems with marginal modifications, the program first tries to read the NAMELIST[*] "DATEIEN" from a file "SYSDATA.DAT". In this NAMELIST for the following keywords a link to the corresponding filenames is expected:

'CFILK':   for control parameters and the rooting distribution,

'CFKONFI':   for parameters describing the site (soil type and composition, dry-soil reflectances), the hydraulic method to be used (see Section 5.5),

'CFNBEFI':   for the crop (type, leaf area index, canopy height),

'CFAMBMET':   for the meteorological boundary conditions.

Optionally for irrigation the keyword 'CFBEREG' is used.

Output to files can be selected with the keywords 'CF16' and 'CF18' and special control parameters. An example for the file "SYSDATA.DAT" is given in Fig. 6.1.

```
 56
&DATEIEN
 CFILK   = 'AMSTEUER.DAT'
 CFKONFI = 'AMBPAR.DAT '
 CFNBEFI = 'C:\CROPS\BEST_KAN.91'
 CFAMBMET = 'E:\DATA\DHD_BS.911'
 CFBEREG  = 'BEREG_WW.91'
 CF18    = 'BEDAT_WW.91'
 /
```

Fig. 6.1   An example of the file "SYSDATA.DAT" for MS-DOS

The **BEKLIMA version** has been created for agrometeorological advice purposes in the AMBER environment under MS-DOS[**]. Its use will be described here briefly; more details can be found in an

---

[*]   This is a FORTRAN expression, available from many compilers.

[**]   A corresponding version has been implemented under NOS-VE recently.

internal report (Löpmeier, 1990). The model runs are controlled by the file "BEKLIMA.STA"[*]. It implies two paths for the input and output of the model, the dates for the start and end of the simulations, the crop to simulate and two filename extensions corresponding to the station to calculate for (*sta*) and the weather station or grid-point of the EM[**]-forecast to supply the meteorological boundary conditions (*stb*). This allows simulations for a lot of stations and crops, since all the recommended meteorological boundary conditions are read from files of path 1 with these extensions (e.g. 'BS1'). Moreover, the height of the canopy, its leaf area index and the dates J_b and J_e of the two phenological stages for the plant senescence (see Tab. 4.1) have to be given. An example for the control file "BEKLIMA.STA" is given in Fig. 6.2.

```
 0
C:\zamf\beklima\input\1994              {=path 1}
C:\zamf\beklima\output\1994             {=path 2}
1994                                    {    > ja=94}
'bs1', 087, 172,'348',   6 , 2, 0.1, 0.5 ,-1 ,-1 ,1
{sta}    {Jb}   {Ja}  {stb}       {crop}
```
Fig. 6.2   An example for the file "BEKLIMA.STA" with additional explanations in wavy brackets

In the BEKLIMA version the **meteorological boundary conditions** are read from the following files of path 1 (*stb*='348' in the example of Fig. 6.2) with hourly values of:

-       TL_*ja*.*stb*   : reference air temperature T_r at the reference height (see Section 3.3),
-       RF_*ja*.*stb*   : reference relative humidity of the air at the reference height,
-       VV_*ja*.*stb*   : wind speed u_r at the height z_u (see Section 3.5),
-       RR_*ja*.*stb*   : precipitation,
-       RG_*ja*.*stb*   : global radiation (see Section 2.1),
-       NG_*ja*.*stb*   : total amount of clouds (see Section 2.1).

If available, even the data of the files with

-       WW_*ja*.*stb*   : weather information (key codes) (see Section 3.6) and
-       RNL_*ja*.*stb*   : the incident long-wave radiation (see Section 2.7)

are evaluated as boundary conditions. These files are direct access files with 366 records, each with the day of the year followed by 24 hourly values. The direct access easily allows the completion of the

---

[*]   In this section the small italic portions of the symbolic names are replaced by numbers or characters in the actual names.

[**]   **E**uropa-**M**odell, numerical weather prediction model of the Deutscher Wetterdienst

data during the year.

The **soil properties**

-        dry soil reflectance in the visible range,

-        dry soil reflectance in the near infra-red range,

-        mass fraction of clay particles,

-        mass fraction of silt particles,

-        mass fraction of organic matter and

-        dry bulk density

are supplied by the file "*sta*.PAR" (='bs1.PAR' in the example of Fig. 6.2). The fractions of clay and silt particles can be evaluated from the soil classification (see Appendix A6.1).

The **starting values** are supplied by the files "*sta*.BOD" or "*sta*.ZWI":

the temperatures and water contents for all soil layers considered, the amount of water or snow at the soil surface and the amount of intercepted water. The file "*sta*.BOD" is used for the initial start of the simulations. Intermediate values of the quantities are written by the model to the file "*sta*.ZWI" to allow for the continuation of the simulations during subsequent runs. These files even include the root distributions.

The state of the crop development is optionally supplied by the file "WURZ_*crop*.sta", where *crop* is the keycode of the regarded crop, chosen in "BEKLIMA.STA" (Fig. 6.2) . This file includes the days of the year of the two phenological stages J_b and J_e (see Section 4.1), the leaf area index, the height of the canopy and the rooting distribution. The file can be generated by other sub-models of the AMBER system.

The **results of the program BEKLIMA** are stored to different files. Hourly values of the resulting microclimate (see Section 3.3) are written into the following files of directory 1:

-        TLO_*ja.sta* :   the air temperature $T_{ca,o}$ in the upper part of the canopy (see Section 3.3),

-        RFO_*ja.sta* :   the relative humidity of the air at the same height,

-        TLU_*ja.sta* :   the air temperature $T_{ca,u}$ in the lower part of the canopy (see Section 3.3),

-        RFU_*ja.sta* :   the relative humidity of the air at the same height,

-        BEN_*ja.sta* :   the amount of dew or water intercepted by the plants,

-        TB05_*ja.sta* :   the soil temperature at the depth of 5 cm,

-        TB10_*ja.sta* :   the soil temperature at the depth of 10 cm.

These files have the same format as the files with the meteorological boundary conditions.

Additionally, an extract of the results giving daily overviews is written to the file "BEKLIMA.LS2" in path 2. Moreover, for plot purposes, a variety of daily results is supplemented to a direct access file "BEKLI_*ja.sta*".

6.3 Some examples for model results

This section gives some examples of results of the model AMBETI/BEKLIMA. The purpose is not to present the results themselves, but to demonstrate the broad variety of simulated quantities in the soil-plant-atmosphere system. The simulations for most of the results presented here were started several days or even weeks before the plotted period in order to make the results less sensitive to the starting values. Further evaporation courses will not be presented, since the corresponding examples can be found in Section 4.1.

At first, several profiles of hourly soil temperatures for bare soil during a sunny day are shown in Fig. 6.3. This figure gives a good impression of the model's capability to simulate the temperature regime with its strong variations in the top soil. Of course, a prerequiste for these detailed results is the fine resolution used for the top soil layers (see Section 5.1).
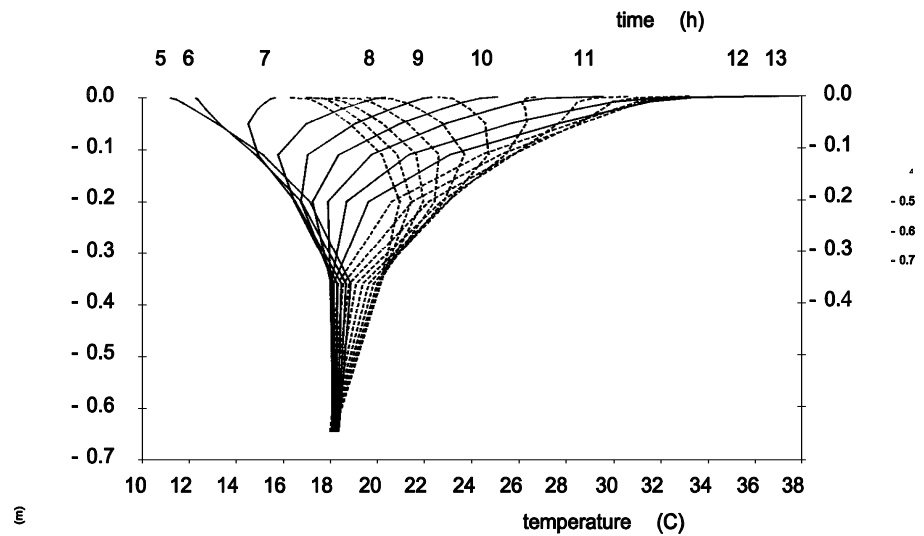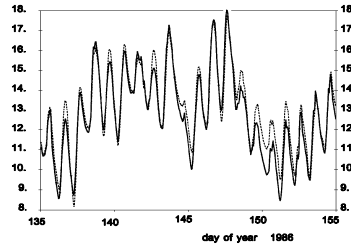

Fig. 6.3   Hourly temperature profiles for bare soil (5 h to 24 h, dashed profiles from 14 h to 24 h)

Fig. 6.4 allows the comparison of simulated and measured soil temperatures in a crop of winter barley. Generally the agreement is good. The deviations, mainly during the 149th and 150th day of year, are probably due to colder precipitation than estimated.

Fig. 6.4   Comparison of measured (-----) and simulated (____) soil temperatures in a depth of
                       5 cm below winter barley

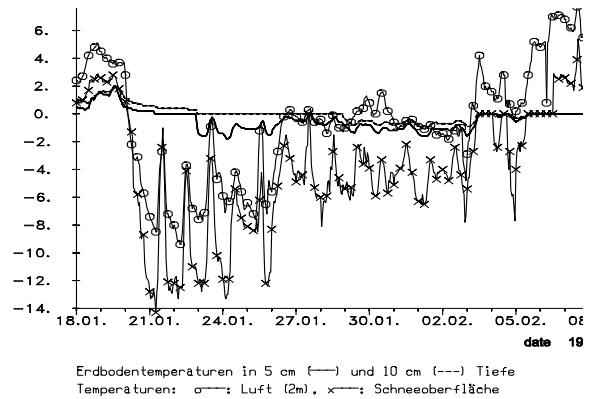**Fig. 6.5**   Soil temperatures 5 cm (____), 10cm depth (-----), x: temp. of snow surface,
                       o: air temp. (2 m)

From Fig. 6.5 the simulated courses of soil temperatures and of the temperature of the snow surface
can be compared with the boundary air temperature at 2 m. During the snow period (January 20th to
February 6th) the top of the snow surface temperature was frequently far below the air temperature, up

to 8 K during the night. At the beginning and the end of the frost period, the soil temperatures remained constant for many hours, i.e., at the phase transition temperature of 0 °C.

In a similar plot (Fig. 6.6), the simulated temperatures of the snow and soil surfaces are plotted together with the input air temperature. The snow cover began to form during the evening of January 28th. In spite of air temperatures down to -12 °C and snow surface temperatures down to even -18 °C, the temperature at the soil surface under the snow cover remained above -3 °C. Of course, this isolating effect of the snow cover is important for the surviving of pests like aphids.
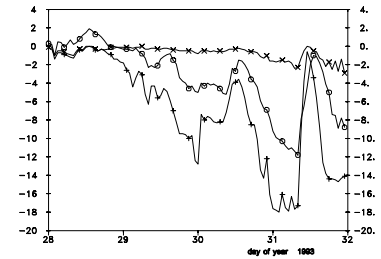
Fig. 6.6   Simulated temperatures of the soil surface (x) and the surface of the snow cover (+); o: air temp. (2 m)

Another example with soil temperatures shows a frost period during January 1993 (Fig. 6.7). Since there was no snow, the soil was deeply frozen (down to about 35cm). The simulations were run on January 6th with meteorological boundary conditions from measurements including January 4th and thereafter from the "Europa Modell" (EM) of the German Weather Service. On January 5th, the properly predicted warming occurred in northern Germany with freezing rain and glazed frost. With these boundary conditions, the model AMBETI/BEKLIMA properly simulated the presented slow warming of the soil with (static) water standing at the soil surface for several days.
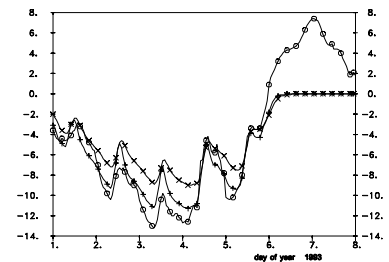
Fig. 6.7   Temperatures at Braunschweig: soil 5 cm (+), 10 cm (x), air 2 m (o)

In the last figure with soil
temperatures, the damping influ-
ence of the canopy is demonstrat-
ed (Fig. 6.8). The model has been
run twice with identical meteo-
rological boundary conditions:
once for bare soil and once for a
crop of winter wheat with the leaf
area index $l_a \approx 3$. Compared with
the bare soil, the plant cover
damped the amplitude of the 5
cm-soil temperature amplitudes
to nearly half. The amplitudes at

Fig. 6.8   Simulated courses of soil temperatures at 5 cm for
                     bare soil (+) and under winter wheat (x); o: air
                     temperature (2 m)

the soil surface (not presented) exceeded those at the depth of 5 cm by factors ranging between 1.5 and
2.4. At the bare soil surface, the maximum-minimum differences reached 34.7 K on the 5th of May.
Since the temperature, humidity and wind speed at the height of 2m, that have been used as boundary
conditions here, in reality are effected by the fluxes, it would be preferable to use input quatities from a
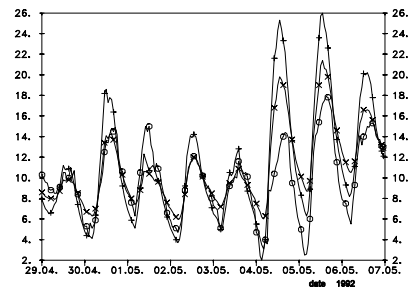higher reference height.

In Fig. 6.9 the relative humidities
measured and simulated for the
lower part of winter barley are
plotted together with the relative
humidity of the boundary condi-
tion. The simulated values are
mostly in good agreement with
the measured ones. These relative
humidities exceed the boundary
humidities from outside the
canopy by about 10% relative
humidity during the day and 20-
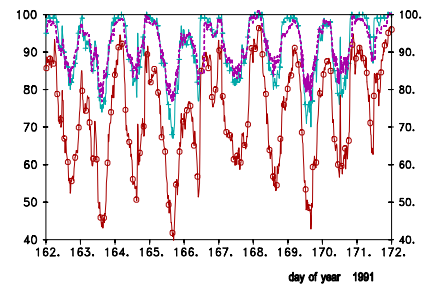30% relative humidity during the
night. Such strong differences, of

Fig. 6.9   Relative humidities for winter barley: o=reference
                     (2 m); in the lower part of the canopy:
                     measured (----); simulated (+___)

course, influence many plant diseases remarkably.

Another comparison of humidities simulated for the lower part of a crop of winter wheat is given with Fig. 6.10. Two courses of relative humidities, one for high and the other for low soil water contents, are presented together with the reference humidity. During the night the differences between the two variants are low, but d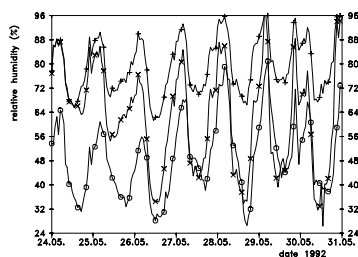uring the day the differences are up to 30% relative humidity. These effects of the soil water contents are due to the differences in transpiration as well as soil evaporation. In the moist variant, the simulated humidities exceed the boundary humidities by up to 40% r.h.. The maximum temperatures (not plotted) in the lower part of the moist crop were exceeded by 5-6 K from those of the dry crop.

Fig. 6.10   Relative humidities simulated for low (x) and high (+) soil water supply
o=reference (2 m)

Fig. 6.11 allows the comparison of measured and simulated daily durations of leaf wetness, which is an important input quantity for phytopathological models. Three sensors have been fixed to different leaves of spring barley, each of these consists of a grid of thin metal wires. In accordance with visual controls, the decrease of the electrical resistance between neighboured wires is interpreted as the beginning of leaf wetness. For the comparison with these leaf wetness sensors, leaves are interpreted as wet if the simulated amounts of dew or intercepted water exceed 0.029 mm

Fig. 6.11   Durations of daily leaf wetness in spring barley: measured (+, x, Y), simulated (----)

on the one-sided leaf area (see Sections 3.4 and 4.3). The agreement seems to be acceptable, especially if the difficulty of the measurements and the large deviations between the different sensors are taken into account.
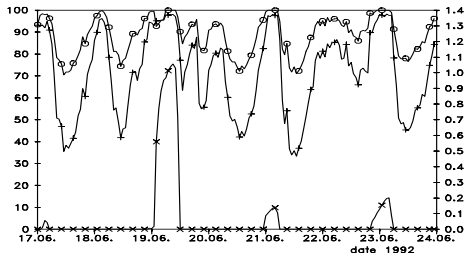
Fig. 6.12   Simulated courses of dew and interception (x) and relative humidities for the upper
                       (+) and lower (o) parts of the canopy

Simulated courses of leaf wetness are presented in Fig. 6.12 together with the relative humidities calculated for the upper and lower parts of a crop of winter wheat. During the period of nine days there were three nights with dew formation and one precipitation event (June 19th).
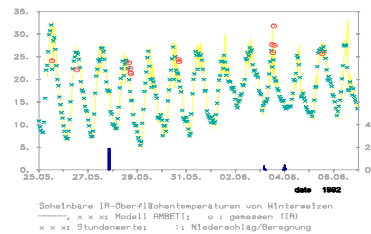
Fig. 6.13   Simulated (____x) and measured (O) apparent surface temperatures for winter
                       wheat

A comparison of remotely sensed and simulated "apparent surface temperatures" (see Section 2.7) for a crop of winter wheat is given in Fig. 6.13. These temperatures may be used as an indicator for water stress. As pointed out by Braden and Blanke (1993) the apparent surface temperatures can even be used for the remotely sensed control of large-sized model results for many pixels.

6.4   Summary and conclusions

The model AMBETI, presented in this paper, is a sophisticated model of transports and budgets of heat and water in the soil-plant-atmosphere system. To a large extent, the model works deterministically and only the bulk stomatal resistance needs calibration. The model consists of highly developed sub-models for the radiation components absorbed by the plants on the one hand, and by the ground cover (soil or snow) on the other hand. The aerodynamic transports are also calculated separately for the plants and the ground surface. The interception of precipitation is considered in a realistic manner. The formation and melting of a snow cover on the soil surface is simulated. Soil chill is considered during the calculation of the soil heat and water budgets. These capabilities of the model allow its application during the whole year including rainy and frost periods. The various effects of these weather events on the soil-plant-atmosphere system can be evaluated. Moreover, the water vapour transport in the upper soil layers is calculated for the proper determination of evaporation as well as the temperatures and water contents in the top soil.

The model AMBETI/BEKLIMA is used for research purposes and for routine applications in the Agrometeorological Section of the German Weather Service. This means daily model runs for many different meteorological boundary conditions and locations of Germany, each with a variety of different site parameters. This intensive application gave the opportunity of thoroughly testing and validating the model.

The model yields a broad variety of outputs like soil temperatures and water contents, evaporation, transpiration and other fluxes of heat and water. Moreover, microclimatic conditions in the canopy including leaf wetness and surface temperatures are calculated. Several results of the model are presented as examples.

Literature

Anderson, M.C.: Stand structure and light penetration, II. A theoretical analysis, J. Appl. Ecol., 3, 41--54, 1966.

Ångström, A.: The albedo of various surfaces of ground, Geofiska Annaler, 7, 323-342, 1925.

Bavel, C.H.M. van, and D.I. Hillel: Calculating potential and actual evaporation from a bare soil surface by simulation of concurrent flow of water and heat, Agric. Meteorol., 17, 453-376, 1976.

Benzler, J.H., et al.: Bodenkundliche Kartieranleitung (Ed.: Bundesanstalt für Geowissenschaften und Rohstoffe), Hannover, 1992.

Biologische Bundesanstalt für Land- und Forstwirschaft: Entwicklungsstadien bei Getreide, Merkblatt Nr. 27/1, Braunschweig, 1979.

Braden, H.: Simulationsmodell für den Wasser-, Energie- und Stoffhaushalt in Pflanzenbeständen, Berichte des Instituts für Meteorologie und Klimatologie der Universität Hannover 23, Diss., Technische Universität Braunschweig, 1982.

Braden, H.: Ein Energiehaushalts- und Verdunstungsmodell für Wasser- und Stoffhaushaltsuntersuchungen landwirtschaftlich genutzter Einzugsgebiete, Mitteilgn. Dtsch. Bodenkundl. Gesellsch., 42, 294-299, 1985.

Braden, H.: Modellierung meteorologischer Parameter im Bestand sowie der Blattbenetzung in Abhängigkeit von Meßdaten aus dem wetterdienstlichen Meßnetz, Int. Symp. "Computergestützte Prognosen und Entscheidungsmodelle im Pflanzenschutz" 29., 30. Nov. 1993, Bonn-Bad Godesberg, Broschüre des Bundesministeriums für Landwirtschaft, in press, 1994.

Braden, H. and Th. Blanke: About the use of remotely sensed surface temperatures for controlling estimates of evapotranspiration, Modeling Geo-Biosphere Processes, 2, 53-66, 1993.

Brooks, R.H., and A.T. Corey: Hydraulic properties of porous media, Hydrol. Pap. 3, 1964.

Brooks, R.H., and A.T. Corey: Properties of porous media affecting fluid flow, Journal of the Irrigation And Drainage Division, J. Irrig. Drain. Div., Am. Soc. Civ. Eng., 92 (IR2), 61-88, 1966.

Brutsaert, W.: Evaporation into the atmosphere, D. Reidel Publ. Comp., Dordrecht/Holland, pp. 299, 1982.

Busscher, W.J. and D.D. Fritton: Simulated flow through the root xylem, Soil Sci., 125 (1), 1978.

Campbell, G.S.: A simple method for determining unsaturated conductivity from moisture retention data, Soil Sci., 117, 311-314, 1974.

Campbell, G.S.: Soil physics with BASIC; Transport models for soil-plant systems, Development in

Soil Science, 14, Elsevier, Amsterdam, 1985.

Cass, A., G.S. Campbell and T.L. Jones: Enhancement of thermal water vapor diffusion in soil, Soil Sci. Soc. Am. J., 48, 25-32, 1984.

Cowan, I.R.: The interception and absorption of radiation in plant stands, J. Appl. Ecol., 5, 367-379, 1968.

Cowan, I.R.: Light in plant stands with horizontal foliage, J. Appl. Ecol., 8, 579-580, 1971.

de Vries, D.A.: Thermal properties of soils, In: W.R. van Wijk (Ed.). Physics of Plant Environment, J. Wiley, NY, 210-235, 1963.

de Vries, D.A.: Heat transfer in soils, In: D.A. de Vries and H.H. Afgan (Eds.). Heat and Mass Transfer in the Biosphere, Part 1, Transfer Processes in the Plant Environment, Sripta Book Comp., Washington DC, 5-28, 1975.

Denmead, O.T. and B.D. Millar: Water transport in wheat, in: Heat and Mass Transport in the Biosphere, (Eds.: D.A. de Vries and N.H. Afgan), J. Wiley, Washington, D.C., 395-402, 1975.

Dickinson, R.E., A. Henderson-Sellers, P.J. Kennedy and M.F. Wilson: Biosphere-Atmosphere Transfer Scheme (BATS) for the NCAR Community Climate Model, NCAR Technical Note, National Center for Atmosperic Research, Boulder, Colorado, 1986.

Dirmhirn, I.: Das Strahlungsfeld im Lebensraum, Akad. Verlagsgesellschaft, Frankfurt/M., 1964.

Feddes, R.A., P.J. Kowalik, and H. Zaradny: Simulation of field water use and crop yield, Simulation Monographs, Pudoc, Wageningen, 1978.

Gardner, W.R.: Some steady state solutions of the unsaturated moisture flow equation with application to evaporation from a water table, Soil Sci., 85, 228-232, 1958.

Gardner, W.R.: Dynamic aspects of water availability to plants, Soil Science, 89 (2), 63-73, 1960.

Gates, D.M. and W. Tantraporn: The reflectivity of deciduous trees and herbaceous plants in the infrared to 25 microns, Science, 115, 613-616, 1952.

Gates, D.M., H.J. Keegan, J.C. Schleter, and V.R. Weidner: Spectral properties of plants, Applied Optics, 4 (1), 11-20, 1965.

Genuchten, M.Th. van: A closed-form equation for predicting the hydraulic conductivity of unsaturated soils, Soil. Sci. Soc. Am. J., 44, 892-898, 1980.

Goudriaan, J.: Crop micrometeorology: A simulation study, Pudoc, Wageningen, 1977.

Graser, E.A. and C.H.M. van Bavel: The effect of soil moisture upon soil albedo, Agric. Meteorol., 27, 17-26, 1982.

Hack, A., H. Bleiholder, L. Buhr, U. Meier U. Schnock-Fricke, U. Weber und A. Witzenberger: Einheitliche Codierung der phänologischen Entwicklungsstadien mono- und dikotyler Pflanzen. - Erweiterte BBCH-Skala, Allgemein - Nachrichtenblatt Deutscher Pflanzenschutzdienst, 44, 12, 265-270, 1992.

Hansen, G.K.: Resistance to water flow in soils and plants, plant water status, stomatal resistance and transpiration of italian ryegrass, as influenced by transpiration demand and soil water depletion, Acta Agric. Scand., 24, 83-92, 1974.

Hillel, D.: Soil and Water, Physical Priciples and Processes, Academic Press, N.Y., 1971.

Hoogland, J.C., R.A. Feddes and C. Belmans: Root water uptake model depending on soil water pressure head and maximum extraction rate, Acta Horticulturae, 119, 123-136, 1981.

Hoyningen-Huene, J. von und A. Bramm: Die wägbare Unterdrucklysimeteranlage in Braunschweig-Völkenrode - Aufbau und erste Erfahrungen, Landbauforschung Völkenrode, 28 (2), 95-102, 1978.

Hulugalle, N.R. and S.T. Willatt: The role of soil resistance in determining water uptake by plant root systems, Aust. J. Soil. Res., 21, 571-574, 1983.

Jolly, P.G.: Derivation of solar angles using vektor algebra, Solar Energy, 37(6), 429-430, 1986.

Kasten, F. and G. Czeplak: Solar and terrestrial radiation dependent on the amount and type of cloud, Solar Energy 24, 177-189, 1980.

Kasten, F.: Strahlungsaustausch zwischen Oberflächen und Atmosphäre, VDI Berichte Nr. 721, 131-158, 1989.

Kücke, M. und P. Löffler: Untersuchungen zum Wurzelwachstum von Getreide und Zuckerrüben auf unterschiedlich schweren Standorten, Mitteilg. Dtsch. Bodenkundl. Gesellsch. 59/II, 741-744, 1990.

Larcher, W.: Ökologie der Pflanzen, Uni-Taschenbücher 232, Ulmer, Stuttgart, 1976.

Löpmeier, F.-J.: AMBER- Agrarmeteorologische Beratung, 124-130, Ed.: F. Kuhlmann, 3. Int. Computerkongreß - Integrierte entscheidungs-orientierte Datenverarbeitung in der Landwirtschaft, Frankfurt a.M. - Bad Soden, 27.-30.Mai 1990, Deutsche Landwirtschafts-Gesellschaft (DLG), Gießen, 1990.

Löpmeier, F.-J.: Fernerkundungdaten für agroklimatische Zwecke, Abschlußbericht BMFT 07 KF114-6, ZAMF, Deutscher Wetterdienst, 1991.

Marsal, D.: Die numerische Lösung partieller Differentialgleichungen in Wissenschaft und Technik, Bibliogr. Inst., Mannheim, 1976.

McInnes, K.J.: Thermal conductivities of soils from dryland wheat regions of Eastern Washington, M.S. Thesis, Washington State University, Pullman, 1981.

Mualem, Y., 1976: A new model for predicting the hydraulic conductivity of unsaturated porous media, Water Resour. Res., $\underline{12}$(3), 513-521, 1976.

Myneni, R.B., G. Asrar, and E.T. Kanemasu: Light scattering in plant canopies: The method of Successive Orders of Scattering Approximations (SOSA), Agric. For. Meteorol., $\underline{39}$, 1-12, 1987.

Oke, T.R.: Boundary Layer Climates, Methuen, London, 1978.

Philip, J.R. and D.A. de Vries: Moisture movement in porous materials under temperature gradients, Trans. Amer. Geophys. Un., $\underline{38}$, 222-232, 1957.

Rawls, W.J. and D.L. Brakensiek: Prediction of soil water properties for hydrologic modeling, Proceedings of the symposium watershed management in the eighties, (Ed.: E.B. Jones), American Society of Civil Engineers, New York, 293-299, 1985.

Richter, O. and M. Kücke: A new model for root growth, submitted to Bulletin of Mathematical Biology, 1994.

Ross, J.: Radiative transfer in plant communities, in: Vegetation and the Atmosphere, (Ed.: J.L. Monteith), Vol. 1, Acad. Press, London, 13-55, 1975.

Scheffer, F., und P. Schachtschabel: Lehrbuch der Bodenkunde, 13. Aufl., 1992.

Schrödter, H.: Zur aktuellen Evapotranspiration von Pflanzenbeständen in Abhängigkeit von der phänologischen Entwicklung, Kali-Briefe, $\underline{15}$, Nr.11, 673-690, 1981.

Schulze, R.: Das Strahlenklima der Erde, Wiss. Forschungsber., Bd. 72, Steinkopff Verlag, Darmstadt, 1970.

Slabbers, P.J.: Practical prediction of actual evapotranspiration, Irrgat. Sci., $\underline{1}$, 185-196, 1980.

Slatyer, R.O.: Plant-water relationships, in: Experimental Botany, (Ed.: JF. Sutcliffe and P. Mahlberg), Vol. 2, Academic Press, London, 1967.

Slavik, B.: Methods of studying plant water relations, in: Ecological Studies 9 (Eds.: J. Jacobs et. al.), Springer, Berlin, 1974.

Smith, R.E.: OPUS: An integrated Simulation Model for Transport of Nonpoint Source Pollutants at the Field Scale, Volume I, Documentation, USDA ARS publication ARS-98, 1992.

Thom, A.S.: Momentum, mass and heat exchange of plant communities, in: Vegetation and the Atmosphere, (Ed.: J.L. Monteith), Vol. 1, Academic Press, London, 57-109, 1975.

Thomas, Ch.W.: On the transfer of visible radiation through sea ice and snow, Journal of Glaciology, $\underline{4}$, 481-484, 1963.

Thompson, N., I.A. Barrie and M. Ayles: The Meteorological Office Rainfall and Evaporation Calculation System: MORECS (July 1981), Hydrological Memorandum No. 45, 1981.

Tietje, O., and M. Tapkenhinrichs: Evaluation of pedo-transfer functions, Soil Sci. Soc. Am. J., 57, 1088-1095, 1993.

Tietje, O., and V. Hennings: Bewertung von Pedotransferfunktionen zur Schätzung der Wasserspannungskurve, Z. Pflanzenernähr. Bodenk. 156, 447-455, 1993.

Vereecken, H., J. Maes, J. Feyen and P. Darius: Estimating the soil moisture retention characteristic from texture, bulk density, and carbon content, Soil Science, 148, No. 6, 390-403, 1989.

Vereecken, H., J. Maes, J. Feyen: Estimating unsaturated hydraulic conductivity from easily measured soil properties, Soil Sci., 149, 1-12, 1990.

Waggoner, P.E., G.M. Furnival and W.E. Reifsnyder: Simulation of the microclimate in a forest, Forest Sci., 15, 37-45, 1969.

Westing, A. und H. Söchtig: Bestimmung der Wurzeldichte in Böden unterschiedlicher Profiltiefe unter Weizen, Gerste und Zuckerrüben, Mitteilg. Dtsch. Bodenkundl. Gesellsch. 43/II, 697-701, 1985.

Widger, W.K., jr. and M.P. Woodall: Integration of the Planck blackbody function, Bull. Amer. Meteor. Soc., 57, 1217-1219, 1976.

Zadoks, A., T. T. Chang and C. F. Konzak: A decimal code for the growing stage of cereals, Weed Research 14, 415-421, 1974.

Zelitch, I.: Photosynthesis, photorespiration, and plant productivity, Acad. Press, New York, 1971.

Ziegler, H.: Physiologie, In: Lehrbuch der Botanik, (founded by E. Strasburger), Fischer Verlag, Stuttgart, 31. Ed., 213-476, 1978.

List of the main symbols

Symbol	Meaning	Unit
c_p	specific heat of the air	J K^{-1} kg^{-1}
c_{pl}	specific heat of the plant elements	J K^{-1} kg^{-1}
$C_{h,i}$	specific heat in soil layer i	J m^{-3} K^{-1}
C_{ph}	specific heat of melting	C_{ph}= 3.32 $_{10}^{5}$ J/kg of water
d_s	stem diameter	m
d_{sn}	height of snow	m
D_v	diffusivity for water vapour in the soil	m s^{-2}
f_h	vertical soil heat flux density	W m^{-2}
$f_{vz,0}$	evaporative flux density	mm$_{(H2O)}$ (= kg m^{-2})
f_w	vertical soil water flux density	kg$_{(H2O)}$ m^{-2} s^{-1}
g	gravitational acceleration	g≈9.81 m s^{-2}
G	ground heat flux density	W m^{-2}
h_r	reduction function for the saturated water content of stressed water	
H_{pl}	vertical flux density of sensible heat to the plants	W m^{-2}
H_{sa}	vertical flux density of sensible heat to the soil surface	W m^{-2}
K	extinction coefficient (Chapter 2)	
K_u	hydraulic conductivity in the soil	kg$_{(H2O)}$ s m^{-3}
K_s	saturated hydraulic conductivity in the soil	kg$_{(H2O)}$ s m^{-3}
l_a	leaf area index	m$^2_{(leaf)}$/m$^2_{(ground)}$
m_c	mass fraction of clay	kg/kg
m_o	mass fraction of organic material	kg/kg
m_u	mass fraction of silt	kg/kg
m_s	mass fraction of sand	kg/kg
p_a	plant area index ($p_a=l_a+s_a$)	m^2/m^2
P_i	amount of intercepted precipitation	mm$_{(H2O)}$ (= kg m^{-2})
P_r	amount of precipitation	mm$_{(H2O)}$ (= kg m^{-2})
$Q_{ph,i}$	latent heat of melting in soil layer i	J m^{-2}
r	reflection coefficient of leaves	
r_a	resistances for the vertical aerodynamic transports between the	s m^{-1}

reference height and the level of the main energy exchange inside the canopy

r_{ac}	aerodynamic resistance inside the <u>c</u>anopy (see Chapter 3)	
r_{ap}	aerodynamic resistance at the <u>p</u>lant elements (see Chapter 3)	
r_{as}	aerodynamic resistance at the <u>s</u>oil surface (see Chapter 3)	
r_g	reflectivity of the ground surface (soil or snow)	
r_{pl}	resistance for transpiration and evaporation of the plants	s m^{-1}
r_{st}	bulk stomatal resistance	s m^{-1}
r_s	reflection coefficient for stems	
R_g	global radiation	W m^{-2}
R_l	incident long-wave radiation	W m^{-2}
$R_{n\,pl}$	net radiation of the plants	W m^{-2}
$R_{n\,g}$	net radiation of the ground surface	W m^{-2}
s_a	stem area index	m^2/m^2
t	time	s
t	transmission coefficient of leaves	
T_d	transmitted portion of diffuse radiation	
T_{IR}	transmitted portion of thermal radiation	
T	temperature	K
T_r	temperature at reference height	K
T_{ca}	temperature in the canopy	K
T_{pl}	plant temperature	K
$T_{s,i}$	temperature of soil layer i	K
T_{ph}	temperature of phase transition liquid < > frozen	K
u_r	wind speed at reference height	m s^{-1}
V_{sa}	vertical evaporation flux density at the soil surface	kg m^{-2} s^{-1}
V_{pl}	vertical evaporation flux density from the plants	kg m^{-2} s^{-1}
w	volumetric (soil) water content	m$^3_{(water)}$/m^3
w_r	residual (soil) water content	m$^3_{(water)}$/m^3
w_s	saturated (soil) water content	m$^3_{(water)}$/m^3
w_{sn}	water content of the snow	kg$_{(water)}$/m^2
z_c	canopy height	m
z_r	reference height	m
z_s	length of stems	m

z_0	roughness length		m
Δz	increment of vertical length		m

β	angle of incidence		rad
γ	psychrometer constant ($\gamma = \rho\, c_p/\lambda$)		kg m^{-3} K^{-1}
ε_{pl}	relative emissivity of the plants		
ε_g	relative emissivity of the ground surface		
θ	relative water content		
λ	angle of leaf inclination	(Chapter 2)	rad
λ	specific latent heat of vaporization	(Chapter 3)	J kg^{-1}
λ_h	thermal conductivity of the soil		W m^{-1} K^{-1}
λ_w	wave length of radiation		µm
ρ	density of the air		kg m^{-3}
ρ_{ca}	absolute humidity of the air inside the canopy		kg m^{-3}
ρ_v	water vapour density in the pore space of the soil		kg m^{-3}
ρ_d	reflectance of the canopy for diffuse radiation		
ρ_{IR}	reflectance of the canopy for thermal radiation		
ρ_β	reflectance of the canopy for direct radiation		
σ	Boltzmann constant		5.67 10^{-8} W K^{-4} m^{-2}
φ_a	volume fraction of air in the soil		
φ_s	volume fraction of solids in the soil		
ψ	matric (water) potential		J/ kg
ψ_{pl}	plant water potential		J/ kg
$\psi_{t,i}$	total water potential in soil layer I		J/ kg $= m^2/s^2$

Appendix

A1.1 Overview over the sub-programs

Name	Contents	(Section/Chapter)

PINTER   third degree polynom interpolation
MSOITE   soil heat budgets (5.1, 5.2)
SOIWAM   soil water budgets (5.4)
PSYKU   hydraulic soil properties (5.5)
BOPAR   soil composition and thermal properties (5.3)
HYPAR   pedo-transfer functions (5.6) according to
CAMPB   Campbell (1985)
VEREEC   Vereecken (1989, 1990)
RABRAS   Rawls and Brakensiek (1985)
METIER   (organization)
DATKOR   control of met. bound. conditions and parameterization of R_g, R_l (6.1)
FRHOW   water vapour conversion
EINGAB   input (AMBETI-version) (6.1)
METIET   aerodynamic resistances (3.5), interception of precipitation (4.3)
STRAHL   radiation components (2)
TRARED   transmission and reflection (2.2b)
TRADIR   transmission of direct radiation (2.3)
HSUN   sun elevation (2.1)
METPEB   energy budgets (3.1), aerodynamic transports (3.2, 3.3), bulk stomatal
              resistance (4.1), plant water conduction (4.2)
MSURF   energy budget at the soil surface (3.1)
SNOWAE   melting of the snow cover (3.6)
SOIVAP   water vapour transport in the upper soil (5.6)

A2.1   On fitting the reflection and transmission coefficients to results of a "Successive Orders of Scattering Approximations (SOSA)" model

The transmitted and reflected portions of the incident radiation calculated according to Sections 2.3 and 2.4 are compared with the results of the "Successive Orders of Scattering Approximations (SOSA)" model (Braden, 1982) in order to improve the results of the method presented. The resulting model combines a straightforward method with the proper results of an involved SOSA model. The direct use of the SOSA model in the model AMBETI is not appropriate, because it would take too much computing time.

In the SOSA model, the plants are divided into several thin horizontal layers, each with small amounts of plant area ($p_a=l_a+s_a \leq 0.1$)[*]. In each layer nine classes of inclinations of the plant elements are considered, each with the same uniform and non-correlated distribution over the azimuths. Though real crop canopies do more or less violate these assumptions, it seems to be acceptable to use the model because radiation transfer models for realistic geometries are not available.

For the nine classes of inclination, incident radiation is considered to be scattered by the plant elements of the top layer. The scattering is considered for reflection and transmission in up to 18 classes of inclination (nine upward and nine downward). The probabilities for the scattering at the plant elements, and the transmission through the leaves, are calculated from the portions of plant area projected in the direction of the respective incident radiation.

For the nine classes of inclination, the unscattered remainder of the incident radiation, together with the radiation scattered downward by the top layer, is considered to be scattered at the second layer of plant elements. These calculations are continued until the bottom layer is reached and then the process begins in the opposite direction with the components scattered upward until the top layer is reached. No reflection is considered at the ground surface because it will be taken into account afterwards. The whole procedure must be repeated several times until finally all important multiple scattering processes are accounted for. The recursion is stopped when the last recursion does not deviate by more than 0.1‰ of the radiant emittances in each layer.

Up to this point a normal SOSA model (Myneni et al., 1987) has been described. The model used has the following additional features (Braden, 1982):

-        The probabilities for scattering are determined separately for each class of incident radiation

---

[*]   This is recommended, because multiple scattering inside one layer will be omitted.

and each class of inclination of the plant elements.

-        Leaves and upright stems with distinct optical properties can be considered.

-        The distribution of the leaf inclinations can be chosen freely.

-        Leaves are allowed to have different coefficients for reflection and transmission ($t \neq r$).

-        The top and bottom faces of leaves are allowed to have different optical properties.

-        Leaves are allowed to reflect with a specular component.

-        The diffuse reflection of the plant elements is considered to be Lambertian.

For the radiation reflected by and transmitted through the leaves the angular distribution of the radiant emittances are considered in relation to the individual position of the plant elements.

A3.1 The calculation of the plant-canopy-air fluxes and plant temperature in the "no-microclimate" option

In this option, the energy budget Equation (3.3) is used with (3.1), (3.2), (3.2a) and (3.6):

$$R_{nspl} + \varepsilon_{pl} (a_{plu} R_l + a_{plo} \varepsilon_g \sigma T_{sa}{}^4 - a_{ple} \sigma T_x{}^4) - B_{RL} (T_{pl}-T_x)$$

$$+ \rho c_p (T_r - T_{pl})/(r_{ap} + r_a) + V_{pl} + c_{pl} (T_{plo} - T_{pl})/\Delta t = 0 \qquad \text{(A3.1)}$$

with the abbreviation

$$B_{RL} = 4 \varepsilon_{pl} a_{ple} \sigma T_x{}^3 \quad . \qquad \text{(A3.2)}$$

Solving (A3.1) for T_{pl} leads to

$$T_{pl} = \{ R_{nspl} + H_{RLX} + \rho c_p T_r/(r_{ap}+r_a) + c_{pl} T_{plo}/\Delta t + V_{pl} \}/N_{RRBW} \qquad \text{(A3.3)}$$

with the abbreviations

$$H_{RLX} = \varepsilon_{pl} (a_{plu} R_l + a_{plo} \varepsilon_g \sigma T_{sa}{}^4 - a_{ple} \sigma T_x{}^4) + B_{RL} T_x \qquad \text{(A3.4)}$$

and

$$N_{RRBW} = B_{RL} + \rho c_p/(r_{ap}+r_a) + c_{pl}/\Delta t \qquad . \qquad \text{(A3.5)}$$

When this expression for T_{pl} is introduced into (3.7) and (3.7a), V_{pl} is resolved to give

$$V_{pl} = \{ [\rho_r - \rho_s(T_x) + \Delta_\rho T_x] N_{RRBW} \qquad \text{(A3.6)}$$

$$- \Delta_\rho [R_{nspl} + H_{RLX} + \rho c_p T_r/(r_{ap}+r_a) + c_{pl} T_{plo}/\Delta t] \}$$

$$/ \{ N_{RRBW} (r_{ap} + r_a + r_{pl})/\lambda_{pl} + \Delta_\rho \} \qquad .$$

Then T_{pl} and the sensible heat flux H_{pl} are calculated from (A3.3) and (3.6), respectively.

A3.2 The calculation of the plant-canopy-air fluxes and plant temperature in the "microclimate" option

As already stated in Sections 3.2 and 3.3, the actual values of T_{pl}, T_{ca} and ρ_{ca} are determined with known values of T_{sa} and ρ_{sa}. For this purpose, Equations (3.1), (3.2), (3.2a), (3.7a), (3.12) and (3.13) are inserted into the energy budget Equation (3.3):

$$R_{nspl} + \varepsilon_{pl} (a_{plu} R_l + a_{plo} \varepsilon_g \sigma T_{sa}^{4} - a_{ple} \sigma T_x^{4}) - B_{RL} (T_{pl} - T_x)$$

$$+ \rho c_p (T_{ca} - T_{pl})/r_{ap} + \lambda_{pl} [\rho_{ca} - \rho_s(T_x) - \triangle_\rho (T_{pl} - T_x)]/(r_{ap} + r_{pl})$$

$$+ c_{pl} (T_{plo} - T_{pl})/\triangle t \quad = \quad 0 \tag{A3.7}$$

Solving (A3.7) for T_{pl} leads to

$$T_{pl} = \{ R_{nspl} + H_{RLX} + \rho c_p T_{ca}/r_{ap}$$

$$+ \lambda_{pl} [\rho_{ca} - \rho_s(T_x) + \triangle_\rho T_x]/(r_{ap} + r_{pl}) + c_{pl} T_{plo}/\triangle t \}/N_{RRBX} \tag{A3.8}$$

with the abbreviations (A3.3 and A3.4) and

$$N_{RRBX} = B_{RL} + \rho c_p/r_{ap} + \lambda_{pl} \triangle_\rho/(r_{ap}+r_{pl}) + c_{pl}/\triangle t \quad . \tag{A3.9}$$

From (3.12), (3.14) and (3.16) T_{ca} is obtained as

$$T_{ca} = [T_r r_{ap} (r_{ac} + r_{as}) + T_{pl} r_a (r_{ac} + r_{as}) + T_{sa} r_a r_{ap}]/N_{RN1} \tag{A3.10}$$

with the abbreviation

$$N_{RN1} = r_a (r_{ac} + r_{as}) + r_{ap} (r_a + r_{ac} + r_{as}) \quad . \tag{A3.11}$$

In a similar way ρ_{ca} is eliminated from (3.13), (3.15) and (3.17) with the linearization (3.7a) and

$$N_{RN2} = \lambda_{pl} \, r_a \, (r_{ac} + r_{as}) + (r_{ap} + r_{pl})[\, \lambda_{sa} \, r_a + \lambda \, (r_{ac} + r_{as}) \,] \tag{A3.12}$$

giving

$$\rho_{ca} = \{ \, [\, \lambda \, \rho_r \, (r_{ac} + r_{as}) + \lambda_{sa} \, \rho_{sa} \, r_a \,] \, (r_{ap} + r_{pl})$$

$$+ \lambda_{pl} \, [\, \rho_s(T_x) + \triangle_\rho \, (T_{pl} - T_x) \,] \, r_a \, (r_{ac} + r_{as}) \, \}/N_{RN2} \qquad . \tag{A3.13}$$

Now, (A3.10) and (A3.13) are introduced into (A3.8) and after some elementary operations for T_{pl} the expression

$$T_{pl} = (\, N_{H2} + \lambda_{pl} \, N_{H0} \, / \, N_{RN2} \,)/N_{H1} \tag{A3.14}$$

is found with the abbreviations

$$N_{H2} = R_{nspl} + H_{RLX} + \rho \, c_p \, [\, T_r \, (r_{ac} + r_{as}) + T_{sa} \, r_a \,]/N_{RN1} + T_{plo} \, c_{pl}/\triangle t \qquad , \tag{A3.15}$$

$$N_{H1} = B_{RL} + c_{pl}/\triangle t + \rho \, c_p \, (r_a + r_{ac} + r_{as})/N_{RN1}$$

$$+ \lambda_{pl} \, \triangle_\rho \, [\, \lambda_{sa} \, r_a + \lambda \, (r_{ac} + r_{as}) \,]/N_{RN2} \qquad , \tag{A3.16}$$

$$N_{H0} = \{ \, \lambda \, \rho_r \, (r_{ac} + r_{as}) + \lambda_{sa} \, \rho_{sa} \, r_a$$

$$+ [\triangle_\rho \, T_x - \rho_s(T_x)] \, [\lambda_{sa} \, r_a + \lambda \, (r_{ac} + r_{as})] \, \}/N_{RN2}. \tag{A3.17}$$

With (A3.14) T_{ca} and ρ_{ca} can be obtained from (A3.10) and (A3.13), respectively. The plant-canopy-air fluxes of sensible and latent heat are finally determined from (3.12) and (3.13).

A5.1   The pedo-transfer coefficients of Rawls and Brakensiek (1985) and of Vereecken et al. (1989, 1990)

Rawls and Brakensiek (1985) empirically related the quantities used in the hydraulic functions (see Chapter 5.5) to the basic soil properties total porosity φ_a , mass fraction of clay m_c , mass fraction of sand m_s . Each quantity is expressed by means of incomplete mixed second order polynoms of the properties in the form

$$P(a_i,\varphi_a,m_c,m_s) = a_0 + a_1\ \varphi_a + a_2\ m_c + a_3\ m_s$$
$$+ a_4\ \varphi_a^2 + a_5\ m_c^2 + a_6\ m_s^2 + a_7\ \varphi_a m_c + a_8\ \varphi_a m_s$$
$$+ a_9\ \varphi_a m_c^2 + a_{10}\ \varphi_a m_s^2 + a_{11}\ m_c\varphi_a^2 + a_{12}\ m_c m_s^2 + a_{13}\ m_s\varphi_a^2 + a_{14}\ m_s m_c^2$$
$$+ a_{15}\ \varphi_a^2 m_c^2 + a_{16}\ \varphi_a^2 m_s^2$$

The saturated hydraulic conductivity K_s (cm/h) is given by

$$K_s = \exp\{\ P(a_i,\varphi_a,m_c,m_s)\ \}\qquad.$$

The residual water content (m^3/m^3) is given by

$$w_r = P(b_i,\varphi_a,m_c,m_s)\qquad.$$

The saturated water content is determined from

$$w_s = P(c_i,\varphi_a,m_c,m_s)\qquad.$$

For the "bubbling-pressure" ψ_b (cm) Rawls and Brakensiek give the relation

$$\psi_b = -\exp\{\ P(d_i,\varphi_a,m_c,m_s)\ \}\qquad.$$

The exponent of the Brooks and Corey retention function (5.26) is determined from

$$1/b = \exp\{\ P(e_i,\varphi_a,m_c,m_s)\ \}$$

The contents of sand and clay, $m_{s,US}$[*)] and m_c, respectively are expressed in % and the total porosity $\varphi_a = 1 - \varphi_s$ in m^3/m^3 (see Section 5.3). The coefficients are listed in Tab. 5.5.

Table A5.2 The coefficients of the polynoms $P(a_i, \varphi_a, m_c, m_s)$

i	a_i	b_i	c_i	d_i	e_i
0	-8.96847	-0.0182482	0.01162	5.3396738	-0.7842831
1	19.52348	0.02939286	0.98402	-2.48394546	-1.062498
2	-0.028212	0.00513488	-0.002236	0.1845038	
3		0.00087269	-0.001473		0.0177544
4	-8.395215				1.11134946
5	-0.0094125	-0.00015395	0.0000987	-0.00213853	-0.00273493
6	0.00018107				-0.00005304
7			-0.010859	-0.61745089	
8	0.077718	-0.0010827	0.003616	-0.04356349	-0.03088295
9	0.02733	0.00030703	-0.000096	0.00895359	0.00798746
10	0.001434			-0.00072472	
11		-0.0023584	0.0115395	0.5002806	-0.00674491
12	0.0000173			-0.00001282	-0.00000235
13			-0.002437		
14	-0.0000035			0.0000054	
15	-0.019492	-0.00018233		-0.00855375	-0.00610522
16	-0.00298			0.00143598	0.00026587

For the use of the van Genuchten functions (5.23 and 5,25a) (method No. 2) $\alpha = 1/\psi_b$, $n = 1 + 1/b$ and $m = 1 - 1/n$ is used. The hydraulic conductivity according to Brooks and Corey (1964) is calculated with the exponent $a = 3 + 2b$ in (5.27) (methods No. 1, 4 and 5). For the modification of Smith (1992) (method No. 5) the retention is calculated from (5.23) with $n = 5$ and $m = 1/(5b)$.

In method No.3 according to Vereecken et al. (1989, 1990) besides the dry bulk density ρ_b (in g/cm^3), the USDA-texture (m_c, m_u and m_s, see footnote in Section 5.3) and the organic carbon content C_{org}, all

---

[*)] For reasons of simplicity in the following m_s and m_u is written instead of $m_{s,US}$ and $m_{u,US}$, respectively.

expressed in %, are used in the regression of the coefficients. For the saturated hydraulic conductivity Vereecken et al. (1990) used the organic matter content m_o instead of the organic carbon content. The conversion is achieved by $m_o = 1.72\ C_{org}$. The residual and saturated water contents (m^3/m^3) are determined from

$$w_r = 0.015 + 0.005*m_c + 0.0139*C_{org}$$

and

$$w_s = 0.81 - 0.283*\rho_b + 0.0013*m_c \qquad .$$

The retention function (5.23) is used with m=1 and α (in cm^{-1}) is given by

$$\alpha = \exp\{ -2.486 + 0.025*m_s - 0.351*m_o - 2.617*\rho_b - 0.023*m_c \},$$

$$n = \exp\{ 0.053 - 0.009*m_s - 0.013*m_c + 0.00015*m_s^2 \}$$

For the saturated hydraulic conductivity (5.28) (cm/h) Vereecken et al. (1990) give the coefficients

$$K_s = \exp\{ 20.62 - 0.96*\ln(m_c) - 0.66*\ln(m_s) - 0.46*\ln(m_o) - 8.43*\rho_b \},$$

$$b = \exp\{ -0.73 - 0.01877*m_s + 0.058*m_c \}$$

and

$$v = \exp\{ 1.186 - 0.194*\ln(m_c) - 0.0489*\ln(m_u) \} \qquad .$$

For the use in the equations of Section 5.4 the hydraulic conductivities are converted from (cm/h) to ($kg_{(H2O)}\ s\ m^{-3}$) by multiplication with the factor 10/3600 ($kg_{(H2O)}\ m^{-3}/s$)/(cm/h) and by division with the gravitational acceleration $g \approx 9.81\ m\ s^{-2}$. The water potentials are converted by multiplying 10 cm = 0.1 m with g=9.81 m/s^2 giving 10 cm^,=0.981 J/kg.

A6.1   The main particle size fractions for the German soil classification

In many cases the particle size fractions have not been measured, but the soil has been characterized according to mapping instructions (Benzler et al., 1982). Tab. A6.1 relates the 28 soil types to the corresponding particle size fractions[*)], that are needed as input quantities of the model AMBETI (see Section 6.1).

Table 6.1   The German soil classification and the corresponding mass fraction of the main particle sizes of clay (c), silt (u) and sand (s)

soil type	abbrev.	m_c	m_u	m_s
		%	%	%
Schluff	U	4.00	88.00	8.00
sandiger Schluff	Us	4.00	65.00	31.00
sandig-lehmiger Schluff	Uls	12.50	57.50	30.00
schwach lehmiger Schluff	Ul2	10.00	77.50	12.50
mittel lehmiger Schluff	Ul3	14.50	75.25	10.25
stark lehmiger Schluff	Ul4	21.33	74.33	4.33
schwach sandiger Lehm	Ls2	20.00	45.00	35.00
mittel sandiger Lehm	Ls3	19.00	34.33	46.67
stark sandiger Lehm	Ls4	21.00	21.50	57.50
schluffiger Lehm	Lu	23.50	60.00	6.50
schwach toniger Lehm	Lt2	30.00	42.50	27.50
mittel toniger Lehm	Lt3	40.00	40.00	20.00
schluffig-toniger Lehm	Ltu	37.50	56.25	6.25
sandig-toniger Lehm	Lts	35.00	27.67	37.33
schwach sandiger Ton	Ts2	58.00	9.00	33.00
mittel sandiger Ton	Ts3	43.00	9.00	48.00
stark sandiger Ton	Ts4	30.00	9.00	61.00
lehmiger Ton	Tl	55.00	31.50	13.50
Ton	T	76.66	11.67	11.67
Sand	S	2.50	5.00	92.50
schwach schluffiger Sand	Su2	2.50	17.50	80.00
mittel schluffiger Sand	Su3	4.00	32.50	63.50
stark schluffiger Sand	Su4	4.00	45.00	51.00
schluffig-lehmiger Sand	Slu	11.50	45.00	43.50
schwach lehmiger Sand	Sl2	6.50	15.00	68.50
mittel lehmiger Sand	Sl3	10.00	23.50	66.50
stark lehmiger Sand	Sl4	14.67	29.33	56.00
schwach toniger Sand	St2	10.00	6.25	83.75
mittel toniger Sand	St3	19.00	9.33	71.67

[*)]   Center of the corresponding area in the soil triangle.